THE INTRINSICALLY DISORDERED NUCLEAR LOCALIZATION SIGNAL AND PHOSPHORYLATION SEGMENTS DISTINGUISH THE MEMBRANE BINDING AFFINITY OF TWO CYTIDYLYLTRANSFERASE ISOFORMS

by

Melissa Dennis
B.Sc., Simon Fraser University, 2004

THESIS SUBMITTED IN PARTIAL FULFILLMENT OF
THE REQUIREMENTS FOR THE DEGREE OF

DOCTOR OF PHILOSOPHY

In the
Department of Molecular Biology and Biochemistry

SIMON FRASER UNIVERSITY

Fall 2010

Approval

Name:	**Melissa Dennis**
Degree:	**Doctor of Philosophy**
Title of Thesis:	**The Intrinsically Disordered Nuclear Localization Signal and Phosphorylation Segments Distinguish the Membrane Binding Affinity of Two Cytidylyltransferase Isoforms**

Examining Committee:

Chair: **Dr. Frederic F. Pio**
Associate Professor, Department of Molecular Biology and Biochemistry

Dr, Rosemary Cornell
Senior Supervisor
Professor, Department of Molecular Biology and Biochemistry

Dr. Mark Paetzel
Supervisor
Associate Professor, Department of Molecular Biology and Biochemistry

Dr. Lisa Craig
Supervisor
Associate Professor, Department of Molecular Biology and Biochemistry

Dr. Edgar C. Young
Supervisor
Associate Professor, Department of Molecular Biology and Biochemistry

Dr. Glen Tibbits
Internal Examiner
Professor, Department of Kinesiology

Dr. George Harauz
External Examiner
Professor, Department of Molecular and Cellular Biology
University of Guelph

Date Defended/Approved: December 3 2010

Declaration of
Partial Copyright Licence

Abstract

Membrane phosphatidylcholine (PC) homeostasis is maintained in part by a sensing device in the key regulatory enzyme, CTP: phosphocholine cytidylyltransferase (CCT). CCT responds to decreases in membrane PC content by reversible membrane binding and activation. Two prominent isoforms, CCTα and β_2, have nearly identical catalytic domains and very similar membrane binding amphipathic helical (M) domains, but have divergent and structurally disordered amino-terminal (N) and carboxy-terminal phosphorylation (P) regions. I found that the anionic membrane binding affinity of purified CCTβ_2 was weaker than CCTα by at least an order of magnitude. Using chimeric CCTs, insertion/deletion mutants and truncated CCTs I showed that the stronger affinity of CCTα can be attributed in large part to the secondary electrostatic membrane binding function of the polybasic nuclear localization signal (NLS) motif, present in the unstructured region of region N of CCTα, but lacking in CCTβ_2. The membrane partitioning of CCTβ_2 in cells enriched with the lipid activator, oleic acid, was also weaker than that of CCTα, and was elevated by incorporation of the NLS motif. Thus, the polybasic NLS can function as a secondary membrane-binding motif not only *in vitro* but also in the context of cell membranes. A comparison of phosphorylated, dephosphorylated, and region P truncated forms showed that the *in vitro* membrane affinity of CCTβ_2 is more sensitive than CCTα to phosphorylation status, which antagonizes membrane binding of both isoforms. These data provide a model wherein the primary membrane binding motif, an amphipathic helical domain, works in collaboration with other intrinsically disordered segments, which modulate membrane binding strength. The NLS reinforces, while the phosphorylated tail antagonizes the attraction of domain M for anionic membranes.

Keywords: CTP: phosphocholine cytidylyltransferase; membrane binding; phosphorylation; nuclear localization signal; intrinsically disordered region

For my parents

Acknowledgements

Even now, I remember the excitement of walking into the lab for the first time. I knew it was where I belonged.

Thank you to my Senior Supervisor, Dr. Rosemary Cornell, for giving me the opportunity to find my passion and pursue it. I am grateful for your encouragement, your wisdom and above all, your unparalleled enthusiasm for science.

Thank you to my External and Internal Examiners, Dr. George Harauz and Dr. Glen Tibbits. Your kind words and thoughtful input are greatly appreciated and will be remembered.

To my Supervisory Committee – Dr. Lisa Craig, Dr. Mark Paetzel and Dr. Edgar Young – thank you so very much for your enthusiasm for my work and my future. As well, thank you for your professional (and personal) guidance as I start my career.

To members of the Cornell Lab – past and present – thank you for all that you have taught me. I would like to acknowledge Dr. Joanne Johnson, Jillian Smith and Dr. Theresa Kitos for "showing me ropes". I would like to offer a special thanks to Dr. Svetla Taneva for her advice, both scientific and personal, and for making me feel like I have something to contribute. I will miss you.

Thank you to Jacqueline Gleave and Dennis Villanueva for their unwavering support. To my sister and brother-in-law, Lori Dennis and Clayton Evoy, for teaching me about balance and for being such a wonderful example. Special thanks to Matthew Wright – I could not imagine having gone through this with anyone else. Thank you for keeping me sane (mostly), for cheering me on and holding me up.

Lastly, and above all, thank you to my parents – Doug and Julie Dennis. None of this would have been possible without you both. Thank you for your patience, your confidence, your guidance and your love. Words are not enough.

Table of Contents

List of Figures

List of Tables

Glossary

ADP	adenosine 5'-diphosphate
ATP	adenosine 5'-triphosphate
BS^3	bis(sulfosuccinimidyl) suberate
BSA	bovine serum albumin
CCT	CTP: phosphocholine cytidylyltransferase
CD	circular dichroism
CDP	cytidine 5'-diphosphate
CMP	cytidine 5'-monophosphate
CTP	cytidine 5'-triphosphate
$Cu(Phe)_3$	copper phenanthroline
DAG	diacylglycerol
DEAE	diethylaminoethyl
DMEM	Dulbecco's Modified Eagle Medium
DMSO	dimethyl sulfoxide
dNTP	deoxynucleotide triphosphate
DPPC	dipalmitoyl-phosphatidylcholine
DTT	dithiothreitol
EC_{50}	concentration of lipid required for half-maximal activity or membrane binding

EDTA	ethylenediaminetetraacetic acid
ER	endoplasmic reticulum
FBS	fetal bovine serum
GCT	CTP: glycerol-3-phosphate cytidylyltransferase
GFP	green fluorescent protein
GuHCl	guanidine hydrochloride
HEPES	(*N*-[2-hydroxyethyl) piperazine-*N'*-[ethanesulfonic acid])
IDR	intrinsically disordered region
K_p	molar partition coefficient
KP_i	a mixture of K_2HPO_4 and KH_2PO_4 to give the indicated pH of the phosphate buffer
LC	liquid chromatography
LUV	large unilamellar vesicle
lysoPC	lysophosphatidylcholine
MALDI	matrix-assisted laser desorption ionization
MLV	multi-lamellar vesicle
MS	mass spectrometry
MWCO	molecular weight cut-off
NaP_i	a mixture of Na_2HPO_4 and NaH_2PO_4 to give the indicated pH of the phosphate buffer
NE	nuclear envelope
Ni-NTA	nickel-nitrilotriacetic acid
NLS	nuclear localization signal
NMR	nuclear magnetic resonance

OA	oleic acid
OK	okadaic acid
PBS	phosphate buffered saline
PC	phosphatidylcholine
PCR	polymerase chain reaction
PE	phosphatidylethanolamine
PG	phosphatidylglycerol
PM	plasma membrane
PMSF	phenylmethylsulfonyl fluoride
PP_i	pyrophosphate
PPIα	protein phosphatase I, α subunit
SDS-PAGE	sodium dodecyl sulfate polyacryamide gel electrophoresis
S.E.M.	standard error of the mean
SLV	sucrose-loaded vesicle
SUV	small unilamellar vesicle
TEV	tobacco etch virus (protease)
Tris	tris (hydroxymethyl) methylamine
UTR	untranslated region

1: Introduction

1.1 Functional Non-Redundancy of Different Forms of Regulatory Enzymes

Most regulatory enzymes come in different forms that perform the same enzymatic reaction within the cell. This suggests a high degree of functional redundancy which may act as a safeguard ensuring the proper regulation of cellular metabolism and other functions. Alternatively, it may provide a means of strict and specialized regulation of vital events within the cell.

Variation in regulatory enzymes allows for alternative chemical modifications such as lipidation, acetylation, phosphorylation and glycosylation. Phospholipase D1 (PLD1), for instance, is present as two forms, PLD1a and PLD1b, as a result of alternative splicing. PLD1b is glycosylated which may target it to a membrane compartment (1), PLD1a on the other hand is palmitoylated and this is critical for its enzymatic activity (2). Sometimes the same chemical modification can have various effects among protein forms. The ten Protein Kinase C (PKC) forms all undergo a "priming phosphorylation" of a conserved threonine in the activation loop of the kinase domain. Most PKCs are then further phosphorylated on their carboxy-terminal V5 domain to maintain a catalytically-competent state. The requirement for and the effect of these secondary phopshorylations is variable among PKC forms. For example, PKCβII requires constitutive phosphorylation of V5 for catalysis but this is dispensable for PKCα (3).

Variation in protein forms also allows for interaction with many different binding partners or substrates leading to a multitude of downstream effects. For example, the function of dual-specificity MAPK phosphatase (DUSP) forms is dependent on the substrate that each of these phosphatases acts on (4). Although there is some overlap, each DUSP form interacts with a distinct subset. Inducible-nuclear DUSP-1, -2, -4 and -5 act on ERK, JNK and p38 MAPKs whereas DUSP-6, -7 and -9 are cytoplasmic and ERK specific. DUSP-8, -10 and -16 are both cytoplasmic and nuclear and inactivate p38 and JNK. Aside from protein binding partners, variation among protein forms allows for the interaction with different membranes as well. PLD1 appears to interact with sub-cellular membranes (endoplasmic reticulum (ER), Golgi, nuclear envelope (NE)) whereas PLD2 is localized mainly to the PM (plasma membrane; 5).

Multiple protein forms allow for the participation in different signaling pathways leading to various cellular responses. The phospholipase A_2 (PLA_2) family is classified into three groups based on their location and dependence on calcium and each group has been implicated in different cellular processes and signaling cascades (6). Cytosolic PLA_2 is calcium-dependent and may be associated with receptor-activated signaling owing to its translocation to the membrane. Calcium-independent $iPLA_2$ appears to be involved in phospholipid remodeling and homeostasis whereas the secretory PLA_2 produces pro-inflammatory lipid mediators.

Catalytic domains among enzyme families tend to be highly conserved but variation in their regulatory domains is yet another way in which isoforms can be specialized. The ten forms of PKC all have a highly conserved catalytic domain but the amino-terminal regulatory domains are variable and are the basis by which PKCs are

classified (3). While they all have a pseudo-substrate domain, they vary in their membrane binding domains. Conventional and novel PKCs both have a C1 domain that binds specifically to diacylglycerol (DAG) whereas the atypical PKCs have an unusual C1 domain that binds to phosphatidylinositol (3, 4, 5)-triphosphate or ceramide. There is also variation in PKC C2 domains. The C2 domain found in conventional PKCs binds to anionic membranes in a calcium-dependent manner. The C2 domain of novel PKCs is not dependent on calcium. Atypical PKCs lack a C2 domain and instead have a PB1 regulatory domain for protein-protein interactions. Differential tissue expression, sub-cellular localization and expression level combined with variation in post-translational modifications and regulatory domains provide a means of specializing enzyme forms for distinct functions, and are therefore not merely redundant.

1.2 Regulation of Protein Function by Intrinsically Disordered Regions

Although most of the protein forms mentioned above contain the same or very similar catalytic domains, they also contain various flanking and/or regulatory domains that distinguish their activation, function and location. Traditionally, function is associated with a distinct structure, but relatively recent studies have indicated that intrinsically disordered regions (IDRs) may also perform specific functions. IDRs can be defined as those which lack a rigid secondary and tertiary structure. Instead, they are either devoid of any structural propensity or fluctuate among a variety of conformations. Based on bioinformatic studies of eukaryotic genomes approximately 50% of proteins are predicted to contain long intrinsically disordered regions (7). The identification and characterization of these unstructured regions has garnered much attention in recent years

and consequently many reviews have been published in this area (7-11). It has become apparent that IDRs, despite a lack of structure *per se*, are important functional components of an ever-increasing group of proteins.

One of the best defined IDR-containing proteins is cAMP response element binding protein (CREB). This transcription factor participates in the regulation of a multitude of genes and can receive signals from many different upstream pathways including those involving protein kinase A, calcium-calmodulin kinases, MAP kinase and many more (12). After phosphorylation by one of these kinases, the kinase inducible domain (KID) of CREB binds to the KIX domain of the CREB binding protein (13). Unbound KID is disordered but forms two helices upon binding to KIX (14). Shoemaker, Portman and Wolynes (15) proposed a "fly-casting model" whereby IDRs may help a protein contact a binding partner by increasing the capture radius (Figure 1.1 A). Weak, long range initial contacts by an IDR would strengthen upon coupled folding and binding to its partner. Furthermore, coupled folding and binding would decrease the energy penalty associated with increased order. KID was found to form many weak intermediate interactions with KIX which are stabilized when KID is fully folded and bound to KIX, thereby confirming the fly-casting model for this interaction (16). In this way, an IDR can function as a regulator of protein-protein interactions.

Perhaps owing to their flexible nature (allowing access of modifying enzymes), IDRs also tend to be sites of phosphorylation (Figure 1.1 B; 17) which can also regulate binding events and interactions. Modulation of DNA binding by the Ets-1 transcription factor has been attributed to multiple phosphorylation sites within its labile autoinhibitory helix which serve to fine-tune its affinity for DNA (18). The degree of helicity increases

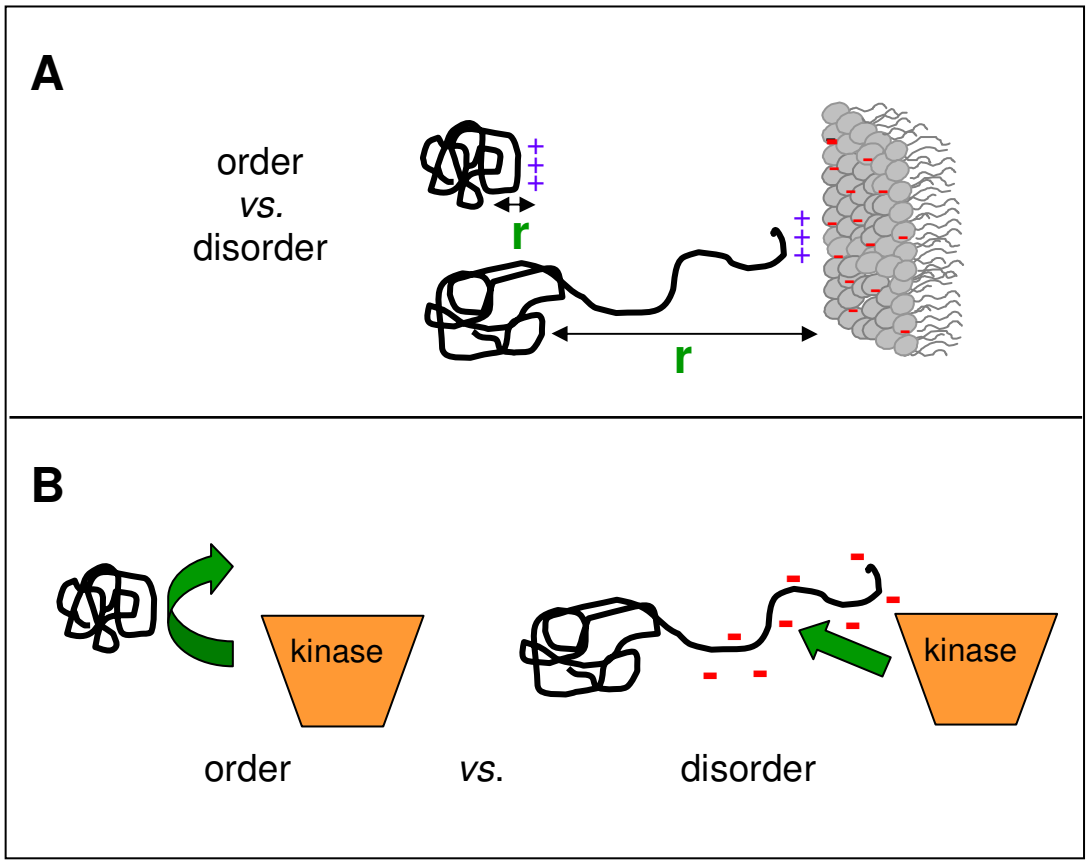

Figure 1.1 Functions of Intrinsically Disordered Regions

A. "Fly-cast model" of protein disorder. Long disordered regions housing binding motifs (in this case, a polybasic membrane binding motif) increase the capture radius (r) of the protein. The protein with disorder can sample a larger area when searching for potential binding partners. *B*. Disordered regions allow greater access of modifying enzymes such as kinases, glycosidases, *etc.* Folded proteins may limit access of modifying enzymes by steric hindrance.

with increased phosphorylation and DNA binding affinity is reduced. The phosphorylated and disordered cyclin-dependent kinase inhibitor Sic1 interacts with one site on Cdc4 via transient multivalent interactions with local order surrounding phosphorylation sites (19). The interaction of the disordered R region and nucleotide binding domain 1 (NBD1) of the cystic fibrosis transmembrane conductance regulator (CFTR) is also regulated by phosphorylation. There are areas of helical propensity within the unstructured R region and these helices are stabilized upon NBD1 binding (20). Phosphorylation of the R region was found to coincide with a decrease in helical content and NBD1 binding. Although the effects are variable, these examples describe how phosphorylation within regions of structural disorder can regulate molecular interactions.

The examples discussed highlight the functional importance of IDRs in transcription factors and protein inhibitors. The unstructured nature of IDRs perhaps make them ideal for protein-protein and protein-DNA interactions which can be easily identified in the types of aforementioned proteins. The many reviews published concerning the function of IDRs have, as of late, not addressed the function of IDRs in the regulation of metabolic enzymes. Perhaps as more IDR-containing proteins are identified, metabolic enzymes that are regulated by IDRs may come to the forefront.

1.3 Non-Redundant Isoforms in Lipid Metabolism - Function, Structure and Regulation of CTP: phosphocholine Cytidylyltransferase

Non-redundant protein forms are abundantly exemplified in many lipid metabolic enzymes (21), not just PLA_2 as mentioned above. Differential tissue expression and sub

cellular localization of enzyme forms involved in the production and catabolism of glycerolipid precursors, phospholipids, sterol and eicosanoids is thought to establish spatially distinct lipid pools for signaling and binding events (21). Phosphatidylcholine (PC) is the most abundant phospholipid component in most eukaryotic membranes and the rate of synthesis is regulated by CTP: phosphocholine cytidylyltransferase (CCT). CCT catalyzes the second rate-limiting step in the *de novo* synthesis of PC where the cytidine group from CTP is transferred onto phosphocholine to yield CDP-choline and inorganic pyrophosphate (Figure 1.2). CCT catalysis is discussed in greater detail in section 1.3.2.2. CCT has a mechanism to sense the phospholipid content of membranes, which is described in sections 1.3.2.3 and 1.3.4. Its activation is dependent on the PC content; therefore, CCT maintains phospholipid homeostasis (Figure 1.3; 22). There are two forms of mammalian CCT; the well-characterized and ubiquitous CCTα and the less abundant and much less investigated CCTβ. Since its discovery in 1998 (23), various studies have indicated that CCTβ performs distinct roles within cells and is not merely a "back-up" for the archetypal CCTα.

1.3.1 CCTβ is not a Redundant Isoform

In mammals there are two CCT genes encoding CCTα and CCTβ (23-25). The two genes give rise to four separate versions of CCT due to alternative splicing and initiation sites. They are often referred to as CCT isoforms in that they carry out identical reactions (and I will refer to them as such); but strictly speaking CCTα and β are paralogs, related by a gene duplication event followed by subsequent evolution that maintained a common function (CDP-choline synthesis), but allowed acquisition of new functions. The CCTα gene contains two transcription initiation sites in the untranslated

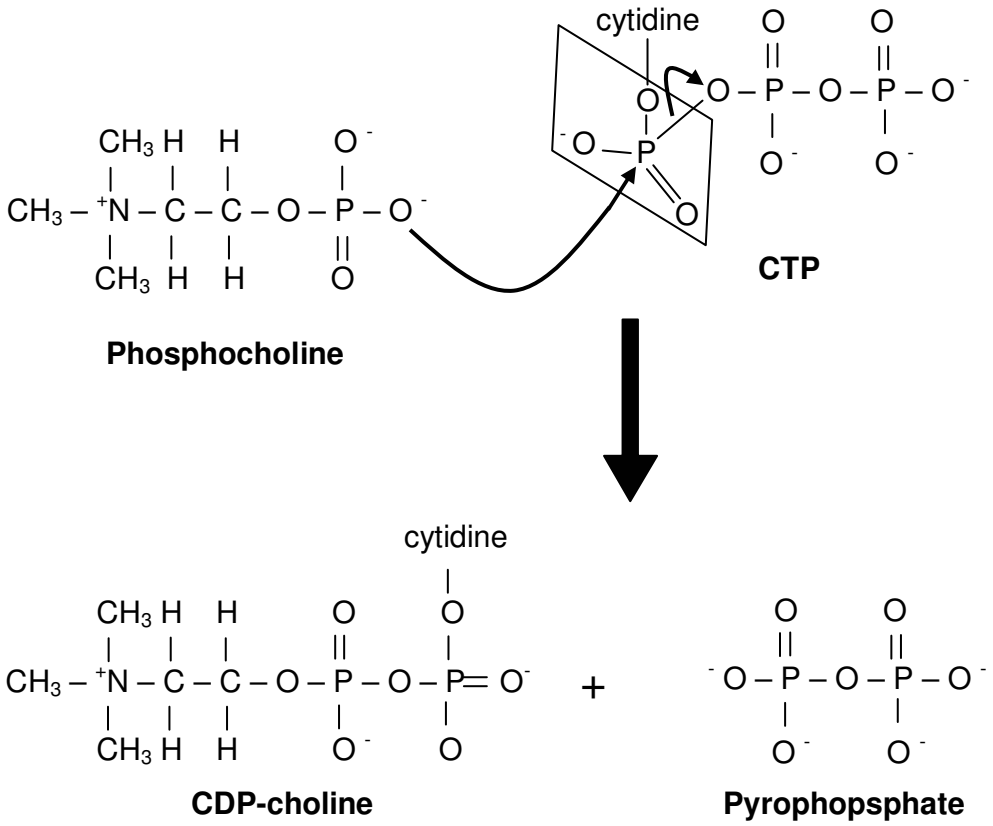

Figure 1.2 CCT Catalytic Reaction

Phosphocholine carries out a nucleophilic attack on the α-phosphate P-O bond thereby displacing pyrophosphate and producing CDP-choline.

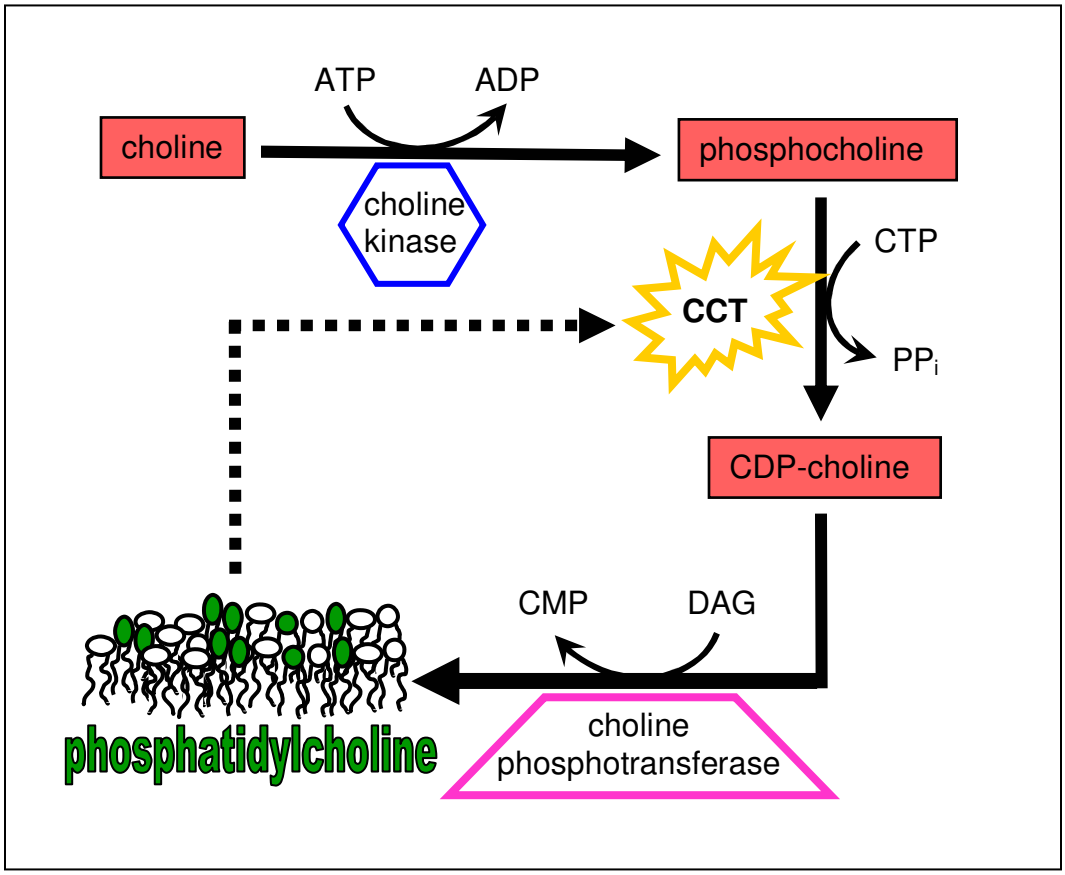

Figure 1.3 Role of CCT in Phospholipid Homeostasis

CCT catalyzes the second, rate-limiting step in the *de novo* synthesis of phosphatidylcholine (PC). The activity of CCT is itself regulated by the lipid content of the membrane. CCT senses the PC-requirement of the membrane and is activated when PC is low.

region which yield the same protein (25). There are three variations of CCTβ as a result of alternative splicing of the gene and an alternate start site (see section 1.3.2) (25). Northern analysis of murine and human tissue showed that while CCTα is expressed ubiquitously, CCTβ isoforms are expressed 10 times less than CCTα, with the exception of the adult brain, reproductive organs, and embryonic tissue (23, 25-27). CCTα is essential for cell proliferation and survival. Homozygous CCTα -/- mouse embryos fail to develop past the blastula stage (28), and a conditional mutation in the CCTα gene in CHO cells results in apoptosis at the non-permissive temperature (29). However, targeted disruption of the CCTα gene in mouse macrophages causes no deleterious phenotype as CCTβ_2 is up-regulated (30). This suggests that CCTβ_2 may perform a redundant role in cells by serving as a backup to CCTα.

A critical role for CCTβ in specific tissues is, however, indicated by its expression pattern. As mentioned, CCTβ is expressed in the adult brain and reproductive organs and the various isoforms of CCTβ are present at various stages in development (23, 25, 26). A critical role for CCTβ_2 is evidenced by reduced fertility and gonadal defects in mice as a consequence of disruption of CCTβ_2 (27). As well, CCTβ_2 is specifically up-regulated and activated in growing neuronal cells in culture in response to neuronal growth factor (31) and plays a critical role in neurite outgrowth and branching (32). These results, together with the differential tissue expression and sub-cellular localization of mammalian CCTβ isoforms (see section 1.3.2.1), suggest that they may perform vital functions in some tissues and cell types.

Mammals are not the only organisms that have different forms of CCT. Two forms of CCT, one cytosolic (CCT2) and one nuclear (CCT1), have been characterized in

Drosophila melanogaster (33, 34). Disruption of the CCT1 gene is lethal indicating that CCT2 cannot compensate (35). This suggests that CCT2 is not a redundant form and that CCT1 and CCT2 perform distinct functions. Distinct roles for CCT forms in *Arabidopsis thaliana* have been identified. The transcription and expression of AtCCT2 is up-regulated in response to cold treatment whereas AtCCT1 remains unchanged (36). Under normal circumstances AtCCT2 is able to compensate for the disruption of the AtCCT1 gene, and vice versa. The authors propose that AtCCT2 plays a unique and special role in the response of *A. thaliana* to cold.

1.3.2 Domain Organization of CCT

In this section I describe the domain organization, structure and functions focusing on mammalian CCTs, but CCTs from yeast to humans have similar domain organization. CCTα functions as a homodimer in both its soluble and membrane bound forms, as evidenced by chemical cross-linking experiments (37, 57). The quaternary structure of CCTβ has not been elucidated. All mammalian CCTs have a similar domain structure: the amino-terminal segment (segment N), the catalytic domain (domain C), the membrane-binding domain (domain M) and the carboxy-terminal phosphorylation segment (segment P). The domain/segment borders are approximate and are based on the exon boundaries for the CCTα gene (24). The first exon is untranslated, exons 2 and 3 (residues 1-39 and 40-72, respectively) comprise region N, exons 4-7 (residues 73-236) comprise domain C, exon 8 (residues 237-299) encodes domain M and exon 9 (residues 300-367) makes up region P. The approximate boundaries for each domain/segment of CCTα have also been confirmed via biochemical means (discussed in following sections). While the domain structure of CCTα has been well-studied, this area remains

relatively unexplored for CCTβ. Of the β isoforms, CCTβ_2 most closely resembles CCTα. CCTβ_1 is identical to CCTβ_2 except for a truncated carboxy-terminal segment, and CCTβ_3 is identical to CCTβ_2 except for a truncated amino-terminal region. Based on sequence similarity, I have divided the sequence of CCTβ_2 into putative domains. Domain C and domain M are well-conserved between CCTα and β_2 isoforms, both having 98% sequence similarity (Figures 1.4, 1.5, Table 1.1). In contrast, the amino acid sequence of N and P regions differ having only 54% and 75% sequence similarity, respectively. How these divergent portions affect the function of CCTα as compared to CCTβ_2 has not been determined.

1.3.2.1 Structure and Function of Region N

The amino-terminal region of CCT is the most poorly conserved among isoforms, having only 54% sequence similarity between CCTα and β_2 isoforms (Figures 1.4, 1.5, Table 1.1). The most distinguishing feature of the N region is the presence of a nuclear localization signal (NLS) sequence in CCTα. The sub-cellular localization of CCTα is still an area of much debate as CCTα is found in the nucleus in many (26, 40, 41), but not all cells (42-45). CCTβ_2, on the other hand, lacks the polybasic NLS sequence in its N region and is expressed in the cytoplasm (23). The 21-residue CCTα sequence ^{8}KVNSRKRRKEVPGPNGATEED^{28} is necessary and sufficient to localize a β-galactosidase fusion protein to the nucleus in CHO cells (46). Deletion of the classic polybasic NLS sequence (^{12}RKRRK^{16}) found within the larger 21-residue sequence resulted in disruption of the exclusively nuclear localization of CCTα (46). More recently Chen and Mallampalli (47) found that the monoubiquitination of the N region of CCTα can impede nuclear import by masking the NLS. Although the α-importin that

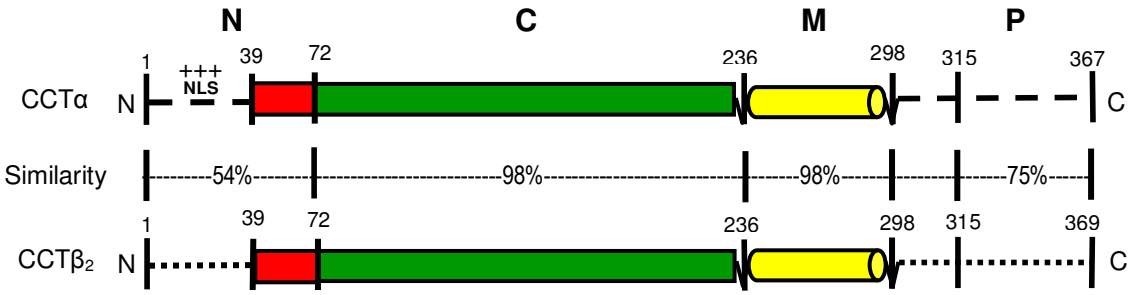

Figure 1.4 Domain Organization and Sequence Conservation of CCTs

Rat CCTα and β_2 sequences were aligned using ClustalW, and the % similarity was calculated (see Table 1.1). Domain and region boundaries are approximate. Structured regions shown as rectangles, lipid-inducible helical domains as cylinder, and disordered regions as dashed lines

Figure 1.5 Sequence Alignment of CCT Isoforms

Rat CCTα and CCTβ$_2$ sequences (NCBI accession number NP_511177.2 and NP_775174.1, respectively) were compared by ClustalW. This program designates G P S N D Q E R and K as hydrophilic residues. (*) identical, (:) conserved; (.) semi-conserved. Elements involved in catalysis are indicated by grey boxes. The polybasic NLS in CCTα is boxed. The tandem 11-mer repeats within the amphipathic helical domain M are underlined.

Domain/Region	Residues	% Identity	% Similarity
Amino-Terminal	1 - 72	22	54
Catalytic	73 - 236	90	98
Membrane Binding	237 - 298	76	98
Phosphorylation	315 - 369	45	75

Table 1.1 Sequence Comparison of CCTα and CCTβ_2

The % identity and % similarity of CCT isoform domains and regions depicted in Figure 1.4 were determined. 'Similar' residues included conservative and semi-conservative amino acid substitutions. Region N residues 40-72 determined to be part of the catalytic fold (48) were found to be only 39% identical and 67% similar between CCT isoforms. CCTβ_2 residue numbering system was used for comparison of region P as this isoform is longer than CCTα.

binds to the NLS of mammalian CCTα and transports it to the nucleus has not been identified, Kap60 has been shown to interact directly with the yeast CCT homolog (49). The function of CCTα within the nucleus remains unknown and is especially curious given that the other enzymes involved in the synthesis of PC (choline kinase and choline phosphotransferase) are located in the cytosol and ER, respectively (50, 51). It has been proposed, however, that CCTα may play a role in shaping the architecture of the nuclear membrane. CCTα has been found to localize to and be responsible for the formation of nuclear tubules (52, 53). These tubules are hypothesized to increase the surface area of the nuclear membrane exposed to the cytosol to enable signaling and/or nucleo-cytoplasmic traffic (54, 55). Alternatively, a recent publication showed that CCTα localizes to "nuclear speckles" in cells under osmotic stress, and that this may be a means of storage and regulating CCTα activity (56).

Apart from its targeting function, region N of CCTα participates in forming the dimer interface. While this was first evidenced via chemical cross-linking studies (57), the recently published crystal structure of the first 236 amino acids of CCTα ($CCT\alpha_{236}$) showed that residues 40-72 of the "amino-terminal region" are, in fact, part of the catalytic domain fold and residues 41-44 form part of dimer interface (48). It is interesting to note that residues 1-39 and 40-72 comprise two separate exons in the CCTα gene (24). The domain boundaries for domain C of CCTα could therefore be amended to reflect this finding (*i.e.*: region N: residues 1-39 and domain C: residues 40-236). The portion of the N region proximal to domain C is partially conserved (67% similar) between the CCTα and β_2 isoforms (Figure 1.4 and 1.5, Table 1.1) which suggests that residues 40-72 of $CCT\beta_2$ may also form part of the dimer interface. The amino-terminal

39 residues of CCTα_{236} were unresolved in the crystal. In both CCT isoforms this region is predicted to be disordered by multiple algorithms (Figure 1.6) and the CCTα N region is susceptible to proteolysis (39). These results suggest that residues 1-39 are flexible and comprise an intrinsically disordered region in CCT. The role of this region, and residues 40-72 (CCTα numbering), has not been investigated in depth in either isoform although studies involving chimeric CCTs indicate region N of CCTα (residues 1-72) support the notion of catalytic activity within domain C, whereas the corresponding sequence in CCTβ_1 appears to negatively influence CCT activity (23).

1.3.2.2 Structure and Function of Domain C

The catalytic domain of CCT was first defined based on sequence homology between rat CCT and yeast CCT (58). In the next few years the conservation of the catalytic core was confirmed with the sequencing of a bacterial CTP: glycerol-3-phosphate cytidylyltransferase (GCT; 59) and CCTs from *Arabidopsis thaliana* and *Caenorhabditis elegans* (60). Sequence comparison of various members of the cytidylyltransferase family reveals a highly conserved central core (CCTα residues 72-234) flanked by variable regions (Figure 1.4). This central core is also protease resistant and therefore was thought to be an ordered, folded domain (38). Mutational and biochemical analysis have revealed several conserved motifs which are crucial for catalysis. CCTα contains a highly conserved ^{89}HxGH^{92} motif that functions in binding CTP and possibly stabilizing the transition state (61, 62). Mutation resulting in glycine being changed to the more bulky serine resulted in a 25-fold increase in the K_m for CTP while the K_m for phosphocholine was unaffected (61). Mutation of His-89 did not affect CTP binding but decreased V_{max} by 100-fold (62). His-92 was proposed to interact with

Figure 1.6 Segments N and P of CCT Isoforms are Predicted to Form Regions of Intrinsic Disorder

Rat sequences of CCTα and CCTβ_2 (NCBI accession number NP_511177.2 and NP_775174.1, respectively) were submitted to the indicated disorder prediction servers: A. RONN (http://www.strubi.ox.ac.uk/RONN), *B*. DISOclust (http://www.reading.ac.uk/bioinf /DISOclust/DISOclust_form.html), *C*. PrDOS (http://prdos.hgc.jp/) and *D*. POODLE-I (http://mbs.cbrc.jp/poodle/poodle.html). The probability of disorder is plotted against residue number. These servers were selected based on their ability to correctly predict structural order within domain C for which there is biochemical and structural information available (48). Structural domains or portions thereof are shaded (based on 48, 63). Residues 40 - 72 of segment N (red), residues 73 - 220 of domain C (green), and residues 236 - 298 of domain M (yellow). Predicted unstructured segments are white.

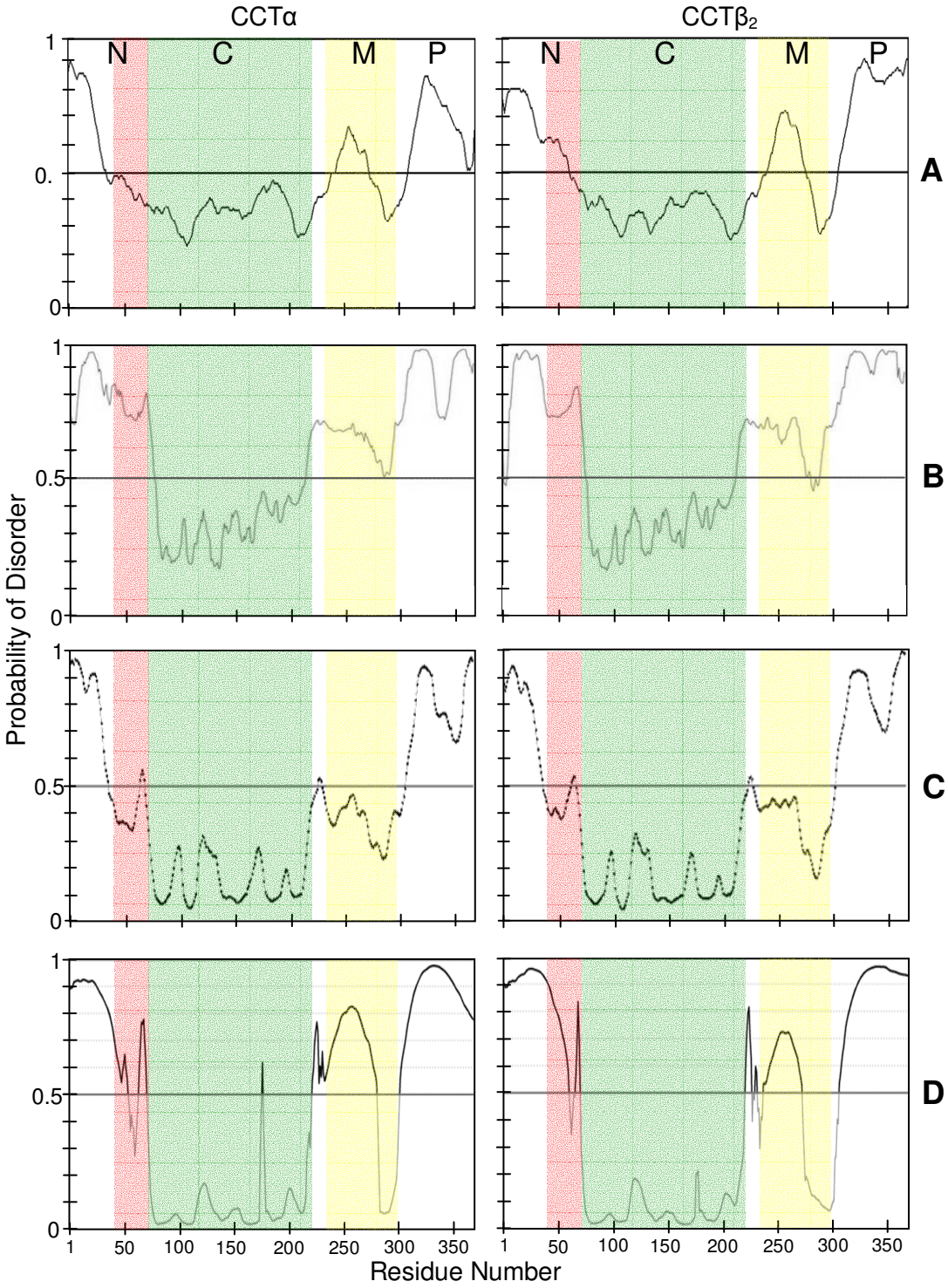
CCTα
CCTβ2
N
C
M
P
A
B
C
D
Probability of Disorder
Residue Number
1
0.5
0
50
100
150
200
250
300
350

phosphates of CTP via hydrogen bonding during catalysis (62). The ^{196}RTEGIST^{202} motif of CCTα is another conserved motif which has been shown to interact with CCT substrates. Mutation of arginine to lysine resulted in a 23-fold increase in affinity for CTP and a 5-fold increase for phosphocholine (64). This mutation (R196K) retains the charge of the side chain and is therefore a conservative substitution. Lysine 122 of CCTα is perhaps the most vital residue involved in catalysis as its mutation results in a 100, 000 -fold decrease in k_{cat}/K_m (64). While these studies have provided some insight into the catalytic mechanism of CCT the structural network responsible for catalysis was still unknown.

As mentioned, bacterial GCT has homology to the central catalytic core of CCT, but lacks the flanking regions. The crystal structure of dimeric GCT was solved in 1999 (65). GCT has an α/β nucleotide binding fold composed of a twisted 5-strand β-sheet surrounded by five α-helices. The conserved HxGH and RTEGIST motifs discussed above are localized to the 'bottom' of this fold and form a pocket for ligand binding, thereby confirming previous mutational and biochemical analysis. As GCT is not regulated and lacks domain M as well as N and P regions found in CCT, the structure offered little insight into the regulation of CCT catalysis. A breakthrough was made 10 years later by Lee *et al.* (48) when the first 236 residues of mammalian CCTα were crystallized in complex with CDP-choline and the structure was solved to 2.2 Å (Figure 1.7). CCTα is also composed of an α/β nucleotide binding fold but has six α-helices instead of the five in GCT. As well, a portion of the N region (residues 40-72) is actually part of the catalytic fold. There is no such sequence in GCT. The nature of the dimer interface was also revealed. The interface is mainly composed of four structural

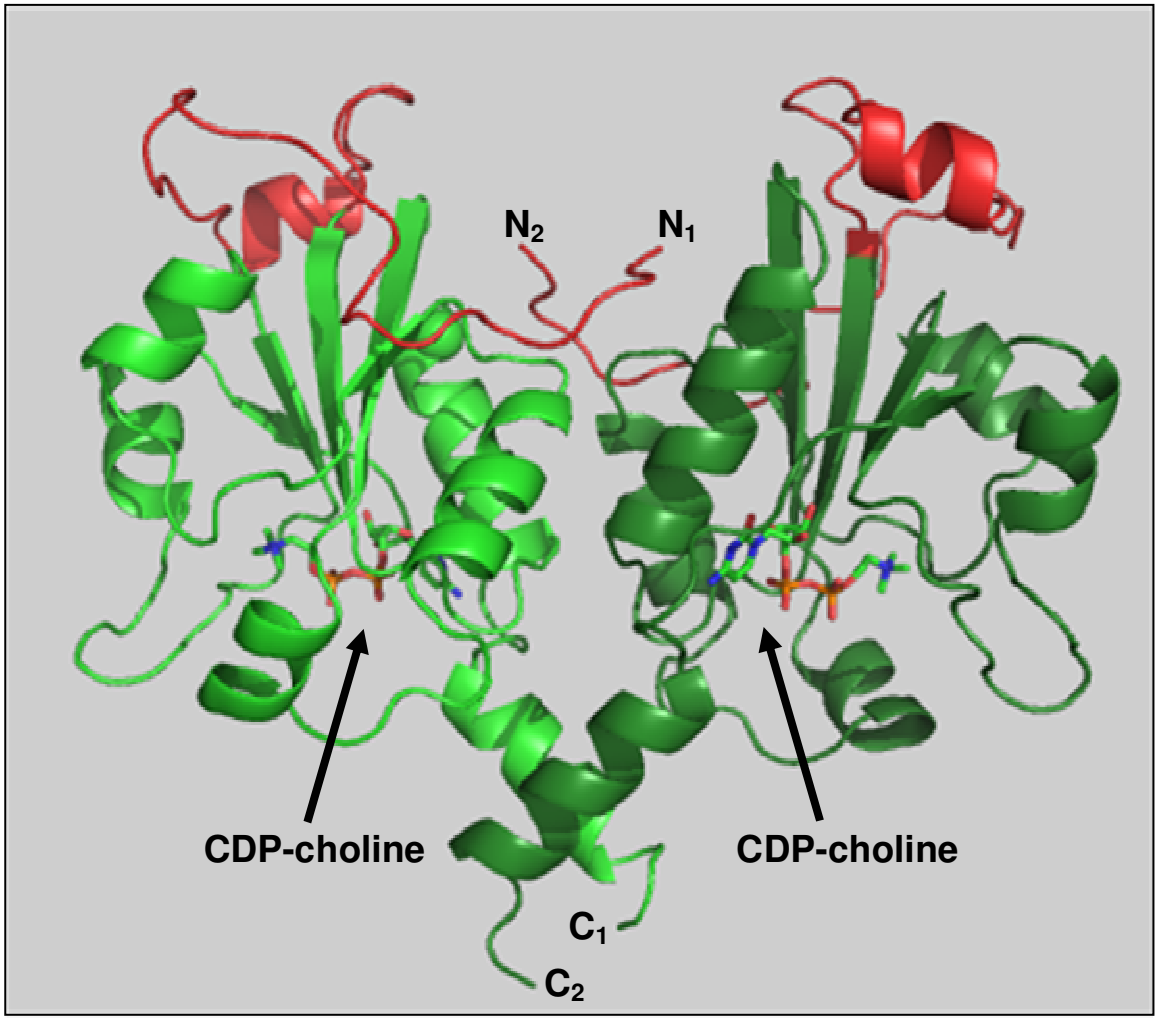

Figure 1.7 Structure of CCTα Residues 1 - 236

The crystal structure of the first 236 residues of CCTα complexed with CDP-choline was solved to 2.2 Å (PDB 3HL4; 48). The structure is dimeric and each CCT monomer is made up of an α/β fold. A 5-stranded β-sheet is flanked by 6 α-helices. Residues 1-39 and ~216-236 were not resolved in the structure. A portion of the amino-terminal region (residues 40-72) is part of the catalytic fold. Domain C (green), region N (red).

interactions including residues 41-44 of region N, and residues 87-105, 124-143 and 206-213 of domain C. Hydrophobic interactions and hydrogen bonding within these regions of CCTα are responsible for dimerization. This work was also accompanied by mutational and biochemical analysis which revealed His-168 and Tyr-173 as functionally important residues not conserved in GCT. Mutation of His-168 resulted in a decrease in V_{max} by 100-fold and its affinity for phosphocholine was specifically reduced suggesting this residue is involved in phosphocholine binding. Mutation of Tyr-173 reduced the V_{max} 20-fold but its affinity for phosphocholine was unaffected, suggesting that this residue interacts with CTP (48). To summarize, the structural and mutational analyses on GCT and CCT have revealed that catalysis occurs by surrounding the α-phosphate of CTP with complementary positive charge utilizing side chains from His, Lys, and Arg as well as some backbone nitrogen atoms. This reorients the α-phosphate for attack by phosphocholine and displacement of pyrophosphate to produce CDP-choline (Figure 1.2). The first 39 residues of region N, domain M and the P region were not included in this structure (due to lack of electron density in the N region and truncation of domain M and region P); therefore, the impact of these regions on domain C and potential inter-domain contacts remain unsolved.

CCTβ_2 contains all of the signature cytidylyltransferase motifs (*i.e.:* HxGH, RTEGIST) and has identical residues to CCTα Lys-122, His-168 and Tyr-173 (Figure 1.5). By no surprise, CCTβ_2 uses CTP and phosphocholine to produce CDP-choline (23, 26) but kinetic analysis of purified CCTβ_2 has not been undertaken. The consequences of subtle differences between C domains among CCT isoforms have yet to be determined. Furthermore, the amino-terminal cap region (residues 40-72), shown to be part of

catalytic fold of CCTα, is only 67% similar to that of CCTβ_2 (Figure 1.4, Table 1.1). The functional consequence of this variation has also not been investigated.

1.3.2.3 Structure and Function of Domain M

The membrane binding domain is a lipid-sensor and is autoinhibitory (66, 67), the details of which will be discussed later. Similar to domain C, domain M was first defined via proteolytic cleavage of CCTα. Limited chymotrypsin digestion of CCTα yields various fragments with cleavage processing from the carboxy-terminus (38, 39). Fragments corresponding to the catalytic domain plus domain M could bind to vesicles composed of activating lipids but further truncation resulted in a loss of this function (38). Domain M is not required for dimerization (38).

The sequence of domain M of CCT isoforms contains three 11-mer repeats (Figure 1.5) that show a high asymmetry of polarity when modeled as a helix (Figure 1.8 A). Two overlapping peptides corresponding to CCTα domain M (residues 236-288) revealed an α-helical structure in the presence of activating lipid vesicles and SDS micelles by circular dichroism (CD; 63, 68) and nuclear magnetic resonance (NMR; Figure 1.8 B; 63). The NMR structure and subsequent mutational and biochemical studies uncovered the mechanism of membrane binding and the basis for membrane selectivity of CCTα. The amphipathic helix is stabilized via hydrophobic interactions of the non-polar face with the lipid core (63, 69). The hydrophobic face of the amphipathic helix of CCTα intercalates into one leaflet of the bilayer (69, 70). Charged and polar residues are exposed to the aqueous environment. As will be discussed in Section 1.3.4, domain M shows high selectivity for anionic lipid surfaces. This is enabled by positively charged lysine residues that are localized to the interface thereby enabling them to

Figure 1.8 Domain M is an Amphipathic α-Helix

A. Amphipathic α-helical M domains of the two CCT isoforms (residues 242-293) are represented as 11/3 helical wheel diagrams (128). The hydrophobic (~120°) and hydrophilic (~240°) faces are delineated by dashed lines. *B.* The structure of domain M in the presence of SDS micelles as determined by NMR (PBD 1PEI; 63). The hydrophobic lipid environment is at the bottom and the aqueous phase is at the top. Interfacial glutamate residues are highlighted in green. Acidic residues (blue), basic residues (red), hydrophobic residues (yellow).

A

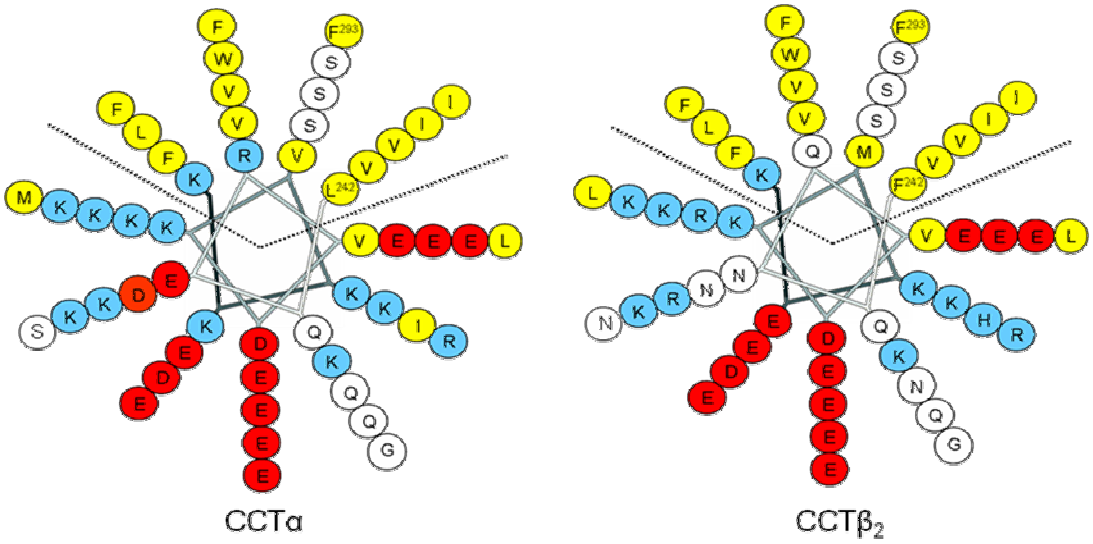

B

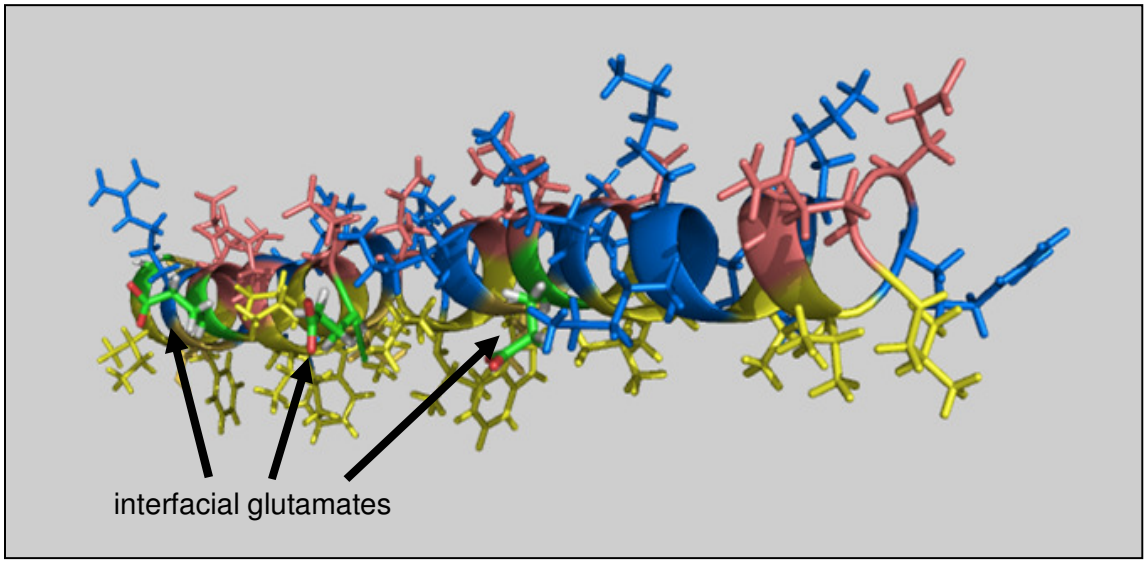

interact electrostatically with negative lipid head groups. Progressive deletion of these positively charged residues weakens the binding affinity of CCTα for anionic lipid vesicles (71). Three conserved serine residues localized to the hydrophobic face of the amphipathic helix contribute to reversible binding by decreasing the hydrophobic driving force (63, 72). There are also three conserved glutamate residues that are exposed to the interfacial region. Somewhat counter-intuitively, these acidic residues contribute to selectivity for anionic membranes. They are selectively protonated at an anionicmembrane surface, where the interfacial pH is lower. Mutation of these acidic residues to glutamine results in an increase in the membrane binding affinity of CCTα (71), indicating that the glutamates are important in generating weak, selective lipid interactions.

While reversible, the binding of domain M to anionic membranes has been shown to be strong enough to tether vesicles *in vitro*. The CCTα dimer with two M domains causes an increase in the apparent absorbance of anionic lipid vesicles at 400 nm resulting from increased turbidity of the sample (73) while a dimer lacking M domains cannot (74). Based on this information, it was postulated that the M domains are oriented on opposite sides of the CCTα dimer (Figure 1.9 A). This model was contradicted when it was found that only one M domain is required for tethering and activation of CCTα (Figure 1.9 B). A heterodimer composed of one wildtype CCTα monomer and a CCT mutant monomer lacking domain M and region P was able to tether anionic lipid vesicles just as well as the wildtype CCTα dimer (74). Binding of one M domain was also sufficient for full activation of the CCT heterodimer, suggesting that the two M domains of the CCT dimer bind to membranes in an alternating manner (74). It is, therefore,

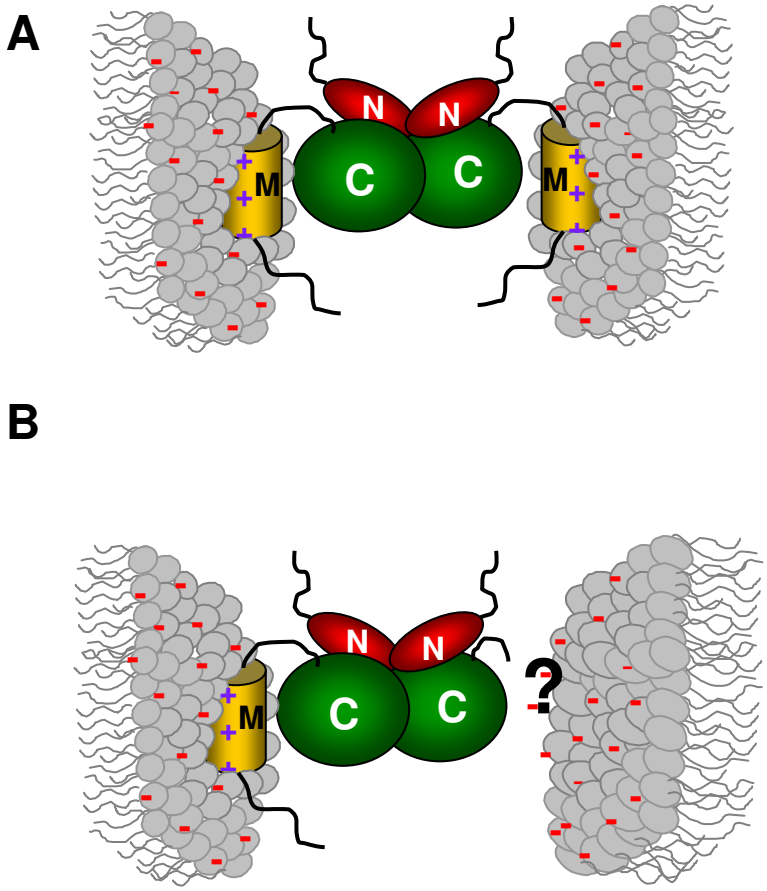

Figure 1.9 The CCTα Dimer can Tether Anionic Lipid Vesicles

A. The original model for vesicle tethering postulated that the two M domains of the CCTα dimer engaged two individual vesicles resulting in vesicles cross-bridged across the dimer interface (73). *B.* Modified model requiring an additional tether: Taneva *et al.* (74) found that a mutant CCTα dimer having only one M domain could tether anionic lipid vesicles. This finding would require a second membrane binding device. The identification of that secondary membrane binding motif was published in Taneva *et al.* (74) and portions of that work are discussed here.

necessary that CCTα house a second membrane binding domain to enable tethering of lipid vesicles. The identification of this binding motif and the tethering ability of CCTβ_2 is discussed in the results section of this work.

The structure of domain M when CCTα is soluble is unknown but CD data suggests a mix of conformers with low helical content (68). Domain M of both CCT isoforms is predicted to have both ordered and disordered sub-regions (Figure 1.6). Like CCTα, CCTβ_1 also showed lipid-dependent activation when activity was assayed in a lipid-depleted cell extract (23), but this area has not been fully investigated and not with CCTβ_2.

1.3.2.4 Structure and Function of Region P

The carboxy-terminal domain of CCT is the phosphorylation region. CCTα is reversibly phosphorylated in cells and phosphorylation attenuates activity (75-79). Region P, like the amino-terminal segment, is a predicted disordered region (Figure 1.6) and this prediction is supported by the extreme protease sensitivity of CCTα P region (38, 39). Protease susceptibility of region P is not dependent on its phosphorylation state, and region P is accessible to proteases when CCTα is soluble or membrane bound (39). The P segment, like domain M, is not necessary for dimerization (38). A possible role for region P as a second membrane binding motif was indicated as a CCTα mutant lacking residues 257-309 (part of domain M and P region intact) was found to be lipid responsive (80). This theory was contradicted, however, by the fact that the P region is equally susceptible to proteolysis when CCTα is membrane-bound (39).

CCTα is phosphorylated on its carboxy-terminus (81, 39) exclusively on 16 serine residues starting at Ser-315 and ending at Ser-362 (82). The average number of phosphate groups on CCTα was found to be 5-6 (39). Based on sequence, MacDonald and Kent postulated that CCTα may be a target for PKC, casein kinase II and glycogen synthase kinase-3 as well as proline-directed kinases (82). CCTα has been found to be phosphorylated by cAMP-dependent protein kinase (83), PKCα, PKCβII, cdc2, casein kinase II and glycogen synthase kinase-3 *in vitro* (81, 84). There is some debate as to whether CCTα is a substrate for MAPK/p44 as several groups have produced contradicting evidence (81, 84-86). In lung epithelial cells, where CCTα is cytosolic, an ERK docking site has been identified (residues 287-300 of domain M) and CCTα was phosphorylated on Ser-315 by p42/44 (86). CCTα has also been shown to be phosphorylated by JNK 1 and 2 in these same cells (87). No published work, however, has shown that phosphorylation *in vitro*, catalyzed by a particular kinase, results in high stoichiometry (*i.e.*: multiple phosphorylations by one kinase) and a significant change in activity, response to lipids, or any other function. Thus, the role of phosphorylation on the activity of CCT remains unclear.

CCTβ is a phosphoprotein and has a putative cdk-5 phosphorylation site in its carboxy-terminus (26). *In vitro* kinase studies showed that CCTβ_2 is not a substrate for Akt (also known as Protein Kinase B) but showed that cyclin-dependent kinase 5 may act on CCTβ_2 indirectly to potentially activate it in the axons of neuronal cells (32) but no other kinases were investigated. This notion of *activation* by phosphorylation has never been observed in CCTα. The phosphorylation state, location of phosphate groups and their effect on membrane binding and activation of CCTβ_2 have not been investigated.

As well, possible functions of region P not related to its phosphorylation have not been examined in either isoform.

1.3.3 Regulation of CCT by Autoinhibition

CCT is an amphitropic enzyme in that it alternates between a soluble/inactive and membrane-bound/active form (Figure 1.10; 22). Domain M is the negative regulator of CCTα activity when it is in soluble form (67). Membrane binding serves to alleviate that inhibition. Deletion of domain M and region P (residues 237-367), but not region P alone (residues 313-367), from CCTα resulted in an enzyme that was constitutively active (67, 78). Over-expression of this mutant ($CCT\alpha_{236}$) in cells resulted in increased synthesis of PC, as evidence by increased incorporation of ^{3}H-choline (78). The specific activity of$CCT\alpha_{236}$ was found to be 50-fold higher than that of wildtype CCTα in the *absence* of activating lipids (67). $CCT\alpha_{236}$ resembles the active conformation of CCTα as the pattern of proteolytic fragments for $CCT\alpha_{236}$ is very similar to CCTα when it is membrane bound (39). Interdomain contacts between domain M and another region(s) of CCT are proposed to be the source of autoinhibition. The location of these proposed interdomain inhibitory contacts was investigated via limited proteolysis of soluble CCTα compared to the membrane-bound form (39). The fragment pattern originating from proteolysis of domain C was the same in the presence or absence of lipids. Domain M was protected from proteolysis by the membrane, as expected, but in the soluble form it showed a mix of exposed (amino-terminal) and protected (carboxy-terminal) sub-domains. This suggests either an interdomain contact between the carboxy-terminal sub-domain ofdomain M and site 'X' of CCT or a folded domain M structure in this sub-domain. Surprisingly, the portion of segment N that forms part of the catalytic fold (48) was less

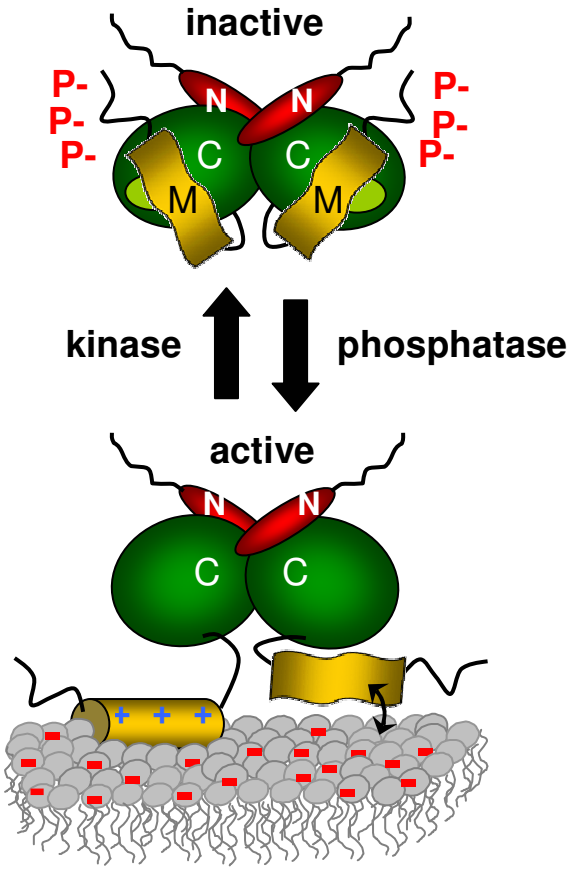

Figure 1.10 Regulation of CCT Activation – Autoinhibition, Activation by Membrane Lipid Content and Dephosphorylation

CCT is regulated by autoinhibition. Domain M silences the active site resulting in a low k_{cat} by an unknown mechanism. Binding of domain M to a membrane alleviates that inhibition. Domain M binding is dependent on the physical properties of the membrane, such as the density of anionic lipids, as shown here. Phosphorylation/dephosphorylation shifts the equilibrium between soluble and membrane-bound forms.

accessible to proteolysis in the presence of lipids, suggesting that this may be the site 'X' of inhibitory contact of domain M (39). Studies are underway to further investigate possible interdomain contacts responsible for the inhibition of CCTα. CCTβ_1 appears to also be regulated by autoinhibition as it is activated by lipid vesicles *in vitro* (23).

1.3.4 Regulation of CCT by Membrane Lipid Content

The membrane binding domain of CCTα serves as a lipid sensor. Its association with membranes is governed by electrostatic interactions, hydrophobic interactions and bilayer curvature, which are dependent on the lipid content of the membrane. In the ER and nuclear membranes (those membranes to which CCT isoforms bind) PC accounts for approximately 50% of the phospholipid species whereas phospholipids with negative head-groups account for 15-20% and phosphatidylethanolamine (PE) 20-30% (88). The proportion of anionic and non-bilayer forming lipids is higher in PC-deficient membranes, to which CCT binds. Examples of specific lipid activators and how CCT interacts with membranes enriched in these lipid activators is discussed below. The characteristics allowing domain M to selectively bind to such membranes is discussed along with its structure in section 1.3.2.3. The binding of domain M to PC-deficient membranes is thought to be a two-step process. Positive residues concentrated in the amino-terminal portion of domain M of CCT interact electrostatically with anionic membranes inducing some helical structure. As the helix is formed the non-polar face is better-defined and then intercalates into the hydrophobic core of the bilayer. This model (Figure 1.10) is based on the results of multiple studies investigating membrane binding both *in vitro* and *in vivo* through various means (discussed below).

In vivo studies revealed that CCTα translocates to and is activated by cell membranes enriched with the anionic lipid oleic acid (OA; 77, 79) indicating specificity for negative membranes. The selectivity of CCTα domain M for anionic lipids has been characterized *in vitro* by measuring the binding and activation of purified CCT by lipid vesicles of various sizes and lipid composition. The activation of CCTα by lipid vesicles increases with increasing mol% anionic lipid and by vesicles composed of more negatively charged head-groups such as phosphatidylinositols, cardolipin and phosphatidic acid (Table 1.2; 89). CCTα therefore binds to membranes based on the overall charge and does not have binding sites for specific lipid monomers. Activation by these same lipids is dependent on the ionic strength of the environment which suggests an electrostatic interaction (89). The association and activation of CCTα by anionic lipid vesicles is sigmoidal suggesting that a threshold of surface charge must be reached for CCTα to bind (89, 90). Similar results were obtained using anionic lipid vesicles and a peptide derived from domain M of CCTα (72). The binding and activation of CCTα by anionic lipid vesicles was enhanced by the addition of DAG (89, 90). The response was more than additive suggesting that the interaction of CCTα with the membrane is not solely electrostatic but involves the synergy of electrostatic and hydrophobic interactions with the membrane bilayer.

CCTα binds to and is activated by lipids that promote stored negative curvature strain (Table 1.2). Lipids with small head-groups and unsaturated acyl chains (Type II lipids) cause deformations in the bilayer as a result of decreased packing of the head-groups and CCTα membrane binding relieves this strain. *In vivo*, choline starvation (which increases the PE/PC ratio) and phospholipase treatment of cells (which

Lipid Activator	Examples	Charge	Curvature Strain
Anionic	PS, PG, PA, OA*, CL, PI, PIP	negative	positive
Type II	DAG, oleyl alcohol, unsaturated PE	neutral	negative

Table 1.2 Types of CCT Lipid Activators

CCT binds to and is activated by membranes enriched with two types of lipid activators: anionic (72, 77, 79, 89, 90) and Type II (52, 91, 92, 93). Examples of anionic lipid activators are phosphatidylserine (PS), phosphatidylglycerol (PG), phosphatidic acid (PA), oleic acid (OA), cardiolipin (CL) and phosphatidylinositol (PI) and phosphatidylinositol monophosphate (PIP). These lipids have an overall negative charge and tend to induce positive curvature strain. Examples of Type II lipid activators include diacylglycerol (DAG), oleyl alcohol and unsaturated phosphatidylethanolamine (PE). These activators have a neutral charge and tend to induce negative curvature strain. See section 1.3.4 for detail and discussion of the mechanism of CCT binding.

generates DAG) caused CCTα to translocate to the membrane and this was reversed by the addition of lysophosphatidylcholine (lysoPC), which promotes positive curvature (91). More direct proof of the affinity of CCTα for non-bilayer forming lipids was provided by *in vitro* vesicle binding and activation studies. CCTα binds to large unilamellar vesicles (LUVs) composed of unsaturated PE and PC and this association is correlated with the calculated curvature strain of these vesicles (92). Again, as observed by Jamil *et al.* (91), lysoPC reversed this effect as CCTα was less active in the presence of PE/PC/lysoPC vesicles (92). DAG has also been shown to promote CCTα binding in the same manner as unsaturated PE. Attard *et al.* (93) measured the activation of CCTα by LUVs containing DAG and unsaturated PE. Based on the calculation of torque tension introduced by these lipids, they postulated that intercalation of the amphipathic helical M domain into the monolayer releases the stored curvature-induced elastic stress and that this is the driving force for CCT binding to Type II lipids.

While extensive work has been published on the activation of CCT by various lipid activators, there is little known about the changes in cell membrane lipid content in response to physiological stimuli that induce CCT membrane binding and activation. During the G_o to G_1 transition, PC synthesis increases as a result of CCTα activity (94). Cell studies suggest that DAG may be the lipid signal inducing CCT activation resulting in increased PC synthesis (95-97). The mechanism by which DAG stimulates CCT remains unknown but evidence suggests that it may require the action of PKC and ERK1/2 (96, 97).

CCTβ_1 is activated by anionic lipid vesicles composed of PC/OA (23) suggesting that it, too, is specifically activated by anionic membranes. The binding and activation of

CCTβ isoforms by negative curvature inducing lipids has not been investigated. Using a scale for interfacial residues (98) the hydrophobic face of domain M of CCTβ_2 appears to be slightly more hydrophobic than that of CCTα (Figure 1.8, Table 1.3). It is possible that CCTβ_2 binding and activation may be more responsive to non-bilayer forming lipids than CCTα.

1.3.5 Regulation of CCT by Reversible Phosphorylation

CCTα activation is regulated by reversible phosphorylation of serine residues in segment P, which attenuates membrane binding and activity (77-79, 90). In this case,phosphorylation is not an "on/off switch" but a means of fine tuning the membrane binding and subsequent activation of CCTα. The mechanism by which phosphorylation attenuates membrane binding and activation of CCTα is unknown but two models have been proposed. The negative charge carried by phosphates may electrostatically repel neighboring domain M from anionic membranes (Figure 1.10). Alternatively, the negatively charged phosphates may neutralize positive residues in domain M responsible for the initial electrostatic interaction with negative membranes.

In vitro studies show that phosphorylation of CCTα is correlated with a weaker membrane binding affinity and activation. Incubation of CCTα supernatant with microsomes and cAMP dependent protein kinase resulted in an increase in phosphorylated CCTα and a 2.5-fold decrease in the activity of the microsomal fraction (83). Phosphorylation of CCTα and the decrease in activity could, however, be reversed by treatment with alkaline phosphatase (83). Homogenates from CCTα-transfected cells treated with a proline-directed kinase inhibitor were found to have higher activity than untreated cell homogenates (84). Studies performed using purified CCTα show more

CCT Isoform (residues 242-293)	**Peak Hydrophobic Moment** $<\mu_H>_{max}$ [a]	**Hydrophobicity of Polar Face** (kcal/mol)[b]	**Hydrophobicity of Non-Polar Face** (kcal/mol)[b]
CCTα	0.69	-35.45	5.57
CCTβ_2	0.58	-33.99	6.67

Table 1.3 Comparison of Domain M Characteristics Between CCT Isoforms

Residues included in calculating hydrophobicity of the polar and non-polar face of the amphipathic domain M can be found in Figure 1.7. [a] Based on Eisenberg *et al.* (99) using EMBOSS (http://bioweb.pasteur.fr/docs/EMBOSS/hmoment.html). [b] Sum of hydrophobicities based on Wimley and White (98) scale for interfacial residues.

directly the full impact of phosphorylation on CCTα membrane binding and activity. CCTα phosphorylation by JNK1 and JNK2 resulted in a 40% decrease in the specific activity although the stoichiometry of CCTα phosphorylation by JNK1 and 2 was not investigated (87). Arnold *et al.* (90) showed more explicitly that phosphorylation increases the anionic lipid requirement of CCTα for membrane binding and subsequent activation. *In vitro* dephosphorylated CCTα required a lower mol% anionic lipid for activation and co-sedimented with sucrose-loaded vesicles at a lower mol% anionic lipid as well (90).

A correlation between phosphorylation status of CCTα and *in vivo* subcellular localization was described by Watkins and Kent (76). CHO cells were treated with phospholipase C (PLC) and then fractionated. CCTα from the soluble fraction of control cells was slower migrating on SDS-PAGE and incorporated ^{32}P whereas CCTα from PLC-treated cells was found largely in the particulate fraction, migrated faster and did not incorporate the label. Treatment of CHO cells with okadaic acid (OK; a phosphatase inhibitor) greatly decreased PLC-induced activation of CCTα (76). Hatch *et al.* (100) showed that OK treatment decreased PC synthesis in hepatocytes and this coincided with increased phosphorylation of CCTα. These data suggest that CCTα is phosphorylated in the soluble form but dephosphorylated when membrane bound. A modulating role for phosphorylation of CCTα *in vivo* was further defined by Wang *et al.* (77). The authors investigated the kinetics of phosphorylation and membrane translocation of CCTα in cells treated with OA. Translocation from the soluble to particulate fraction occurred within 15 minutes of treatment, as did dephosphorylation of CCTα. Removal of OA from the cell media caused a reversal of this translocation within a minute, but it was found that

CCTα did not need be phosphorylated in order to dissociate from the membrane. Similar results were produced using OA enriched hepatocytes and digitonin release. CCTα was found to associate with these membranes in an active but phosphorylated form and dephosphorylation occurred subsequent to membrane binding (79). Mutational studies have also yielded similar results. A CCTα mutant lacking all phosphorylated serines in domain P (CCTα 16Ser→Ala) was found to partition into cell membranes but half of CCTα 16Ser→Ala remained in the soluble fraction (78). Furthermore, a phospho-mimic of CCTα where all serines were mutated to glutamate still partitioned into OA enriched cell membranes (78). These data show that in cells the membrane partitioning of CCTα is influenced negatively by phosphorylation but strong signals from lipid activators within the membrane can overcome the effects of phosphorylation.

Although the research indicating that there is an inverse relationship between CCT phosphorylation in region P and the association with membranes is fairly compelling, the identity of specific kinases and phosphatases that directly regulate CCT's membrane association in cells, and the sites of the key regulatory phosphoserines remains a mystery. Likewise, the effect of phosphorylation on the membrane binding and activation of purified CCTβ isoforms has not been investigated.

1.3.6 Transcriptional Regulation of CCT

CCT isoforms are expressed to differing degrees in various tissues as determined by the distribution of mRNAs (23, 25-27). This suggests that they may be regulated at the transcriptional level by distinct means. CCTα is ubiquitously expressed and is essential in development (28). It is therefore not surprising that its promoter region is similar to those of other house-keeping genes. The 5' untranslated region (UTR) does

not contain a TATA or CAAT box but has GC-rich regions (24). It also has many potential binding sites for transcription factors and regulators. These sites include those for Sp1, AP1, AP2, AP3, Y1, TFIIIA and numerous others. Sp1 binds to the promoter region of CCTα and is responsible for the increase in CCTα mRNA before mitosis (101, 102). The Sp1 binding element at -67/-62 is essential for this response while the site at -31/-9 serves to further enhance transcription (102). Sp1 links the transcription of CCTα to the cell cycle as phosphorylation of Sp1 by cyclin dependent kinase 2 enables Sp1 to bind to the promoter of CCTα (103). Association of cyclin A and cyclin E also serves to increase Sp1 binding (103). Sp3 has also been shown to regulate the transcription of CCTα (and CCTβ) and its expression in a Ras/p42/44^{MAPK} dependent pathway (104). Roles for Sp2 (105), EF-4 (106) and cholesterol/sterol response element-binding proteins (107) in the transcriptional control of CCTα have also been discovered.

The murine promoter regions of CCTβ isoforms 2 and 3 have recently been defined (mice lack the CCTβ$_1$ isoform). Unlike CCTα, the 5'UTR of CCTβ$_{2/3}$ has a TATA-like box upstream of the transcriptional start site (108). The promoter region of CCTβ$_{2/3}$ has potential binding sites for many transcription factors and regulators including SRY, GATA 1/2, AP1, Sox-5, C/EBP a/b, Chop-C, *etc*. and many are active only in specific tissues. The regulation of CCTβ transcription appears to be more complex and tissue specific as evidenced by the developmental dependence of the transcription of CCTβ$_2$ versus CCTβ$_3$ in mice (25) and the tissue-specific expression of CCTβ versus CCTα (23, 25-27).

1.3.7 Possible Regulation of CCT by Intrinsically Disordered Regions

The regulation of protein function by intrinsically disordered regions is a relatively new and expanding field of research. The functions of the disordered N and P regions in CCT are, as yet, not well-defined. The availability of a distinct CCT (CCTβ_2) with divergent N and P segments, but highly similar domains C and M offered the opportunity to further probe the contributions of the divergent and disordered regions to the regulation and membrane binding mechanism of CCT by comparative analysis. I hypothesize that CCT isoforms have evolved similar but distinct modes of regulation to allow for varied control of PC synthesis in different sub-cellular localizations and cell types.

2: *In Vitro* Analysis of the Role of the Intrinsically Disordered Regions of CCT in Membrane Binding

2.1 Introduction

The structure, function and regulation of CCTα has been studied in detail for several decades. CCTβ, on the other hand, was only first identified in 1998 (23) and the amount of experimental data pertaining to this isoform is limited. According to published research, CCTβ has never been purified, its specific activity is unknown, and its membrane binding and activation by different lipids has not been characterized. The secondary, tertiary and quaternary structure of CCTβ has never been determined experimentally. CCTβ functions as a cytidylyltransferase as it catalyzes the synthesis of CDP-choline from CTP and phosphocholine (23) and restores PC synthesis in CHO cells devoid of CCTα (26). CCTβ activity is low in the absence of lipid but increases with the addition of anionic lipid vesicles suggesting that it too is regulated by autoinhibition and binds to membranes electrostatically. Incorporation of ^{32}P into $CCT\beta_1$ suggested that like CCTα, $CCT\beta_1$ is a phosphoprotein but the location and consequence of phosphorylation is unknown in this isoform (23). Region N of $CCT\beta_1$ appears to be inhibitory to catalysis since its activity was increased when residues 1-83 were exchanged for those of CCTα or when residues 1-26 of $CCT\beta_1$ were deleted (23). The basis of the negative effect of region N on CCTβ activity is unknown. Here, I characterize the activity, membrane binding, quaternary structure and phosphorylation of purified $CCT\beta_2$. With that established, I then sought to determine, through comparative and mutational analysis, the

contributions of the intrinsically disordered N and P regions to the membrane binding and activation of CCT *in vitro*.

2.2 Experimental Procedures

2.2.1 Materials

All restriction enzymes were from Invitrogen or Fermentas except for *Bst*BI which was from New England Biolabs. The dNTPs, *Pfu* turbo and all primers were from Invitrogen. Rapid ligation and plasmid preparation kits were from Fermentas. Cell culture supplies were from Gibco-Invitrogen and BD Falconware. Lipids were purchased from Northern Lipids (egg PG; Vancouver, BC, CAN) and Avanti (egg PC; Alabaster, AL, USA). Protein Phosphatase I catalytic subunit (PPIα) used in the *in vitro* dephosphorylation of proteins was from Sigma. BS^3 (bis (sulfosuccinimidyl) suberate) was from Pierce. His-tagged TEV (tobacco etch virus) protease was from Invitrogen. Ni-NTA agarose used in affinity purification of His-tagged proteins was from Qiagen. ^{3}H-DPPC was from Perkin Elmer NEN and ^{14}C-phosphocholine was purchased from Amersham Biosciences. SYPRO Orange was purchased from Sigma. pAX-His-Xa-CCTα was constructed as described by Xie *et al.* (57) and generously provided by Jillian Smith.

2.2.2 Construction of His-tagged CCTs

pAX-His-Xa-CCTα. His-CCTα in the pAX142 mammalian expression vector (109), and in pBSKS(-), was constructed as described by Xie *et al.* (57).

pAX-His-Xa-CCTβ$_2$. The His-tag was added to CCTβ$_2$ by polymerase chain reaction (PCR). The reaction set-up and thermocycler settings can be found in Appendix 1. pCR 2.1 TOPO housing CCTβ$_2$ cDNA (gift from Dennis Vance and Jodi Carter,

University of Alberta) was used as the template for addition of a His-tag. Primers were designed flanking the coding region of CCTβ$_2$ to insert a *Bgl*II site before the start codon, add an extra base to maintain frame after sub-cloning, and a Sal I site after the stop codon. The primer sequences can be found in Appendix 2. The PCR product was sequenced and the *Bgl*II/*Sal*I fragment of the PCR product (CCTβ$_2$ coding sequence) was ligated with the *Bgl*II/*Sal*I fragment of pBSKS(-) His-Xa-CCTα (vector fragment lacking the CCTα sequence) to yield pBSKS(-) His-Xa-CCTβ$_2$. His-Xa-CCTβ$_2$ was then sub-cloned into the pAX142 mammalian expression vector via *Mlu*I and *Sal*I sites.

pAX-His-Xa-CCTβ$_2$ C34S. His-Xa-CCTβ$_2$ C34S was constructed using site-directed mutagenesis (Stratagene). The reaction set-up and thermocycler settings can be found in Appendix 1. Using pBSKS(-) His-Xa-CCTβ$_2$ as a template, complementary primers (Appendix 2) were designed to change codon 34 from TGC to TCC, changing the amino acid from cysteine to serine. A unique *Avr*II site was also engineered by changing codon 38 from CGA to AGG. This was a silent mutation and the new restriction site, as well as sequencing, was used to confirm mutagenesis. pAXHis-Xa-CCTβ$_2$ C34S was constructed by ligating the *Mlu*I/*Ssp*I fragment from pBSKS(-) His-Xa-CCTβ$_2$ C34S (first 83 codons of CCTβ$_2$ C34S with 5' extension housing the His-tag) with the *Mlu*I/*Ssp*I fragment of pAXHis-Xa-CCTβ$_2$ (CCTβ$_2$ sequence lacking first 83 condons housed in the pAX vector).

pAX-His-Xa-CCTα-βN and pAX-His-CCTβ-αN. To construct chimeric CCTs pAXHis-Xa-CCTα and pAXHis-Xa-CCTβ$_2$ were digested with *Mlu*I and *Ssp*I. The insert fragment from pAXHis-Xa-CCTβ$_2$ (first 83 codons of CCTβ$_2$ and the His-tag extension) was ligated to the vector fragment from pAXHis-Xa-CCTα (CCTα missing the first 83

codons and the His-tag extension in pAX) to yield pAXHis-Xa-CCTα-βN. Likewise, the insert fragment from pAXHis-Xa-CCTα (first 83 codons of CCTα with His-tag) was ligated to the vector fragment from pAXHis-Xa-CCTβ$_2$ (CCTβ$_2$ missing the first 83 codons in pAX) to yield pAXHis-Xa-CCTβ-αN.

All His-tagged constructs have a Factor Xa site between the poly-histidine sequence and the CCT start codon. Factor Xa cleaves in the CCTα sequence (74); therefore, the His-tags were not removed after the resultant proteins were purified.

2.2.3 Construction of CCTs with Cleavable His-tag

pAX-His-TEV-CCTβ$_2$. The Factor Xa site was replaced with a tobacco etch virus (TEV) protease site via site-directed mutagenesis initially using pBSKS(-) His-CCTβ$_2$ as a template. The reaction set-up and thermocycler settings can be found in Appendix 1. Complementary primers were designed to insert 15 basepairs to complete the TEV recognition site, delete 9 basepairs of spacer sequence and engineer a new *Nde*I site for confirmation of mutagenesis. The mutation to form the *Nde*I site was silent. The primer sequences can be found in Appendix 2. Mutagenesis was confirmed via *Nde*I digest and sequencing. His-TEV-CCTβ$_2$ was sub-cloned into the pAX mammalian expression vector via *Mlu*I/*Ssp*I digest of pBSKS(-) His-TEV-CCTβ$_2$ and pAXHis-Xa-CCTβ$_2$ (exchanging codons 1-83 of CCTβ$_2$ and the His-Xa tag with codons 1-83 of CCTβ$_2$ and the His-TEV tag).

pAX-His-TEV-CCTα. pAX-His-TEV-CCTα was constructed by swapping the coding region of CCTβ$_2$ in pBSKS(-) His-TEV-CCTβ$_2$ with that of CCTα in pAXHis-Xa-CCTα by *Bgl*II/*Sal*I digest. His-TEV-CCTα was sub-cloned into pAX by digesting

pBSKS(-) His-TEV-CCTα and pAXHis-Xa-CCTα with *Mlu*I/*Eco*RV. The insert fragment consisting of His-TEV-CCTα (condons 1-170) was ligated to the vector fragment of CCTα (codons 171-367) in pAX to yield pAXHis-TEV-CCTα.

pAX-His-TEV-CCTαΔNLS. pAX-His-Xa-CCTαΔNLS was constructed as described by Taneva *et al.* (74). Briefly, codons 12-16 of CCTα were deleted by site-directed mutagenesis (reaction set-up and thermocycler settings Appendix 1) using a pair of complementary primers (Appendix 2) and pBSKS(-) His-Xa-CCTα_{236} as the template. The resultant amino acid sequence of the amino-terminal portion of CCTαΔNLS is: GRSM[1]DAQSSAKVNS*EVPG, where '*' is the deleted RKRRK sequence. The GRS sequence from a portion of the TEV recognition site remained intact after cleavage of the tag. The mutation was confirmed by sequencing. The *Mlu*I/*Ssp*I fragment of pBSKS(-) His-Xa-CCTα ΔNLS (codons 1-78 with the His-tag and Xa site) was ligated with the *Mlu*I/*Ssp*I fragment of pAX-His-Xa-CCTα (pAX vector housing codons 83-367 of CCTα) to yield pAX-His-Xa-CCTαΔNLS. The Factor Xa site was replaced with the TEV recognition by digesting pAX-His-Xa-CCTαΔNLS with *Bgl*II and *Eco*RV. The insert fragment containing CCTα ΔNLS codons 1-168 and an 8 basepair 5' extension was ligated to the *Bgl*II/*Eco*RV fragment of pBSKS(-) His-TEV-CCTα to yield pBSKS(-) His-TEV-CCTαΔNLS. The *Mlu*I/*Eco*RV fragment of pBSKS(-) His-TEV-CCTαΔNLS (includes His-TEV and CCTα ΔNLS codons 1-170) was ligated with the *Mlu*I/*Eco*RV fragment of pAX-His-TEV-CCT (pAX vector with CCTα codons 171-367) to yield pAX-His-TEV-CCTαΔNLS.

pAX-His-TEV-CCTβ+NLS. His-TEV-CCTβ+NLS was constructed by site-directed mutagenesis. The reaction set-up and thermocycler settings can be found in

Appendix 1. Complementary primers were designed to exchange codons 7-9 and 11-15 of CCTβ_2 for those of CCTα thereby adding the polybasic nuclear localization signal (^{12}RKRRK^{16}; CCTβ_2 already has a K at codon 16) and mutating acidic residues to those of CCTα. The resultant amino acid sequence of the amino-terminal portion of CCTβ+NLS is: GRSM^{1}PVVTT**AKVSSRKRR**KSLSN, where mutated residues are in bold. The primer sequences can be found in Appendix 2. A unique *Bst*BI site was also engineered via silent mutation to confirm mutagenesis by diagnostic digest. pBSKS(-) His-TEV-CCTβ_2 was used as template and mutagenesis was confirmed by sequencing. His-TEV-CCTβ+NLS was sub-cloned into pAX via *Mlu*I/*Ssp*I digest of pBSKS(-) His-TEV-CCTβ+NLS and pAXHis-TEV-CCTβ_2.

2.2.4 Expression and Purification of CCTs

Adherent COS-1 cells were maintained in Dulbecco's Modified Eagle Media (DMEM)/ 0.37% $NaHCO_3$ with penicillin and streptomycin supplemented with 5% fetal bovine serum (FBS). Cells were passaged, on average, every three days by diluting them 1:10 in media. Cells passaged more than 20 times were discarded.

Transfection. COS-1 were plated 2.5×10^6 cells per 15 cm dish one day prior to transfection. On average, ten 15 cm plates were used for large scale protein expression and purification. Transient transfection of COS-1 with pAX142 vector containing CCT constructs was performed using the calcium-phosphate method. Cells were washed twice in 12.5 ml warm TS buffer (140 mM NaCl, 25 mM Tris pH 7.4, 5 mM KCl, 0.5 mM Na_2HPO_4, 1 mM MgCl, 1 mM $CaCl_2$). Cells were incubated in 20 µg of plasmid DNA and 1 mg/ml DEAE in 2.5 ml TS per 15 cm dish for 40 minutes at 37°C, 5% CO. The plasmid DNA mixture was then aspirated and the cells were incubated in 12.5 ml of

warmed modified media (DMEM, 10 mM HEPES pH 7.4, 5% FBS, 0.4 mM chloroquine) for 3 hours at 37°C, 5% CO. The media was then aspirated and the cells were washed twice with warm TS buffer. COS-1 cells were shocked for 2 minutes with 10 ml of warm TS/20% glycerol per dish at room temperature. The glycerol was aspirated and the cells were washed twice with warm TS. Cells were incubated in DMEM/0.37% $NaHCO_3$/penicillin-streptomycin/ 5% FBS at 37°C, 5% CO until harvest. The duration of transfection was 64 hours, with the exception of His-Xa-CCTα-βN and His-TEV-CCTα ΔNLS which were transfected for 48 hours to limit protein aggregation due to over-expression.

Harvesting and Lysing Cells. Media was aspirated and cells were washed three times with 12.5 ml of warm PBS per 15 cm dish. 5 ml of warm PBS/2.5 mM EDTA was added to each dish and cells were incubated for 5 minutes at 37°C, 5% CO. Cells were then scraped off of the plates and collected in two 50 ml tubes. Plates were washed with 5 ml cold PBS to remove any remaining cells and this was added to the 50 ml tubes. Cells were then centrifuged at 300 x g for 4 minutes and the supernatant was removed by aspiration. Cells were resuspended in 7.5 ml cold PBS, transferred to one 15 ml tube and centrifuged again. The supernatant was removed by aspiration and the cell pellet was then resuspended in 0.75 ml per plate of hypotonic buffer (20 mM KP_i pH 7.4, 1% NP-40, 2 mM DTT, 1 mM PMSF) supplemented with protease inhibitors (listed in Appendix 3). Cells were lysed by sonication on ice for 6 x 20 seconds. A 1/10 volume of cold binding buffer (5 mM NaP_i pH 8.0, 0.5 M NaCl, 15 mM imidazole; working concentrations) was added to the cell lysate. The mixture was centrifuged at 15 000 x g at 4°C for 10 minutes, and the supernatant was transferred to a new tube.

Purification Using Ni-NTA Agarose. A 1/8 volume of a cold 50% Ni-NTA slurry was washed with buffer to remove ethanol and then added to the supernatant in a 15 ml tube. The mixture was rotated at 4°C for 1 hour. The slurry was then transferred to a column at 4°C and allowed to settle. The flow-through was collected and the Ni-NTA column was washed with a 10 x column volume of cold wash buffer 1 (50 mM NaP_i pH 8.0, 500 mM NaCl, 25 mM imidazole, 1% NP-40). The column was then washed with a 10 x volume of cold wash buffer 2 (50 mM NaPi pH 8.0, 100 mM NaCl, 25 mM imidazole). The purified His-tagged CCT was then eluted using a 10 x column volume of cold elution buffer (50 mM NaPi pH 8.0, 100 mM NaCl, 350 mM imidazole, 0.25 mM Triton X-100, 2 mM DTT). Fractions of approximately 200 µl were collected in 1.5 ml microfuge tubes on ice. Samples of each purification fraction were run on SDS-PAGE and stained with Coomassie (0.2% Coomassie Brilliant Blue R, 45% methanol, 10% acetic acid). Those fractions containing pure protein were transferred to separate dialysis bags (10 000 MWCO tubing) and dialyzed against 500 x volume of dialysis buffer (10 mM Tris pH 7.4, 100 mM NaCl, 0.25 mM Triton X-100, 2 mM DTT) at 4°C for 3 hours with one change of dialysis buffer. 20 mM K_2HPO_4 pH 7.4 was used for His-Xa-CCTα, β_2 and β_2 C34S. Pure dialyzed protein was then aliquoted into small volumes and stored at -80°C or, where required, the His-tag was removed immediately (described below).

Purification of His-TEV-CCTα_{312}. His-TEV-CCTα_{312} was found to be insoluble in cell lysates and was therefore denatured and re-folded *in vitro.* Briefly, the cell homogenate (20 mM KP_i, 1% NP-40, 500 mM NaCl, 15 mM imidazole, 5 mM NaP_i, pH 8.0) was centrifuged at 15 000 x g for 10 minutes at 4°C. The protein pellet was then dissolved in 6 M guanidine hydrochloride (GuHCl) and centrifuged at 15 000 x g for 15

minutes at 4°C. The supernatant was then dialyzed at 4°C in three stages: *i*) 4 hours against 100 mM NaCl, 20 mM NaP_i pH 7.4, 0.25 mM Triton X-100, 2 mM DTT and 3 M GuHCl, *ii*) 3 hours against the same buffer but with 1.5M GuHCl, *iii*) overnight against the same buffer without GuHCl. The protein sample was dialyzed against a 500 x volume of buffer in each step. The resultant protein was then centrifuged at 15 000 x g for 30 minutes at 4°C. The $CCT\alpha_{312}$ in the supernatant was then purified as above. Pure dialyzed protein was then aliquoted into small volumes and stored at -80°C or, where required, the His-tag was removed immediately (described below).

Cleavage of the His-tag. The His-tag was removed from constructs with TEV protease recognition sequences using 0.5 units of His-tagged TEV per µg of CCT. The protease was added to pure His-tagged CCT and the mixture was rotated at 4°C overnight. After incubation NaCl was added to a final concentration of 150 mM. 15 mM imidazole and fresh DTT (2 mM) was also added. A 1/8 volume of Ni-NTA agarose bead slurry, washed in dialysis buffer, was then added and the mixture was rotated at 4° for 1 hour. The cleaved CCT was purified by batch method given the small volume. The beads were pelleted by centrifugation at 15 000 x g at 4°C for 2 minutes and the supernatant containing cleaved, untagged CCT was removed. Protein was aliquoted into small volumes and stored at -80°C.

Determination of Protein Concentration. Protein concentration was determined by the method of Bradford (110) using ovalbumin to construct a standard curve. Background absorbance from the buffers was accounted for by subtracting the absorbance of the buffers from the absorbance of the protein.

2.2.5 CCT Activity Assay

Purified CCTs were assayed for enzymatic activity as described previously (111). Briefly, 0.06 - 0.1 µg of purified protein was added to a mixture of 8 mM CTP, 88 mM NaCl, 12 mM $MgCl_2$ and 20 mM Tris pH 7.4. SUVs composed of 1:1 egg PC/egg PG were prepared as described (112) and added to a final concentration of 0.2 mM in a 40 µl reaction volume. Control samples with no lipid added were also included. The reaction was initiated by the addition of 1 mM [^{14}C] phosphocholine (1 mCi/mmol) and was allowed to proceed for 10 minutes at 37°C with agitation. The reaction was stopped by the addition of 1/3 volume of methanol/ammonia (9:1). The radiolabeled product was separated from substrates via thin layer chromatography. 30 µl of each sample was spotted on plastic-backed silica plates and placed in a tank containing 100 ml of 5:5:1 methanol/0.6% NaCl/ammonia for separation. Dried plates were then sprayed with 0.02% dichlorofluorescein to visualize the CDP-choline band. This area was then scraped off of the plate, collected, and the amount of radioactive product was determined by liquid scintillation counting. The dpm of the samples were corrected for background and the specific activity of CCT was determined as nmol CDPcholine/minute/µg CCT.

In experiments investigating the differential lipid response of CCT isoforms, LUVs (3:2 or 3:1 egg PC/egg PG) were used to activate CCT. The preparation of a similar type of extruded vesicle is described in section 2.2.10 except Buffer A (10 mM Tris pH 7.4, 0.5 mM EDTA) was used here instead of the sucrose buffer and salt buffer described in that section. Data were analyzed using GraphPad Prism 4 software by non-linear regression fit to the equation:

$$v = V_{max} [L] / (K_{½} + [L])$$

where [L] is the molar concentration of accessible lipid (½ of total lipid concentration). CCT will only have access to the outside of the vesicle, which effectively reduces the lipid concentration by 50%. The maximal activity V_{max} and the $K_{½}$, an apparent dissociation constant, were determined. The activities of each CCT isoform at each concentration of lipid were normalized to the extrapolated V_{max} values obtained from 3:2 PC/PG LUVs. The respective V_{max} values are reported in Figure 2.5. The normalized data were re-plotted and fit to the equation used to determine partition coefficients (see section 2.2.10). The curve was constrained to 0 and 100%. The $K_{½}$ values were derived from the normalized activation curves: CCTα = 39, 085 ± 5015 M^{-1}, CCTβ_2 = 17, 783 ± 2861 M^{-1}. The $K_{½}$ is equivalent to the reciprocal of K_p, which is described in section 2.2.10. The EC_{50}, from which the K_p value is derived, were compared by f-test using GraphPad Prism 4 software ($\alpha = 0.05$; $p < 0.0001$). The f-test evaluates the variance between models which have been fit to two groups of data, as opposed to a t-test which evaluates the variance between two data sets.

2.2.6 Enzyme Kinetic Analysis

Kinetic analysis of CCT isoforms was analyzed in a similar manner as described in section 2.2.5 but the amount of substrate was modified. Phosphocholine dependence of CCT isoforms was assayed in the presence of 16 mM CTP and 0-5 mM [^{14}C] phosphocholine. The CTP dependence of CCT isoforms was assayed in the presence of 1.5 mM [^{14}C] phosphocholine and 0-20 mM CTP. The kinetic parameters, K_m and V_{max}, were provided by analysis of primary plots (velocity versus concentration; Appendix 7). The velocity versus substrate concentration data were analyzed using GraphPad Prism 4 software and were fit to the Michaelis-Menten equation:

$$v = (V_{max} [S]) / (K_m + [S])$$

where v is the velocity of the reaction at a given substrate concentration [S], V_{max} is the maximal velocity of the reaction and K_m is the concentration of ligand required for half-maximal velocity (Michaelis constant). The values of K_m ± S.E.M. for CTP and phosphocholine are reported in section 2.3.5.

2.2.7 Chemical Cross-linking and Copper Phenanthrolene Treatment

Chemical cross-linking was used to assess the dimeric status of the CCTs. I used conditions which covalently capture subunit interactions between dimers but not random collisions (57). His-tagged proteins in phosphate buffer (20 mM K_2HPO_4 pH 7.4, 100 mM NaCl, 0.15 mM Triton X-100, 2 mM DTT) were added to a 30 µl reaction mixture to a final concentration of 0.4 µM. The reaction mixture (2 mM DTT and 0 or 2 mM PG SUVs) was allowed to equilibrate for 3 minutes in a 37°C shaking water bath. A lysine-specific cross-linker, bis (sulfosuccinimidyl) suberate (BS^3; structure shown in Appendix 4) was used in these experiments. This cross-linker has been used previously to capture specific inter-subunit interactions in CCTα (57). BS^3 was dissolved in DMSO to 100 mM in DMSO. Prior to initiating the reaction, it was diluted in water and added to the samples to a concentration of 1 mM. The samples were incubated for a further 20 minutes. The reaction was stopped by the addition of glycine to a final concentration of 0.1 M and the samples were left at room temperature for 15 minutes. In pre-quenched samples, glycine was added prior to the addition of BS^3. Samples were then analyzed by SDS PAGE and silver stain (113).

Disulfide "cross-linking" of CCTβ_2 was probed using the sulfhydryl oxidizing agent copper phenanthrolene ($Cu(Phe)_3$; structure shown in Appendix 4). This method has been used previously to probe the quaternary structure of CCTα (57). His-tagged CCTs to be treated with $Cu(Phe)_3$ were first reduced by adding 1 mM DTT and incubating for 10 minutes in a 37°C shaking water bath. Reduced His-CCTs were then placed on ice and added to a 30 µl reaction mixture containing 20 mM K_2HPO_4 pH 7.4, 100 mM NaCl and 0 – 2 mM PG SUVs. The protein concentration was 0.34 µM in the reaction and DTT was therefore diluted to approximately 0.06 mM. Samples were equilibrated in a 37°C shaking water bath for 3 minutes. Stocks of $CuSO_4$ and phenanthrolene were mixed during this incubation time and were added to the reaction to a final concentration of 0.4 mM $CuSO_4$ and 1.2 mM phenanthrolene. The reaction was allowed to proceed for 10 minutes in the 37°C shaking water bath and Laemmli buffer was used to stop it. Samples were analyzed by SDS-PAGE and silver staining.

2.2.8 Vesicle Aggregation Assay

CCT-induced aggregation of anionic lipid vesicles (vesicle tethering or cross-bridging) was monitored by measuring the apparent absorbance at 400 nm similar to Taneva *et al.* (74). The absorbance of the lipid mixture alone was recorded every 30 seconds for 3 minutes until a plateau was reached. This absorbance value (*i.e.:* the background) was subtracted from the absorbance of the experimental samples. CCTα alone does not absorb at 400 nm (73). Varying amounts of CCT (0 - 500 nM dimer) were added to the sample mixture (0.1 mM PG SUVs, 10 mM Tris pH 7.4, 2 mM DTT, 130 mM NaCl, 0.65 mM EDTA). Triton X-100 was present in the purified protein stocks and was therefore present in the reaction mixture at a concentration of 0.05 - 0.08 mM which

was kept constant regardless of the volume of protein added. Upon the addition of CCT to the mixture the absorbance at 400 nm was recorded every 30 seconds for 3 minutes. A clear plateau value was reached during this time, and this value was plotted as a function of CCT dimer concentration.

2.2.9 *In Vitro* Dephosphorylation

CCTs were dephosphorylated in the presence of 0.2 mM $MnCl_2$, 10 mM Tris pH 7.4, 100 mM NaCl, 2 mM DTT and 0.25 mM Triton X-100. EDTA was added to 2 mM, K_2HPO_4 (pH 7.7) was added to 20 mM, and $MnCl_2$ was omitted in reactions where PPIα was pre-quenched. Lyophilized PPIα was dissolved in water according the manufacturer's instructions and 2 units/μg CCT was used. Samples were incubated for 45 minutes in a 37°C shaking water bath. The reactions were not quenched at the end but were used immediately in membrane binding assays or stored at -80°C for later use.

The phosphatase was not removed from the untagged CCT samples prior to vesicle binding analysis; thus, as a control, we examined the binding of CCTα and CCTα with pre-quenched phosphatase. The binding curves were not statistically different ($p = 0.1146$; Appendix 5), thus the presence of the phosphatase did not interfere in these binding assays. The phosphatase was, however, removed from His-CCTβ_{313}. The size of PPIα and His-CCTβ_{313} is similar (37 187 Da and 38 334 Da, respectively) and would therefore interfere with identification of band shifts resulting from dephosphorylation. Nickel affinity chromatography was used to remove PPIα from His-CCTβ_{313} using the batch method and solutions identical to those used when purifying His-CCTs (but without dialysis).

Dephosphorylation was confirmed by monitoring a band shift via SDS PAGE and silver stain as well as by whole protein matrix-assisted laser desorption ionization mass spectrometry (MALDI-MS) using an Applied Biosystems Voyager-DE STR (Framingham, MA) mass spectrometer. Liquid chromatography MS (LC/MS) was used to investigate the phosphorylation status of $CCT\beta_{313}$ using an Applied Biosystems MDS-SCIEX API QSTAR Pulsar (Sciex, Thornhill, ON).

2.2.10 Membrane Binding Assay

My analysis of membrane binding used a popular sedimentation-based assay, first developed by McLaughlin and colleagues (114). Since unilamellar phospholipid vesicles in the fluid state have a density near 1.0, a procedure for increasing their density was devised (sucrose loading) in order to separate them from the aqueous phase. The positive aspects of this membrane binding assay are that is it sensitive, can be done with protein species that are not homogeneously pure (since the protein is quantified as a band on a gel) and requires no modification or engineering of the native protein. The negative aspect is that, as in any method based on separation of phases, the separation process can alter the equilibrium between bound and free protein.

Preparation of Sucrose-loaded Vesicles. Multi-lamellar vesicles (MLVs) composed of PC/PG (3:2) and spiked with 0.6 μCi ^{3}H-DPPC/ml lipid were prepared in advance of the binding assay. Lipids dissolved in chloroform were aliquoted into a round bottomed flask and dried to a film under vacuum for 45 minutes. Sucrose buffer (170 mM sucrose, 20 mM HEPES pH 7.5) was added to the dried lipids to make the final concentration 15 mM. Lipids were vortexed and hydrated for 10 minutes. They were then vortexed vigorously for 2 minutes and subjected to five freeze/thaw cycles in liquid

nitrogen and 37°C water with 1 minute of vortexing in between cycles. The MLVs were then aliquoted into 0.5 ml volumes and stored at -20°C.

Sucrose-loaded vesicles (SLVs) were prepared fresh from MLVs for each binding assay. A manual extruder (LipoFast microextruder, Avestin, ON) containing two 100 nm pore membranes was first washed with sucrose buffer then 0.5 ml of PC/PG MLVs were extruded 21 times. 200 µl of SLV suspension was diluted to 1 ml with 800 µl of salt buffer (120 mM NaCl, 20 mM HEPES pH 7.5, 10 mM DTT) and was vortexed for 1 minute. The SLVs were then centrifuged at 100 000 x g for 30 minutes at 20°C. The supernatant (800 µl) was removed and the SLVs were resuspended in the remaining volume by vortexing. The final concentration of lipid was determined by liquid scintillation counting of the lipids before and after extrusion.

Membrane Binding Assay. Binding of various CCT constructs was measured in a sedimentation-based assay. The 60 µl sample mixture was composed of 0.5 µM CCT, 0-5000 µM SLVs, 104 mM NaCl, 19 mM HEPES pH 7.5, 0.7 mM Tris pH 7.4, 20 mM sucrose, and 8 mM DTT. The sample also contained 17 µM Triton X-100 which accompanied the purified CCTs. Liquid scintillation counting of pellet and supernatant fractions ensured that the Triton X-100 did not disrupt the integrity of the SLVs, and that the supernatant was not contaminated with lipid from the pellet fraction. The protein-SLV mixtures were sedimented at 100 000 x g at 20°C for 30 minutes. After ultracentrifugation, 40 µl of supernatant was removed so as not to disturb the pellet and 20 µl of salt buffer was added to the pellet and it was resuspended by vortexing. Equal volumes of supernatant and pellet fractions were run on 10% acrylamide tricine gels. The gels were then stained with SYPRO Orange (Sigma) according to manufacturer's

instructions and visualized using a Typhoon 9410 variable mode imager (GE Healthcare). A blue 488 nm laser was used with the 580 BP 20 filter. Alternatively, a green 532 nm laser was used with the 555 BP 30 filter. The amount of CCT in the pellet versus supernatant was determined via densitometry using Image Quant 5.2 software. The intensity of the pellet band was corrected for contamination by supernatant:

$$\% \text{ Pellet} = [(P - S/2)/(P + S)] \times 100\%$$

where P is the intensity of the pellet band and S is the intensity of the supernatant band. A correction was made for the amount of protein that sedimented in the absence of SLVs as well:

$$\% \text{ CCT Bound} = [(\% \text{ in pellet} - \% \text{ aggregated})/(100 - \% \text{ aggregated})] \times 100\%$$

The % in pellet is as above and the % aggregated is the % pellet in the absence of SLVs. The % aggregated for all proteins analyzed was 27% ± 6 (mean ± S.D., n = 42). His-CCTα-βN was one outlier where the % aggregated was approximately 43%. Therefore, this construct was centrifuged at 100, 000 x g for 30 min at 20°C and the supernatant (now ~22% aggregated) was used in binding assays. Data were compiled from at least two independent experiments and were fit by non-linear regression using GraphPad Prism 4 to the equation,

$$\% \text{ Bound} = [K_p [L] / (1+K_p [L])] \times 100\%$$

where [L] is the concentration of accessible lipid (½ of total lipid). The partition coefficient (K_p) has the units M^{-1} and is a proportionality factor comparing the mole fraction of membrane-bound protein to that of soluble protein (115). Top and bottom

values were constrained to 100 and 0%, respectively. Partition coefficients were calculated from the binding curves,

$$K_p = 1/ [L]$$

when the protein is 50% bound, where [L] is the concentration of accessible lipid (½ of total lipid; 74, 115). The error reported is ± 95% confidence interval with respect to the best fit K_p value. Where applicable, the log EC_{50} values (*i.e.*: the concentration of lipid at which 50% of CCT is bound; K_p derived from this value) of the curves were compared by f-test ($\alpha = 0.05$) using GraphPad Prism 4 software.

2.3 Results

2.3.1 CCTα and CCTβ$_2$ have Different Anionic Membrane Binding Affinities *in Vitro*

Lykidis *et al.* (23) showed that CCTβ$_1$, analyzed in lysates from transfected COS-7 cells, is activated by anionic lipids. In that study neither the activity nor the membrane binding of CCTβ was compared to that of CCTα in side-by-side experiments. As a first step in determining how the divergent regions among CCT isoforms may influence its membrane binding and subsequent activation, I characterized the lipid vesicle binding of CCTβ$_2$ and CCTα in parallel. The CCTβ$_2$ splice isoform was used because it is the most similar in sequence to CCTα (see section 1.3.2). His-tagged proteins were purified and their binding to SLVs composed of PC/PG (3:2) was measured. I found that His-CCTβ$_2$ had a weaker membrane binding affinity than His-CCTα as it requires a higher concentration of anionic lipid to achieve the same proportion of bound enzyme as CCTα (Figure 2.1). Partition coefficients (K_p) were calculated from these curves (Figure 2.1 inset). The K_p for His-CCTα was approximately 40-fold higher than that of His-CCTβ$_2$. These data suggest that the two isoforms have significantly different membrane binding affinities ($p<0.001$).

What could account for this difference in binding affinity for anionic membranes? NMR and CD analyses indicated that residues 242 - 293 contribute to the amphipathic helix responsible for membrane binding of CCTα (63, 68). This region of CCTα and CCTβ$_2$ has several amino acid substitutions that are semi-conservative, but only one non-conservative change when analyzed by ClustalW (Ile-272 in CCTα to His-272 in CCTβ$_2$;

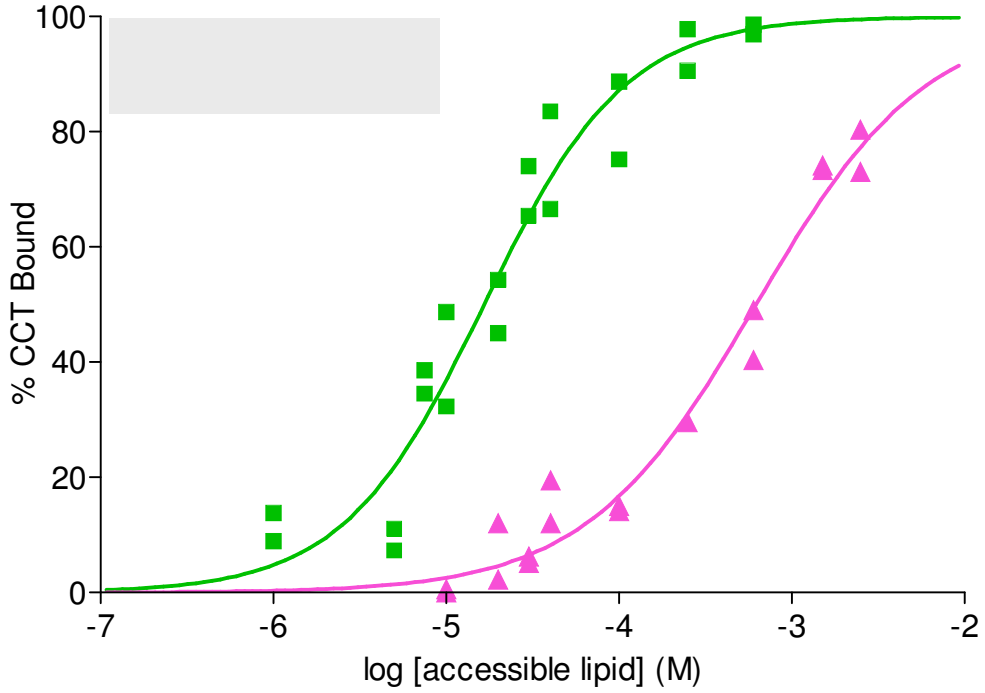

Figure 2.1 CCTβ$_2$ Has a Weaker Binding Affinity than CCTα

Binding analysis of His-CCTα and His-CCT$_2$ to SLVs composed of PC/PG (3:2) at 20°C. Data were compiled from at least two independent experiments and were fit using GraphPad Prism 4 to the equation, % Bound = 100K_p [L] / (1+K_p [L]), (115) where [L] is the concentration of accessible lipid (½ of total lipid, see "*Experimental Procedures*" section 2.2.5). Top and bottom values were constrained to 100 and 0%, respectively. Partition coefficients (K_p) were calculated from the curves where K_p = 1/ [accessible lipid] when protein is 50% bound (115). K_p has units x 10^3, M^{-1}. The error reported is ± the 95% confidence interval with respect to the best fit K_p value.

Figure 1.5, Figure 1.8 A), and this occurs outside the non-polar face of the helix. Both isoforms have the same net charge (0 over residues 242-293). The peak hydrophobic moment and the total hydropathies of the non-polar and polar faces of this region of domain M are also very similar between CCT isoforms (Table 1.3). The subtle differences in M domains seemed unlikely to account for the significantly different lipid response between CCT isoforms. This prediction was borne out of comparative membrane binding analyses of purified constructs containing only the carboxy-terminal tails (domain M and region P) of the two isoforms. These constructs were expressed and purified from a bacterial expression system and were, therefore, not phosphorylated. The induction of α-helical content by PC/PG (3:2) SUVs was monitored. Lipid-induced helix acquisition in domain M coincides with other measures of membrane binding (71, 72). There was little difference in the K_p values calculated from these curves (data not shown, Svetla Taneva, unpublished work). I hypothesized that the divergent regions N and P (when phosphorylated) may influence the membrane-binding and subsequent activation of CCT isoforms. Region N is the most divergent segment between CCT isoforms and analysis of expressed constructs in crude cell lysates suggested that region N of CCTβ_1 negatively influences catalytic activity (23). I therefore focused my initial attention on the role of region N in the lipid response of CCT isoforms by creating region N-swapped chimeric enzymes.

2.3.2 CCTβ_2 is a Dimer and Region N Participates in Forming the Dimer Interface

Before creating CCTα/CCTβ chimeras I needed to ensure that the N regions of CCTα and CCTβ_2 perform analogous structural roles. If so, this would alleviate concerns

about folding disruption in the chimeric enzymes. Region N of CCTα participates in forming the dimer interface and interacts intimately with domain C as revealed in the solved structure of CCTα (residues 1-236; 48), and by chemical cross-linking (57).

I determined the quaternary interactions of CCTβ_2 using the lysine-specific chemical cross-linker bis (sulfosuccinimidyl) suberate (BS^3). I found that, like CCTα (57), a homodimeric ~90 kDa species of CCTβ_2 is trapped in the presence of the cross-linker (Figure 2.2 A). In the presence of the lysine-specific cross-linker many cross-linked species of CCTβ_2 dimer are trapped as a result of different cross-links being made. The addition of activating lipids such as PG reduced the amount of dimer species trapped. This feature is shared with CCTα (Figure 2.2 A; 57), and suggests that upon membrane binding a conformational change occurs that results in an alteration of the dimer interface that abrogates cross-linking. These experiments confirm that CCTβ_2 is a dimer and the dimer interface rearranges upon membrane binding, like that of CCTα, but did not determine whether region N of CCTβ_2, like that of CCTα, participates in forming the dimer interface.

CCTα has a pair of cysteines located in region N which are in the region that forms the dimer interface (48). While there is no evidence that these cysteines form a disulfide bond under physiological conditions, a disulfide bond can be formed between these cysteines when CCTα is oxidized *in vitro* with copper phenanthrolene ($Cu(Phe)_3$), thereby trapping CCTα as a covalently-linked dimer (57). Mutation of Cys-37 in CCTα to serine severely limited trapping of the CCTα dimer upon oxidation. The CCTβ_2 dimer has a pair of cysteines at position 34. To test whether the Cys-34 pair is homologous to the CCTα Cys-37 pair I mutated Cys-34 to serine. This switch did not affect activity or

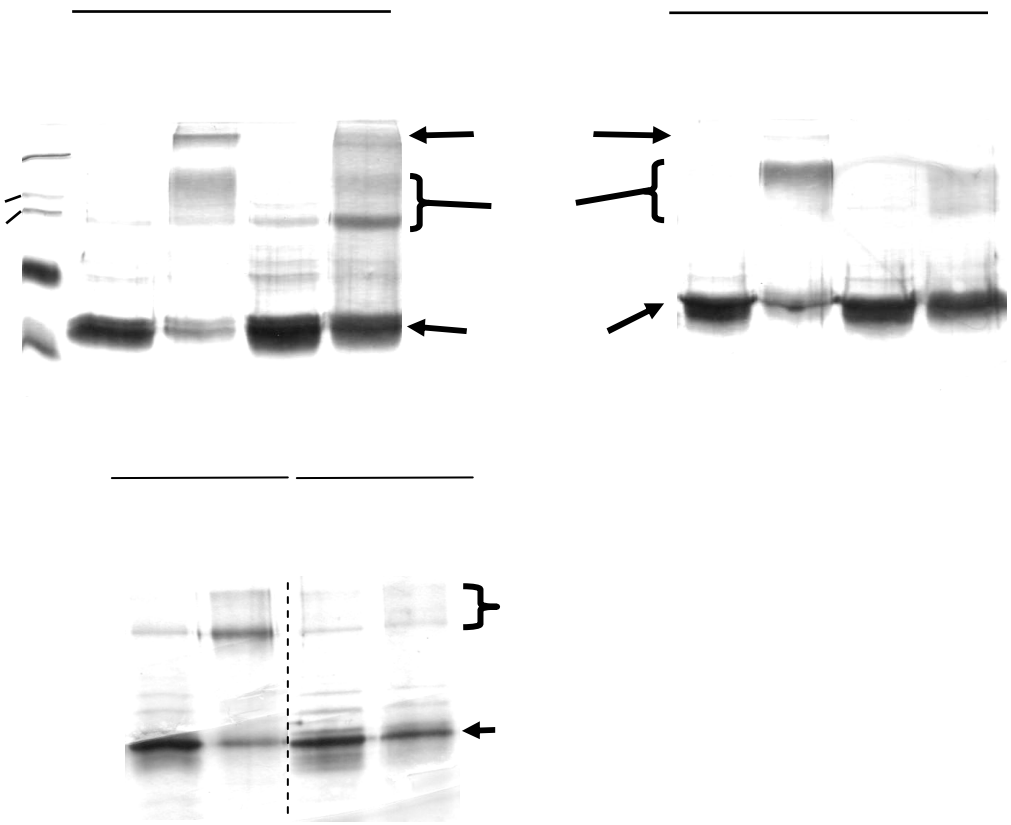

Figure 2.2 Both CCTβ_2 and α are Dimers with Inter-Subunit Contacts Involving Region N

A. BS^3 reactions. Purified His-tagged CCTα or β_2 (0.4 μM) was reacted with BS^3 in the presence or absence of 2 mM PG SUVs. Reactions were pre-quenched (-) or quenched after 20 min at 37^{o}C (+). *B. Copper phenanthrolene reactions.* Purified His-tagged CCTβ_2 or CCTβ_2 C34S (0.34 μM) were either added to 0.4 mM $CuSO_4$ and 1.2 mM phenanthrolene (+) or untreated (-). The samples were electrophoresed on 10% polyacrylamide gels and stained with silver.

Construct	Specific Activity		n
	Without Lipid	With Lipid	
CCTα	0.32 ± 0.03	12.2 ±1.1	3
CCTβ_2	0.62 ± 0.16	6.4 ± 1.3	3
CCTβ_2 C34S	0.30 ± 0.10	9.2 ± 1.0	3
CCTα-βN	0.20 ± 0.04	6.7 ± 0.5	3
CCTβ-αN	1.2 ± 0.4	10.3 ± 0.6	3
CCTαΔNLS	0.24 ± 0.04	10.4 ± 0.9	3
CCTβ+NLS	0.76 ± 0.15	8.1 ± 0.9	3
CCTα_{312}	0.28 ± 0.19	13.9 ± 1.4	4
CCTβ_{313}	0.44 ± 0.06	6.2 ± 0.4	4
CCTαΔNLS$_{312}$	0.27 ± 0.05	11.9 ± 1.3	4

Table 2.1 Specific Activities of Purified CCT Constructs

Specific activities (nmol CDPcholine/min/μg CCT) are averages of at least three independent determinations ± S.D. Saturating concentrations of phosphocholine and CDP-choline were used. Samples with lipid were assayed with saturating concentrations PC/PG (1:1) SUVs. These data show that none of the mutations compromise enzyme activity or regulation by lipids. Constructs shaded in grey contain region N from CCTβ_2, which correlated with a 30 - 40% decrease in enzyme specific activity. The mean specific activity of all constructs containing region N of CCTβ_2 is 7.3 ± 1.2; whereas the mean specific activity of all constructs containing region N of CCTα is 12.2 ± 1.4.

lipid dependence (Table 2.1). The $Cu(Phe)_3$ treated His-CCTβ_2 C34S did not show an increase in disulfide-trapped dimers relative to untreated sample (Figure 2.2 B), similar to that of CCTα C37S (57). These results indicate very similar roles for region N in the quaternary structure of the two CCT isoforms (*i.e.*: forming part of the catalytic fold and dimer interface).

2.3.3 Region N Distinguishes the Membrane Binding Affinity of CCT Isoforms *in Vitro*

Having demonstrated analogous roles of segment N in the quaternary structure of CCTα and β_2 I constructed region N chimeras, swapping the first 83 residues of the two CCT isoforms. The purified segment N swapped mutants were active and activation was lipid-dependent (Table 2.1). Binding of these constructs to PC/PG (3:2) SLVs was measured, and partition coefficients (K_p) were calculated. Exchange of region N of CCTα with that of CCTβ_2 (His-CCTα-βN) resulted in a right shift of the binding curve translating to a 20-fold reduction in K_p (Figure 2.3). The reciprocal mutation of CCTβ_2 (His-CCTβ-αN) resulted in a left shift of the binding curve translating to a > 6-fold increase in K_p value ($p > 0.0001$; Figure 2.3). It is also interesting to note that exchange of region N of CCTβ_2 with that of CCTα increased the specific activity of this construct while the reciprocal mutation decreased the specific activity of CCTα (Table 2.1). This result is discussed in later sections and should be investigated in the future.

2.3.4 The Polybasic NLS Distinguishes the Affinity of CCT Isoforms *in Vitro*

Taneva *et al.* (73) have shown that the CCTα dimer can tether anionic lipid vesicles resulting in an increase in sample turbidity that can be monitored by changes in absorbance at 400 nm. Later, through the use of a heterodimer composed of one wildtype

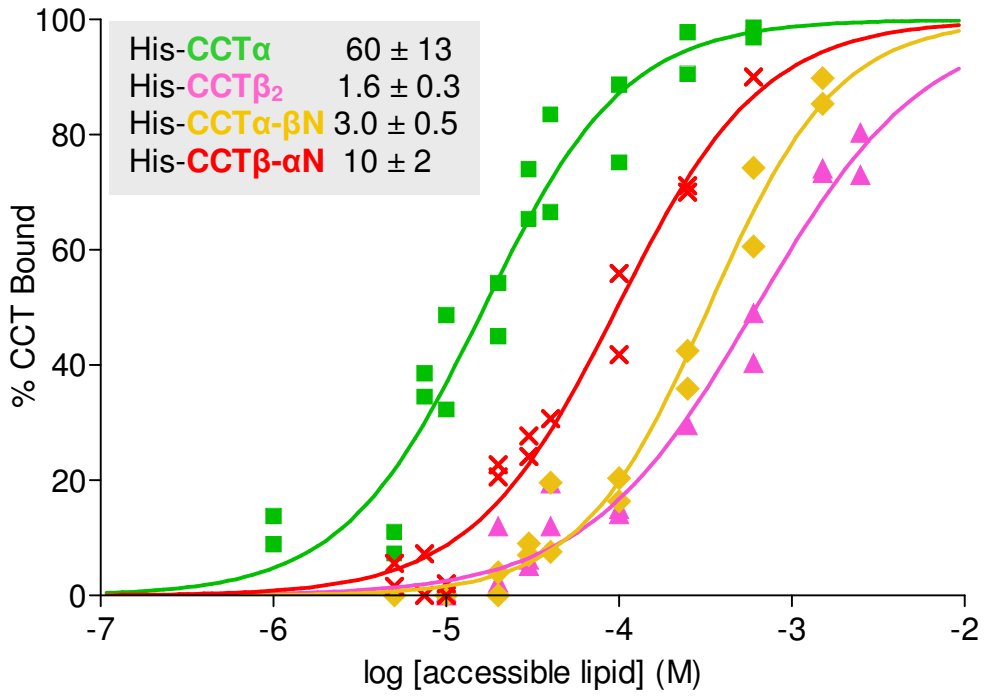

Figure 2.3 The N Segment Distinguishes the Membrane Binding Affinity of CCT Isoforms

Membrane binding was assayed using SLVs composed of PC/PG (3:2) at 20°C. His-tagged region N-swapped chimeras were assayed and compared to His-CCT isoforms in Figure 2.1. Data were compiled from at least two independent experiments and were analyzed as in Figure 2.1. Partition coefficient of each construct is listed. K_p has units x 10^3, M^{-1}.

CCTα monomer and one monomer lacking domain M and segment P we showed that CCTα required only one M domain for full activation and the heterodimer was able to tether anionic lipid vesicles despite having only one M domain (74). These findings suggest the existence of another membrane binding motif to enable CCTα to tether lipid vesicles. I hypothesized that the polybasic NLS is this second membrane binding motif. Furthermore, I postulated that the NLS serves to elevate the membrane binding affinity of CCTα and, since it is absent in $CCT\beta_2$, may explain the large difference in lipid response between CCT isoforms.

To probe this idea, a CCTα mutant lacking the NLS (CCTαΔNLS) and a $CCT\beta_2$ mutant with the NLS sequence from CCTα (CCTβ+NLS) were created. The exact sequences of their amino-termini are provided in section 2.2.3. The poly-histidine tag used in purifying CCT can contribute to membrane binding, when paired with the polybasic NLS (74). His-tagged $CCT\alpha_{236}$ (CCTα lacking domain M and region P) was found to have a K_p value of ~7 x 10^3 M^{-1} in the presence of anionic SLVs even though it lacked domain M. Removal of the poly-histidine tag or the polybasic NLS from $CCT\alpha_{236}$ resulted in no measurable binding to anionic SLVs. The His-tag was therefore cleaved. CCT constructs were active and lipid-dependent (Table 2.1). The binding affinity for PC/PG (3:2) SLVs of untagged CCTαΔNLS and CCTβ+NLS compared to untagged CCTα and $CCT\beta_2$ was determined. Deletion of the NLS reduced the binding affinity of CCTα and the resultant K_p was not significantly different from that of the chimeric His-CCTα-βN ($p = 0.8792$; Figure 2.4; compare inset with Figure 2.3). The addition of the NLS to $CCT\beta_2$ increased its binding affinity as reflected by a ~3-fold increase in K_p ($p <$

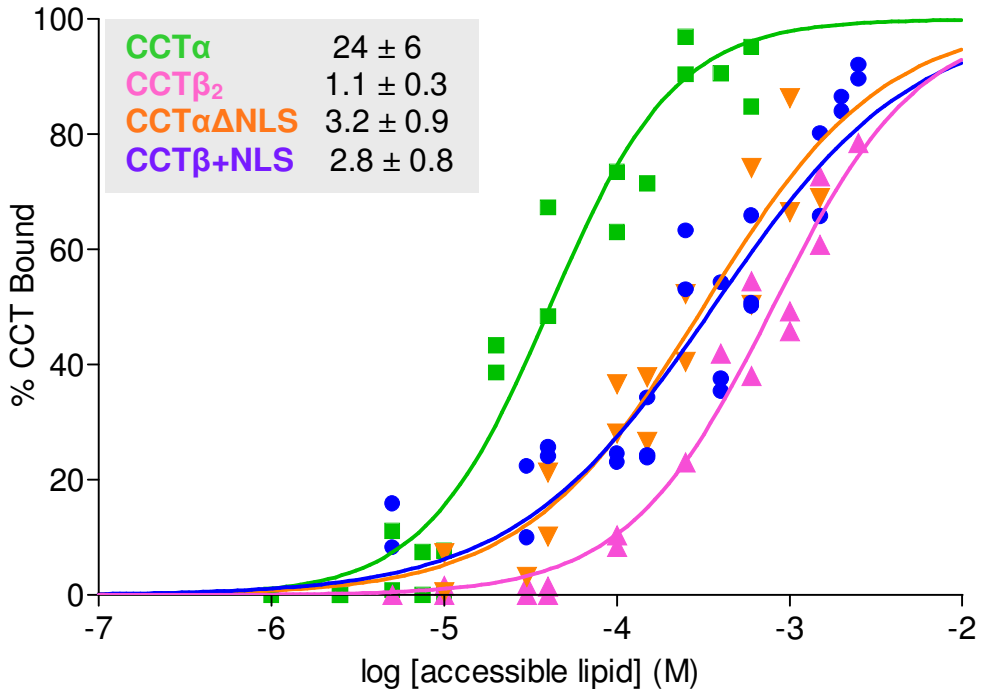

Figure 2.4 The NLS is Responsible for the Difference in Membrane Binding Affinity of CCT Isoforms

Membrane binding of untagged CCT isoforms and NLS mutants was assayed using SLVs composed of PC/PG (3:2) at 20°C. Data were compiled from at least two independent experiments and were analyzed as in Figure 2.1. Partition coefficient of each construct is listed. K_p has units x 10^3, M^{-1}.

0.0001; Figure 2.4). These results support a role for the NLS in distinguishing the affinity of CCTα and CCTβ_2 for anionic vesicles.

2.3.5 Membrane Binding of the NLS Contributes to CCT Activation by Highly Anionic Vesicles

I explored whether the additional binding strength afforded by the NLS motif would translate into more efficient lipid activation of CCTα versus CCTβ_2. Before comparing the anionic lipid requirement for activation of the two isoforms I determined the substrate K_m values, so that the analyses would be done using conditions saturating for substrate. The K_m values for CTP were approximately the same for the two CCTs (CCTα = 1.3 ± 0.4 mM, CCTβ_2 = 0.9 ± 0.4 mM), and the K_m values for phosphocholine were 0.4 ± 0.06 mM for CCTα and 0.25 ± 0.05 mM for CCTβ_2 (Appendix 7). These values are in the range of those reported elsewhere for CCTα (61, 62, 67, 78). A comparison of the lipid requirement for activation of CCTα and β_2 by LUVs composed of either PC/PG (3:2) or (3:1) suggested that CCTβ_2 required a higher lipid concentration for activation (Figure 2.5 A). The maximal activity of CCTβ_2 is lower than CCTα (10.1 ± 1.2 μmol/min/mg *vs.* 14.6 ± 1.4 μmol/min/mg; See also Table 2.1 and a section in the Discussion dealing with this feature), therefore the curves in Figure 2.5 A were normalized (Figure 2.5 B). In the presence of 3:2 PC/PG LUVs there was 2.2-fold stronger response to the lipids on the part of CCTα ($p < 0.0001$). Previous work has shown that NLS binding to membranes requires in excess of 25 mol% anionic lipid (or 3:1 PC/PG; 73). In keeping this, the lipid activation of CCTα and β_2 were coincident when LUVs containing 3:1 PC/PG were used (Figure 2.5 B), reflecting a dependence solely on their highly similar M domains for activation. Thus, when the lipid vesicles are

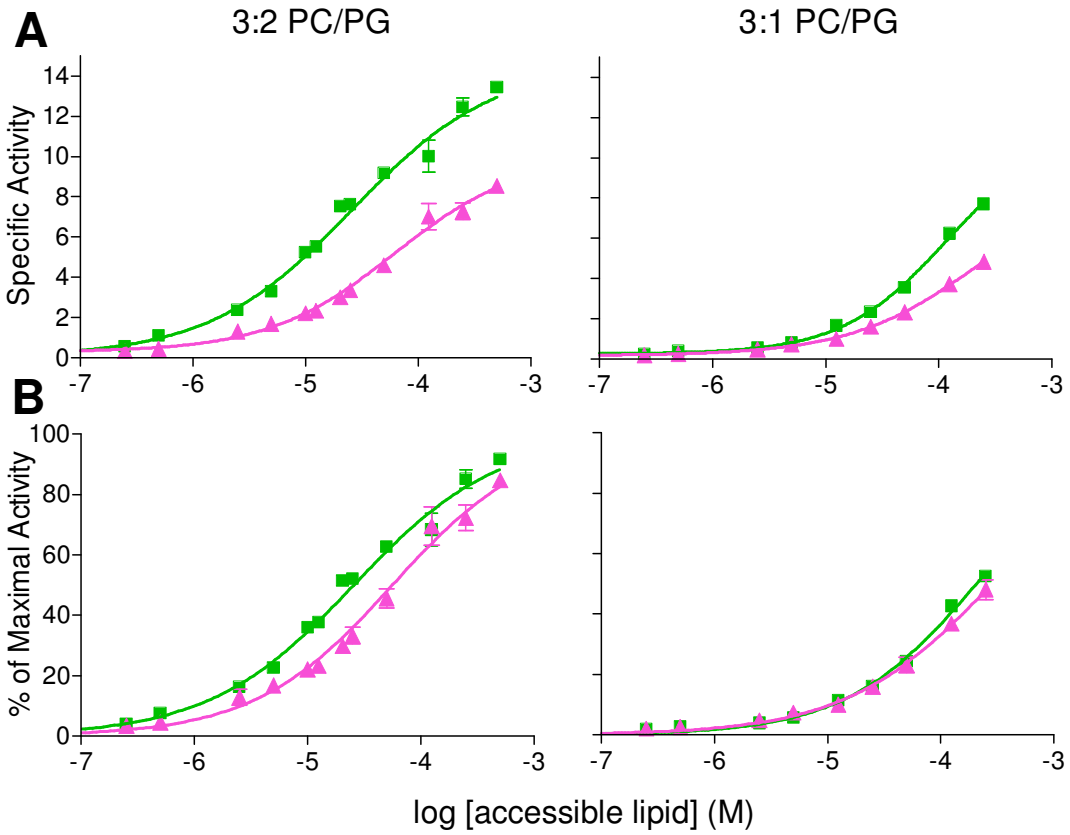

Figure 2.5 CCTβ$_2$ Activity has a weaker response to anionic lipids than CCTα

A. The specific activities (nmol CDPcholine/min/µg CCT) of purified untagged CCT isoforms were measured in parallel as a function of increasing concentrations of the indicated LUVs. [Accessible lipid] = ½ x [total lipid]. Data represent the mean ± S.D. of four independent determinations. The data was plotted as a function of log [accessible lipid] and analyzed using GraphPad Prism 4 by non-linear regression. *B*. The data in Figure 2.5 A were normalized to mean maximal activities of each CCT isoform in the presence of 3:2 PC/PG LUVs (see section 2.2.5; CCTα, 14.6 ± 1.2 nmol/min/µg; CCTβ$_2$, 10.1 ± 1.4 nmol/min/µg). The data were fit using GraphPad Prism 4 to the equation, % Maximal Activity = $100K_p$ [L] / (1+K_p [L]), (115) where [L] is the concentration of accessible lipid (½ of total lipid). CCTα (green), CCTβ$_2$ (pink).

strongly anionic, the binding reinforcement via the NLS motif affects the lipid activation of CCTα. These findings are consistent with a primary role for domain M of CCTα and β_2 in membrane charge sensing and alleviation of inhibition, and an additional contribution of the NLS to CCTα binding and activation only at high anionic lipid content.

2.3.6 The Polybasic NLS is a Membrane Binding Motif and Distinguishes the Vesicle Tethering Activity of CCT Isoforms

I compared the anionic vesicle tethering activity of CCT constructs by monitoring the increased turbidity due to aggregated anionic lipid vesicles (73, 74). Taneva *et al.* (73) previously showed that dimeric CCTα can tether anionic lipid vesicles owing to its high membrane binding affinity. It was assumed that the two M domains of the CCTα were responsible for this tethering and were, therefore, oriented on opposite sides of the dimer. This matter was complicated by the fact that a heterodimer containing only one M domain was able to tether vesicles as well as the wildtype dimer (74). Figure 2.6 A and B show that CCTβ_2 is completely deficient in vesicle tethering function. Swapping the N segments between the α and β_2 isoforms results in loss of function from CCTα and gain of function in CCTβ_2 (Figure 2.6 A). The vesicle tethering activity of CCTα was completely obliterated upon deletion of the NLS sequence (Figure 2.6 B; 74). Figure 2.6 B shows that the CCTβ_2 construct carrying the NLS is nearly as effective as CCTα. These data confirm that the NLS can function as a membrane binding motif (74), and that the NLS accounts for the difference in tethering activity between CCT α and β_2 isoforms.

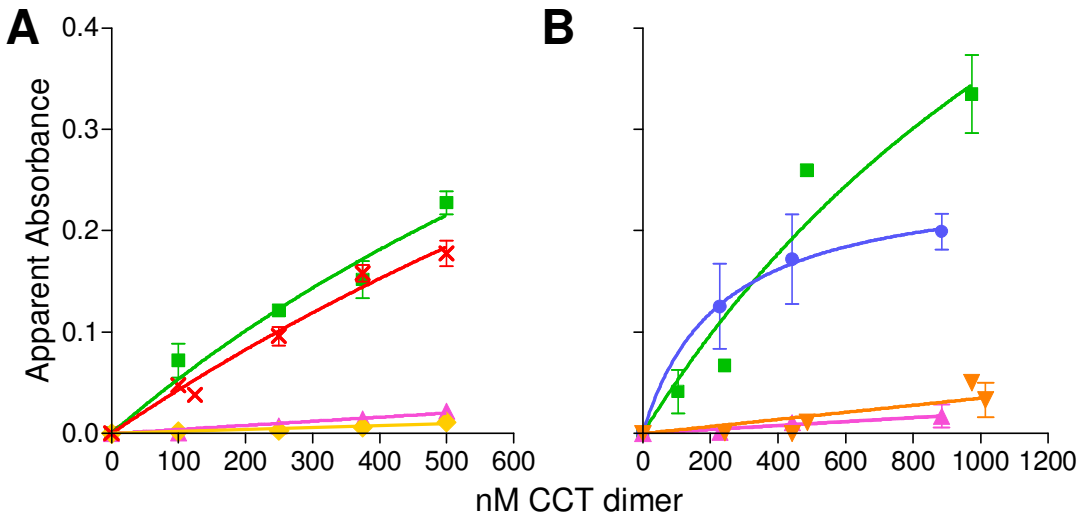

Figure 2.6 CCTβ$_2$ Cannot Tether Lipid Vesicles Because it Lacks a NLS

The increase in apparent absorbance (400 nm) of PG SUVs due to the addition of CCT was monitored for 3 min. The apparent absorbance due to vesicles alone was subtracted from the plateau value of each CCT concentration. The data represent the mean ± standard error or range for at least two independent determinations. *A*. His-tagged CCT isoforms and region N-swapped chimeras, *B*. untagged CCT isoforms and NLS mutants. Some of the data for CCTαΔNLS were contributed by Dr. Svetla Taneva. CCTα (green), CCTβ$_2$ (pink), CCTα-βN (red), CCTβ-αN (yellow), CCTαΔNLS (orange), and CCTβ+NLS (blue).

2.3.7 Dephosphorylation of CCTs Clarifies the Effect of the NLS on Membrane Binding

The NLS, acting in its traditional capacity, targets proteins to the nucleus. Deletion of the NLS from CCTα and addition of the NLS to CCTβ_2 would presumably result in their mislocalization during expression in COS-1 cells. These mislocalized proteins could have alternative phosphorylation states as compared to their wildtype counterparts. CCTα is phosphorylated on serine residues in segment P (82, 39) which antagonizes membrane binding and activation (90, 116). CCTβ_2 is a phosphoprotein (26) but the extent of phosphorylation and its effect on membrane binding had not been investigated when I began this study. Rat CCTα has 16 serine residues in region P while rat CCTβ_2 has 18 serine residues as well as 3 threonine residues in the corresponding region which may also be phosphorylated. If CCT isoforms and the NLS mutant constructs were differentially phosphorylated, this would mask the true contribution of the NLS to membrane binding affinity.

To clarify the contribution of the NLS to membrane binding affinity without the complication of variable and undefined phosphorylation states, purified CCT constructs were dephosphorylated *in vitro*. CCT constructs were incubated with the catalytic subunit of protein phosphatase I (PPIα) which has been successfully used to dephosphorylate CCTα (90). Dephosphorylation of CCTs was confirmed by MS of whole proteins and by monitoring the resultant band shift on SDS PAGE (Figure 2.7). MS analysis gave an average number of 6 phosphates for CCTα, in agreement with previously published work (39), while CCTβ_2 had 7. CCTαΔNLS had an average of 2 phosphate groups while CCTβ+NLS had a remarkable 14. This high degree of

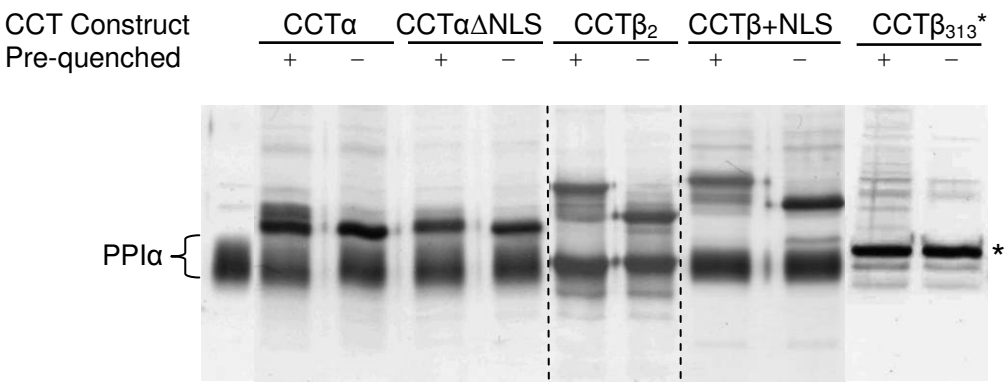

Figure 2.7 ***In vitro*** **Dephosphorylation of CCT Isoforms and Constructs**

One μg CCT was incubated with 2 units pre-quenched (+) or active (-) protein phosphatase I (catalytic subunit; PPIα) for 45 min at 37°C with agitation. *The molecular weight of CCTβ_{313} and PPIα are similar (38 334 Da and 37 187 Da, respectively) therefore His-CCTβ_{313} was re-purified using nickel-agarose after incubation with PPIα. Samples were electrophoresed on 10% acrylamide gels and stained with silver.

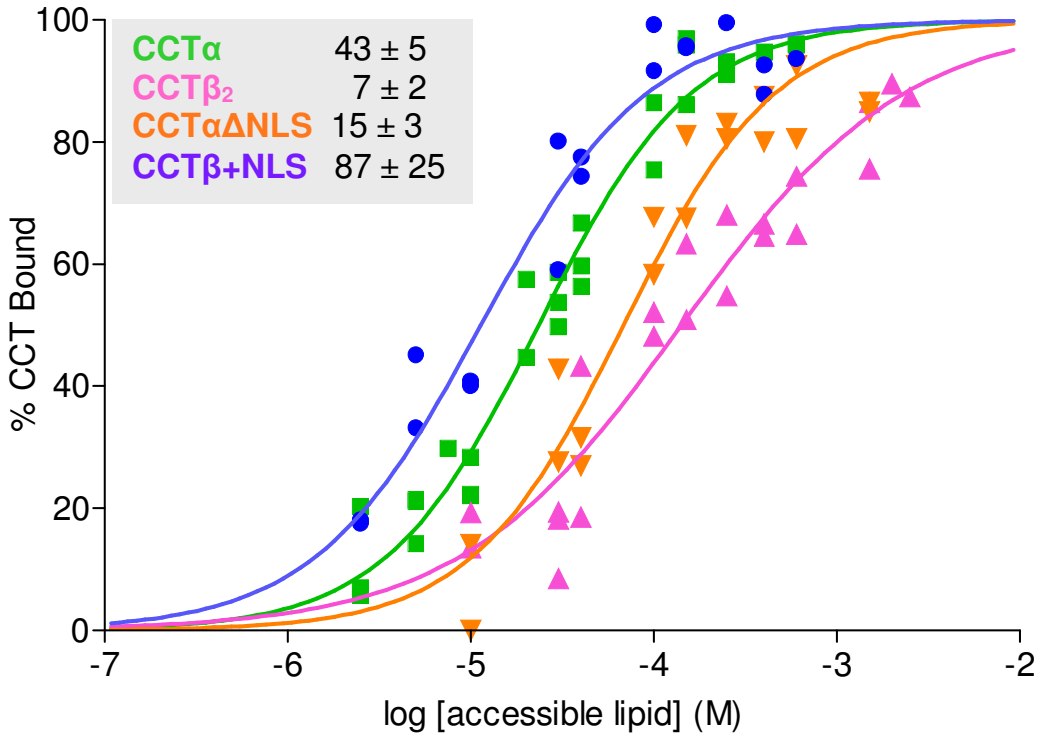

Figure 2.8 Dephosphorylation Reveals Full Impact of NLS on Membrane Binding

Membrane binding of *in vitro* dephosphorylated untagged CCT isoforms and NLS insertion/deletion mutants was assayed using SLVs composed of PC/PG (3:2) at 20°C. Data were compiled from at least two independent experiments and were analyzed as in Figure 2.1. Partition coefficient of each construct is listed. K_p has units x 10^3, M^{-1}.

phosphorylation could explain why addition of the NLS to CCTβ_2 was associated with only a 3-fold increase in membrane binding affinity.

Binding of *in vitro* dephosphorylated CCTα, CCTβ_2, CCTαΔNLS and CCTβ+NLS to PC/PG (3:2) SLVs was measured and K_p values were calculated from the binding curves. The difference in membrane binding affinity between CCT isoforms is evident even when these proteins are dephosphorylated (Figure 2.8). The K_p value of dephosphorylated CCTα is 6-fold higher than that of CCTβ_2. Deletion of the NLS from CCTα reduced binding affinity approximately 3-fold ($p < 0.0001$), and addition of the NLS to CCTβ_2 increased binding affinity more than 10-fold (Figure 2.8 inset). Thus, when phosphorylation is eliminated as a variable, the effect of the NLS on membrane binding affinity is very apparent.

2.3.8 CCTβ_2 Membrane Binding Affinity is More Sensitive to its Phosphorylation Status Than CCTα

Removal of 6 phosphate groups from CCTα increased its K_p value just 2-fold whereas removal of 7 phosphates from CCTβ_2 resulted in a 7-fold increase in K_p value (compare insets from figure 2.4 and 2.8). Furthermore, when the NLS was absent in CCTα, phosphorylation had a greater influence on its membrane binding affinity. Removal of only 2 phosphate groups from CCTαΔNLS resulted in a 5-fold increase in K_p compared to a 2-fold increase in CCTα after removal of 6 phosphates (compare insets from figure 2.4 and 2.8). These data suggest that the membrane affinity of CCTs lacking an NLS is more heavily influenced by phosphorylation than CCTα. Thus, there appears to be an antagonism between membrane attraction by the NLS and membrane repulsion by the phosphorylated P region.

2.3.9 Region P Antagonizes Membrane Binding via its Phosphorylation Status

The results above suggest that phosphorylation of region P influences membrane binding affinity. Can region P also influence the affinity of domain M for membranes via a mechanism unrelated to its phosphorylation status *i.e.*, by the intrinsically disordered region itself? To answer this question I prepared CCTs missing the entire region P (CCTα residues 313-367 and CCTβ_2 314-369). Secondary structure predictions suggested that region P deletion would not affect the integrity of domain M. Furthermore this deletion in CCTα does not affect its specific activity (78, 81, 80; Table 2.1). It is known that phosphorylation is restricted to residues 315-367 in CCTα, but the sites of phosphorylation in CCTβ_2 were unknown. To determine if phosphorylation is restricted to the carboxy-terminal 55 residues in CCTβ_2 I compared the mass of purified CCTβ_{313} before and after dephosphorylation with PPIα using conditions that resulted in loss of 7 phosphates in full-length CCTβ_2. Unlike full-length CCTβ_2, phosphatase treatment produced no band shift on gels (Figure 2.7) and no change in mass as determined by MS (untreated- 38, 334 Da; phosphatase-treated - 38, 334 Da; which agrees with the theoretical mass within an error of 1 Da). This provides evidence that residues 314-369 constitute the phosphorylation region of CCTβ_2.

I measured the binding to PC/PG (3:2) SLVs of the CCTα, CCTαΔNLS, CCTβ_2, and CCTβ+NLS constructs truncated before region P (Figure 2.9). For CCTβ_{313} and CCTαΔNLS$_{312}$ there was little difference in the K_p values when comparing dephosphorylated full-length versus region P-truncated constructs (compare insets from Figures 2.8 and 2.9), in support of the notion that region P modulates membrane binding solely via its phosphorylation status. CCTβ+NLS$_{313}$, although active, formed protein

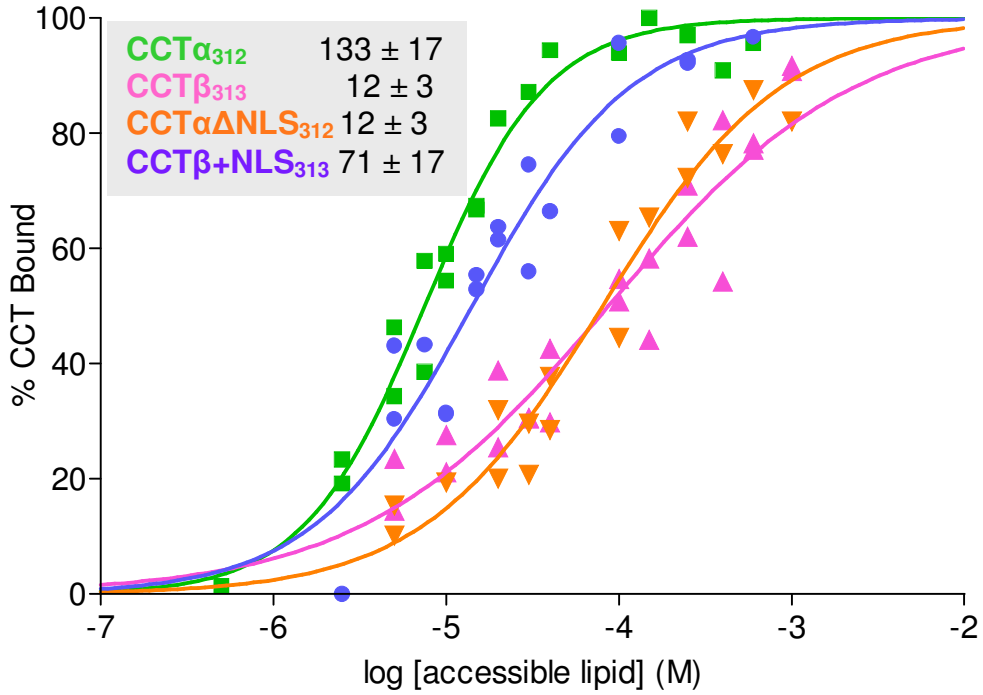

Figure 2.9 Region P Truncation Mimics Effects of Dephosphorylation on Membrane Binding

Membrane binding of segment P truncated untagged CCT isoforms and NLS insertion/deletion mutants was assayed using SLVs composed of PC/PG (3:2) at 20°C. Data were compiled from at least two independent experiments and were analyzed as in Figure 2.1. Partition coefficient of each construct is listed. K_p has units x 10^3, M^{-1}.

aggregates, leading to sedimentation of >50% of the protein in the absence of lipid. The partitioning of the soluble component of this construct into the vesicles, determined after subtracting the insoluble component, yielded a K_p value of 71 ± 17 x 10^3 M^{-1}, that is not different from that of the dephosphorylated CCTβ+NLS construct ($p = 0.2339$). However, given its solubility problems, I am hesitant to make any conclusions based solely on this K_p value. The SLV binding of CCTα_{312}, however, was ~3 times higher than that of dephosphorylated full-length CCTα ($p < 0.0001$). This suggests a negative contribution of region P to binding, *i.e.* region P stabilizes the soluble form of the enzyme especially when the NLS is present. In keeping with this idea, like CCTβ+NLS$_{313}$, the CCTα_{312} construct was more prone to aggregation and losses during purification than the other constructs. Most importantly the role of the NLS is clearly revealed in the region P truncated CCTs (Figure 2.9). P segment truncation of CCTαΔNLS yielded a proteinwhich behaved identically to CCTβ_{313} as the K_p values are not statistically different ($p = 0.6438$) while the K_p of CCTα_{312}, which houses an NLS, is much higher ($p < 0.001$).

2.4 Discussion

S. Taneva, R. B. Cornell and I have identified a novel membrane binding motif; the polybasic NLS (74). The *in vitro* analyses indicate that CCTβ_2 has a weaker binding response to lipids than CCTα and that although differential phosphorylation between isoforms does influence membrane binding affinity, the NLS is largely responsible for this difference. This strongly suggests that the NLS, acting as a secondary membrane binding motif, has a functional consequence. The finding that the NLS can pair with domain M to cross-bridge (tether) two separate bilayers provides insight into the orientation of domains/regions within the CCT dimer. For vesicle tethering to be possible, the M domains and N segments must be on opposite poles of CCT. And yet the NLS couples with domain M to increase binding affinity for vesicles, which would suggest that both motifs engage the same bilayer. The solution to this quandary may be that the N domain is so long and flexible that it can do both.

In vitro analyses of dephosphorylated and region P truncated CCTs also suggested that the effect of segment P on membrane binding affinity is solely due to its phosphorylation. It was unfortunate, however, that region P truncation resulted in solubility problems for constructs also containing an NLS (i.e.: CCTα_{312} and CCTβ+NLS$_{313}$). CCTα_{312} could be refolded *in vitro* but this was not attempted for CCTβ+NLS$_{313}$ due to a lack of material. While this impeded me from accurately measuring the partition coefficient of CCTβ+NLS$_{313}$ it appears that this construct does have high affinity for anionic membranes. This complication also suggests that the P region, even in the absence of phosphorylation, may help to stabilize and solublize CCT.

In the next chapter (chapter 3) I seek to further validate these *in vitro* findings in the context of cellular membranes. Does the NLS function as a secondary membrane binding motif in cells? If the absence of a secondary binding motif (the NLS) in CCTβ_2 has a functional consequence in a cell, I would expect that CCTβ_2 would partition more weakly into cell membranes.

In the final chapter (chapter 4) I discuss the rationale for the evolution of an NLS as a membrane-reinforcing motif in CCTα, the relative roles of phosphorylation as a modifier of the membrane binding affinity of CCTα versus CCTβ_2, and the evolution of regulatory regions as intrinsically disordered.

3: Role of the Intrinsically Disordered Regions of CCT in Membrane Binding in Cells

3.1 Introduction

The goal of this investigation was to substantiate the *in vitro* studies of the membrane binding affinity of CCT isoforms and mutants. I hypothesized that CCTβ_2 has a weaker response to lipids in cells due to its lacking an NLS and, as a consequence, will partition less into OA enriched membranes than CCTα. I aimed to provide evidence that the NLS and phosphorylation are responsible for the difference in membrane binding affinity between isoforms in cells. To do this I needed a reliable method for assessing the differences in membrane partitioning among CCTs.

Three methods are used to assess changes in CCT membrane partitioning (commonly referred to as membrane translocation): cell fractionation (71, 77-79), digitonin release (42, 94), and fluorescence microscopy (129). The latter uses either immunofluorescence of native CCT or fluorescence of expressed GFP fusion constructs. Each method has both advantages and disadvantages. I used a cell fractionation approach to compare CCT membrane partitioning as a function of OA-enrichment of cell membranes. OA can be supplied exogenously to transfected COS cells using a bovine serum albumin (BSA) carrier. OA is largely unsoluble in aqueous solution but can be solublized through the use of a protein carrier. BSA has multiple low affinity binding sites for fatty acid monomers (130), like OA. BSA binds to and solublizes OA but the low affinity with which BSA binds OA enables its release and subsequent partitioning

into cell membranes. Previous work from our lab has established the mol% OA incorporated into cell membranes within the molar ratios of OA/BSA used here (71).

3.2 Experimental Procedures

3.2.1 Materials

All restriction enzymes were from Invitrogen or Fermentas except for *Bst*BI which was from New England Biolabs. dNTPs, *Pfu* turbo and all primers were from Invitrogen. Rapid ligation and plasmid preparation kits were from Fermentas. Cell culture supplies were from Gibco-Invitrogen. Sodium oleate was from Sigma. Fatty acid free bovine serum albumin was purchased from Calbiochem. The ^{14}C-phosphocholine was purchased from Amersham Biosciences.

3.2.2 Construction of Untagged CCTs

Untagged CCTs for *in vivo* partitioning experiments were constructed via site-directed mutagenesis. The reaction set-up and thermocycler settings can be found in Appendix 3. Complementary primers were designed to delete the His-tag and Factor Xa sequence, maintain the Kozak sequence and engineer a *Sca*I site for diagnostic digest (silent mutation). pBSKS(-) His-Xa-CCTα was used as template. The primer sequences can be found in Appendix 4. Mutagenesis was confirmed by sequencing and diagnostic digest. Untagged CCTα was sub-cloned into pAX by ligating the *Mlu*I/*Eco*RV fragment of pBSKS(-) CCTα (CCTα codons 1-170) with the *Mlu*I/*Eco*RV fragment of pAXHis-TEV-CCTα (CCTα codons 71-367 in pAX). Untagged CCTβ$_2$, CCTαΔNLS and CCTβ+NLS in pAX were constructed by sub-cloning the coding sequences from pAXHis-TEV-CCTs into pAX using pBSKS(-) as a shuttle. A shuttle was required because the *Bgl*II site located between the His-tag and CCTx coding sequences was needed for sub-cloning, but there is a *Bgl*II site in the pAX vector. *Bgl*II/*Sal*I fragments of pAXHis-TEV-CCTβ$_2$, -CCTαΔNLS and -CCTβ+NLS (entire coding regions of all

constructs) were ligated with the *Bgl*II/*Sal*I fragment of pBSKS(-) CCTα (pBSKS(-) lacking CCTα). *Mlu*I/*Ssp*I fragments of pBSCCTβ_2, -CCTαΔNLS and -CCTβ+NLS (first ~83 codons of each isoform/ construct) were then ligated with *Mlu*I/*Ssp*I fragment of either pAXHis-TEV-CCTβ_2 or -CCTα (codons 84-367 of CCTα or 84-369 of CCTβ_2 in pAX).

Untagged region P truncated CCTs were constructed by engineering a premature stop codon via site-directed mutagenesis. The reaction set-up and thermocycle settings can be found in Appendix 3. pBSKS(-) CCTα and pBSKS(-) CCTαΔNLS were used as templates and complementary primers were designed to engineer a stop codon at 313 and a *Sal*I site directly after it. Primer sequences can be found in Appendix 4. Likewise, pBSKS(-) CCTβ_2 and pBSKS(-) CCTβ+NLS were used as templates and complementary primers were designed to engineer a stop codon at 314 and a *Sal*I site directly after it. The primer sequences can be found in Appendix 4. Mutagenesis was confirmed by diagnostic digest and sequencing. Untagged CCTα_{312}, CCTαΔNLS$_{312}$, and CCTβ_{313} were sub-cloned into pAX by digesting with *Mlu*I/*Sal*I to liberate the coding sequences and ligating them with the *Mlu*I/*Sal*I pAX fragment.

3.2.3 Membrane Partitioning Assay

CCT partitioning into cell membranes enriched with OA was performed essentially as described in Johnson *et al.* (71). The COS-1 cells were plated 1 x 10^6 cells per 10 cm dish one day prior to transfection. One dish was plated per OA:BSA ratio tested. Transient transfection of COS-1 with pAX142 vector containing untagged CCT constructs was performed as described in Section 2.2.4. Cells were transfected for various durations to obtain similar expression levels (approximately 100 units CCT

activity/mg lysate protein, Appendix 6): CCTα - 20 hours; $CCT\alpha_{312}$, CCTαΔNLS and $CCT\alpha\Delta NLS_{312}$ - 24 hours; CCTβ+NLS - 30 hours; $CCT\beta_2$ and $CCT\beta_{313}$ - 36 hours.

Enrichment of cell membranes with oleic acid was achieved by incubating the cells for 1 hour at 37°C in media containing 1 mM sodium oleate and 0.25-20 mg/ml fatty acid free BSA (molar ratios OA:BSA from 3.3 to 266). Trypan blue exclusion was used to assess the viability of transfected cells treated with and without OA. While transient transfection caused approximately 20-25% cell death, there was little difference in viability between OA-treated and untreated cells. Cells were harvested in 1.5 ml per dish of hypotonic buffer (10 mM Tris pH7.4, 1 mM EDTA, 2 mM PMSF, 2 mM DTT) and lysed by sonication 2 x 30 seconds on ice. NaCl was added to 100 mM and the samples were then centrifuged 100 000 x g for 1 hour at 4°C. The supernatant was removed (cytosol) and the pellet was resuspended by sonication in 10 mM Tris pH 7.4, 100 mM NaCl, 1 mM EDTA, 2 mM PMSF, 2 mM DTT and 1% Triton X-100. The sample was centrifuged again to separate the membrane and Triton-insoluble (particulate) fractions. This protocol routinely yielded ≤ 20% of the total wildtype CCTα or β_2 in the membrane fraction of *untreated* cells. The percent in the particulate fraction varied somewhat among CCT constructs. It ranged from a low value of ~ 1% for $CCT\beta_2$, $CCT\beta_{313}$, and $CCT\alpha\Delta NLS_{312}$, to a high value of 5 -7% for $CCT\alpha_{312}$ and CCTβ+NLS. The units of CCT activity of each fraction were determined as described above in the presence of saturating levels of the activating lipid (250 μM PG SUVs). The activity of each fraction at each OA:BSA treatment was assayed in duplicate. The proportion of CCT partitioning into the membrane fraction was determined from the activity of each fraction:

% CCT in Membrane = 100 (activity in membrane fraction / activity in all fractions)

The proportion of CCT in the membrane fraction versus the total CCT in the cytosol, membrane and particulate fraction for each OA:BSA was plotted. The individual data points (average of duplicates) from at least two independent determinations were analyzed by GraphPad Prism 4 software by non-linear regression fit to the equation:

$$\% \text{ partition} = \%P_{max} [X] / Y_{½} + [X]$$

where % partition is the % of CCT activity in the membrane fraction, $\%P_{max}$ is the maximum partitioning, [X] is the OA:BSA ratio and $Y_{½}$ is the inverse of the OA:BSA ratio required for ½ maximal partitioning. A curve was fit manually to CCTβ_2. These curves were not constrained. Basal and maximum % partitioning was determined as the mean value ± S.E.M. of the baseline and plateau of the curves using GraphPad Prism 4. Bound/Free is the ratio of CCT units in the membrane fraction to the CCT units in the soluble fraction:

bound/free = units in membrane fraction / units in soluble fraction

Where applicable, the top values (*i.e.:* maximum partitioning values of each CCT) and bottom values (*i.e.:* basal partitioning values of each CCT) of the curves were compared by f-test ($\alpha = 0.05$) using GraphPad Prism 4 software.

3.3 Results

3.3.1 CCTβ$_2$ has a Weaker Membrane Binding Affinity in Cells due to the Absence of the NLS

CCTα translocation to COS cell membranes can be promoted by enrichment of membranes with the anionic lipid OA, which can be delivered exogenously from a complex with bovine serum albumin (BSA) (71, 77, 79, 100). This method was used to determine the relative binding affinity of CCTβ$_2$, CCTβ+NLS, and CCTαΔNLS for OA-enriched cell membranes compared to CCTα. These constructs were expressed in COS cells to approximately equivalent levels, as assessed by activity (40 to 50-fold above endogenous levels). Since the specific activities of purified CCTs were not affected by the NLS deletion/insertion (Table 2.1), I was able to use the total lysate activity as a measure of the abundance of each CCT. The membrane partitioning was analyzed as a function of the OA/BSA molar ratio, which we previously showed results in an increase in fatty acid content up to ~30 mol% of total phospholipids (71). My protocol to analyze membrane bound versus soluble CCT was designed so that ≤ 20% of wildtype CCTα would appear in the membrane fraction in untreated cells (see section 3.2.3 and following discussion). The ratio of membrane bound/free CCT is a function of the volume of lysis buffer, which was constant in these analyses. This ratio does not represent how much CCT is membrane bound in the intact cell, but enables measurement of the changes in membrane partitioning due to OA enrichment, and a comparison of the responses of the different CCT constructs.

The CCTβ_2 isoform displayed weaker membrane partitioning than CCTα in both untreated and OA-enriched cells (Figure 3.1). Induction of partitioning into the membrane fraction occurred at approximately the same OA/BSA ratio for CCTα, β_2, and the NLS insertion/deletion mutants. This suggests that they have similar negative charge sensing mechanisms. On the other hand, the partitioning at saturating OA contents varied among the four CCT constructs. The ratio of bound/free CCTβ_2 in OA-saturating conditions was ~10-fold lower than that of CCTα (Figure 3.1 inset) and addition of the NLS to CCTβ_2 increased this ratio from 0.43 to 1.2. These results are consistent with the *in vitro* membrane binding data. On the other hand, deletion of the NLS from CCTα appeared to have only a small (< 2-fold) but significant reduction in the membrane partitioning ($p < 0.005$; Figure 3.1). I considered that the differential phosphorylation status of these constructs could again be masking the impact of the NLS on membrane binding affinity.

The complete set of kinases responsible for the phosphorylation of the 16 sites in CCTα has not been identified (81, 83-87), and the kinases, other than Cdk5 (32) that act on CCTβ2 are unknown. In vitro SLV binding analysis suggested that region P truncation has a similar effect on membrane binding affinity as dephosphorylation. Rather than attempting to inhibit all kinases acting on CCTs I deleted region P. Activity analysis of lysate fractions revealed equal expression of the CCT constructs (data not shown). Because of its poor folding properties (see section 2.3.9), the membrane partitioning of CCTβ+NLS313 is not included in these results. The partitioning results for the other CCT constructs lacking the P region clearly reveal a positive role for the NLS in membrane binding in cells (Figure 3.2). The membrane partitioning (bound/free)

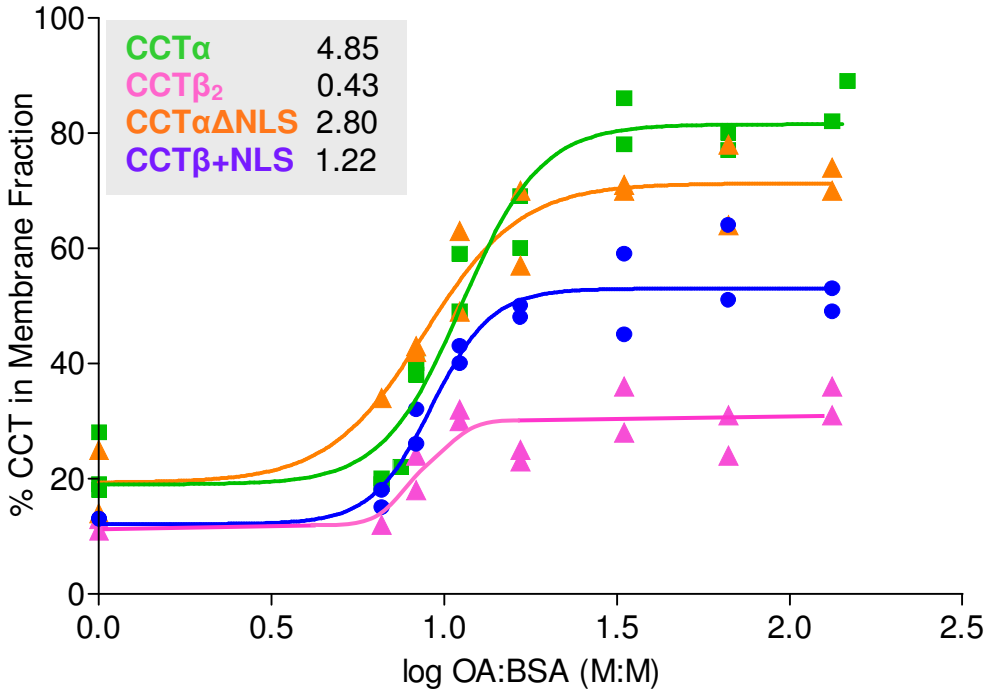

Figure 3.1 Differential Membrane Partitioning of CCT Isoforms to Oleic Acid-Enriched Cell Membranes

COS-1 cells expressing untagged full-length CCT constructs at approximately equivalent levels were treated with OA/BSA in molar ratios of 3.3 to 266 for 1 h at 37°C. Cells were harvested and fractionated, and the CCT activity units in each fraction were determined. The proportion of CCT in the membrane fraction versus the total CCT in the cytosol, membrane and particulate fraction for each OA:BSA was plotted. The individual data points from at least two independent determinations were fit to curves by GraphPad Prism 4, or manually fitted in the case of CCTβ_2. Maximum bound/free ratios for each construct are listed. Bound/free is the ratio of CCT units in the membrane fraction to the CCT units in the soluble fraction at the plateau of the curves.

of CCTβ313 in cells saturated with OA was more than an order of magnitude lower than that of CCTα_{312} (Figure 3.2). Deletion of the NLS from CCTα_{312} resulted in a large reduction in the membrane partitioning to mimic that of CCTβ_2. Unfortunately, due to the ambiguous fit of the data to the curve an f-test was not possible. These effects of NLS addition and deletion on the cell membrane partitioning of region P truncated CCTs were very similar to the effects of the same mutations analyzed *in vitro* (Figure 2.9). These results provide evidence that the NLS is a membrane binding motif in the context of cellular membranes and that the NLS is largely responsible for the difference in membrane binding affinity between CCT isoforms.

A comparison of phosphorylated and dephosphorylated CCT isoforms *in vitro* revealed that the phosphorylation of region P serves to attenuate binding affinity and that the effect was most pronounced in CCTβ_2. The 1.4 to 3-fold increases in basal and maximal cell membrane partitioning of CCTα and CCTβ_2 and NLS mutant constructs upon deletion of the P segment also support an antagonistic role for phosphorylated region P in cells (compare insets from Figures 3.1 and 3.2). Curiously, deletion of region P from CCTαΔNLS resulted in a 3.4-fold *decrease* in cell membrane partitioning, rather than an increase (compare insets from Figures 3.1 and 3.2), suggesting a positive role for region P in the membrane binding of this construct. However, the phosphorylation states of full-length CCTs expressed in cells under these conditions were unknown, making it difficult to assess the contributions of phosphorylation versus the region P protein segment to the membrane binding process. The results of the *in vitro* analyses clearly rule out a positive modulating role for region P on domain M membrane partitioning.

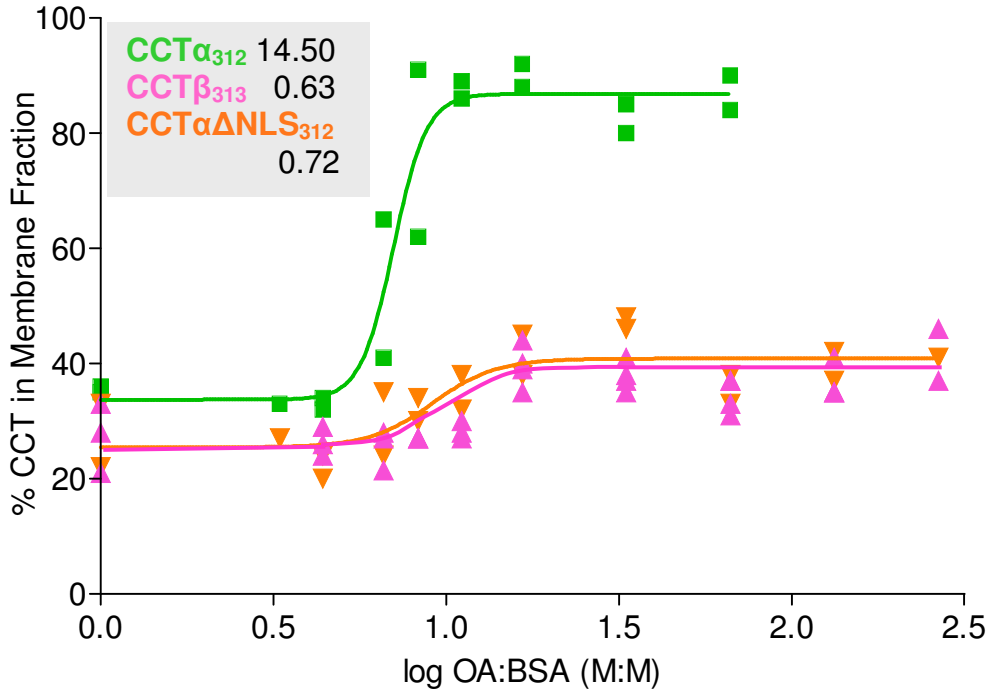

Figure 3.2 Partitioning of Segment P Truncated CCT Isoforms to Oleic Acid-Enriched Cell Membranes

COS-1 cells expressing untagged region P truncated CCT constructs at approximately equivalent levels were treated with OA/BSA in molar ratios of 3.3 to 266 for 1 h at 37°C. Cells were harvested and fractionated, and the CCT activity units in each fraction were determined. The proportion of CCT in the membrane fraction versus the total CCT in the cytosol, membrane and particulate fraction for each OA:BSA was plotted. The individual data points from at least two independent determinations were fit to curves by GraphPad Prism 4, or manually fitted in the case of CCTβ_2. Maximum bound/free ratios for each construct are listed. Bound/free is the ratio of CCT units in the membrane fraction to the CCT units in the soluble fraction at the plateau of the curves.

3.4 Discussion

While these studies are not truly "*in vivo*", I have measured the binding of cellular CCTs to cellular membranes which have a more complex composition than liposomes and are more representative of the conditions in which CCT engages a membrane. Furthermore, I have separated truly membrane associated CCT from CCT in the particulate in an added fractionation step using detergent. This is an advance with respect to other analyses that only separate soluble and particulate fractions. The particulate fraction obtained without detergent-based fractionation may contain aggregated protein as well as membrane associated protein which may skew results. The fractionation method used here is therefore more accurate. These membrane partitioning results have further validated my *in vitro* findings. CCTβ_2 has a weaker affinity for cell membranes than CCTα and this is largely due to the lack of a secondary membrane binding motif, the NLS.

This method, however, does have limitations. The exact anionic lipid content of OA-enriched membranes is unknown in these studies. I assume that enrichment is very similar between trials, but no measurements were performed. Instead, I used OA-enrichment conditions that were identical to those described by Johnson *et al.* (71). In those studies the mol% OA at each OA/BSA ratio was determined by lipid extraction and quantification. Furthermore, the concentration of lipid cannot be varied, as was done *in vitro*. This does not allow for the extraction of a binding constant. Instead, I varied the mol% anionic lipid and was able to determine a bound/free ratio as a measure of membrane binding affinity. Despite this limitation, this method does allow for

comparative analysis between constructs. Another limitation of this method arises from the lysis and homogenization of cells. When most tissues or cells in culture are homogenized and centrifuged CCTα is distributed between the soluble and particulate fractions, the distribution depending on parameters like the dilution factor, salt concentration, and the presence of detergents in the homogenization medium. The homogenization procedure also disrupts the cell's ultrastructure and scrambles membranes. Thus, this method is not appropriate for determining the specific membrane localization of a membrane protein; however, it can be reliable for assessing changes in intrinsic membrane affinity of a given protein in response to a variable. Here, the variables were (i) anionic lipid content of the membranes (which was accomplished by enrichment with different concentrations of OA delivered from BSA in the culture medium) and (ii) the presence or lack of the NLS motif or region P. I compared entire data sets of distributions over a wide range of OA:BSA treatments to draw conclusions about similarities and differences in CCT membrane partitioning.

Investigation of the role of phosphorylation in membrane partitioning was complicated by the fact that the phosphorylation state of untagged CCTs expressed under these conditions is unknown. Thus it is not possible to assess the effect of phosphorylation by comparing the membrane partitioning of full-length CCT and segment P truncated CCTs. Deletion of the P regions did, however, increase the partitioning both in the basal condition and maximum OA enrichment of most constructs, suggesting that the P segment does attenuate membrane binding *in vivo*.

4: Concluding Discussion

4.1 Characterization of CCTβ$_2$ Structure, Activity, and Membrane Affinity

This work represents the first biochemical characterization of purified CCTβ$_2$. I have shown *via* cross-linking studies that CCTβ$_2$, like CCTα, is a homodimer, and that the amino-terminal region in the vicinity of Cys-34 participates in dimerization. Also like CCTα, the amino-terminal 40 residues and the carboxy-terminal ~55 residues are strongly predicted to be intrinsically disordered (Figure 1.5, Appendix 2). Previous analyses of CCTβ$_2$ in cells or partially purified cell extracts showed that it was a phosphoprotein (26, 32). By mass spectrometry of untreated and phosphatase-treated full-length and truncated CCTβ$_2$ purified from a mammalian cell I found that, like CCTα (82, 81, 39), the phosphorylation region of CCTβ$_2$ is confined to the carboxy-terminal residues 314-369. I found that rat CCTβ$_2$ has 30-40% lower V_{max} than rat CCTα (Table 2.1), even though their catalytic domains are 90% identical (Figure 1.4, Table 1.1). This difference was maintained despite NLS deletions/additions, dephosphorylation, and/or region P truncations. However when the entire N regions were swapped (residues 1-83), the V_{max} values also switched; *i.e.:* CCTα V_{max} became 35% lower than that of CCTβ$_2$ (Table 2.1). This suggests that a portion of the N region can influence the catalytic function of CCTs. Lykidis *et al.* (23) obtained a similar result when assaying the activity of the same N region chimeras in cell lysates. Since residues 40-72 of the N region crown the catalytic domain and contribute many contacts to the catalytic dimer (48), it

may be that this segment, which is just 67% similar between isoforms, functions less effectively as a dimer stabilizer in the β versus α isoform. This intriguing idea warrants further investigation.

I have shown here that while CCTβ_2 does bind to anionic lipid vesicles, the binding is weaker than that of CCTα; *i.e.* requires a higher molar lipid concentration for an equivalent binding response. Insertion of the NLS sequence of CCTα caused an increased in membrane affinity *in vitro* (Figure 4.1, Table 4.1) and in cells (Figure 4.2, Table 4.2), and this was especially marked when CCTβ_2 was dephosphorylated, indicating that the NLS distinguishes the membrane affinities of the two isoforms. Dephosphorylation or deletion of the carboxy-terminal 55 residues from CCTβ_2 resulted in a 7 to 10-fold increase in membrane binding affinity, indicating that the phosphorylation region antagonizes membrane binding, as it does for CCTα. Thus while the structure and regulatory mechanisms of CCTβ_2 resemble those of CCTα, there may be rather large differences in the relative impact of regulatory processes.

4.2 The NLS can Function as a Secondary Membrane-Binding Motif *In Vitro* and in Cells to Distinguish the Membrane Affinities of Two Natural CCT Isoforms

In collaboration, I have identified the polybasic NLS as a secondary membrane binding/tethering motif *in vitro* (74). Portions of the work presented here contributed to that publication (*i.e.:* the CCTα NLS deletion mutant used in the vesicle aggregation assay). In that paper we also speculated on the biological function of CCT membrane tethering. We postulated that the NLS and domain M of CCTα may be responsible for the membrane stacks observed in cells where CCTα is over-expressed. Gehrig *et al.* (53)

Figure 4.1 Binding of CCT Constructs to Anionic Sucrose-loaded Vesicles

SLV binding curves were aligned to allow for comparison of all constructs. CCTα-derived constructs (green), CCTβ_2-derived constructs (pink), CCTαΔNLS-derived constructs (orange), CCTβ+NLS-derived constructs (blue), His-CCTα/β-N (yellow) and His-CCTβ/α-N (red).

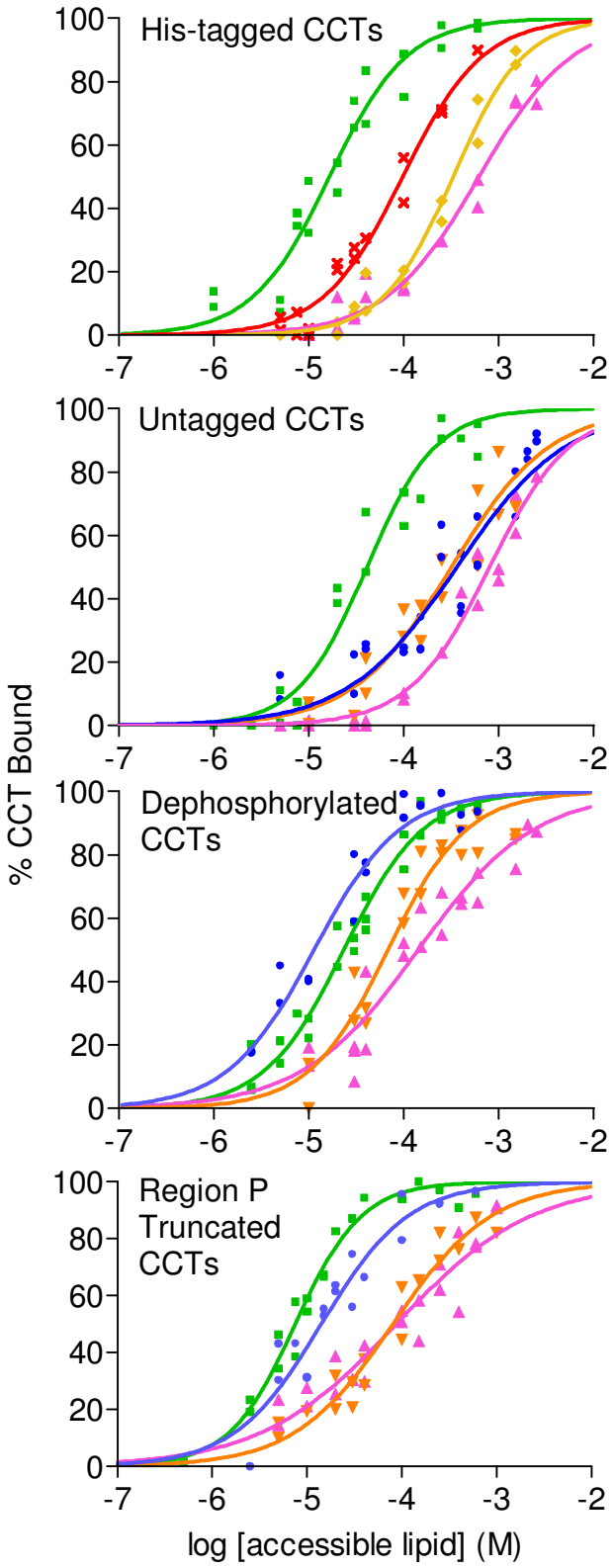
His-tagged CCTs
Untagged CCTs
Dephosphorylated CCTs
Region P Truncated CCTs
% CCT Bound
log [accessible lipid] (M)
100
80
60
40
20
0
-7
-6
-5
-4
-3
-2

	Construct	Phosphorylation State	Partition Coefficient (K_p) (x 10^3, M^{-1})	r^2 Value for Curve Fit
1	His-CCTα	ND	60 ± 13	0.94
	His-CCTβ_2	ND	1.6 ± 0.3	0.97
	His-CCTα-βN	ND	3.0 ± 0.5	0.98
	His-CCTβ-αN	ND	10 ± 2	0.97
2	CCTα	6	24 ± 6 [b]	0.95
	CCTβ_2	7	1.1 ± 0.3	0.94
	CCTαΔNLS	2	3.2 ± 0.9	0.90
	CCTβ+NLS	14	2.8 ± 0.8	0.87
3	dephosCCTα	0	43 ± 5	0.97
	dephosCCTβ_2	0	7 ± 2	0.91
	dephosCCTαΔNLS	0	15 ± 3	0.93
	dephosCCTβ+NLS	0	87 ± 25	0.92
4	CCTα_{312}	0 [a]	133 ± 17	0.97
	CCTβ_{313}	0	12 ± 3	0.90
	CCTαΔNLS$_{312}$	ND	12 ± 3	0.94

Table 4.1 Partition Coefficients and Phosphorylation State for CCT Constructs

The average number of phosphate groups on full-length CCT isoforms and constructs and CCTβ_{313} was determined by mass spectrometry of whole proteins. Partition coefficients were calculated from the binding curves in Figure 4.1 where K_p = 1/ [accessible lipid] when protein is 50% bound (74, 115). The error reported is ± 95% confidence interval with respect to the best fit K_p value. ND = not determined and/or no published data. [a]Phosphorylation status of rat CCTα_{312} is based on previous analyses (39, 81, 82). [b]This K_p value is similar to that determined previously for CCTα and 1:1 PC/PG SLVs (74). CCTβ+NLS$_{313}$, which was heavily aggregated, is not included in this list.

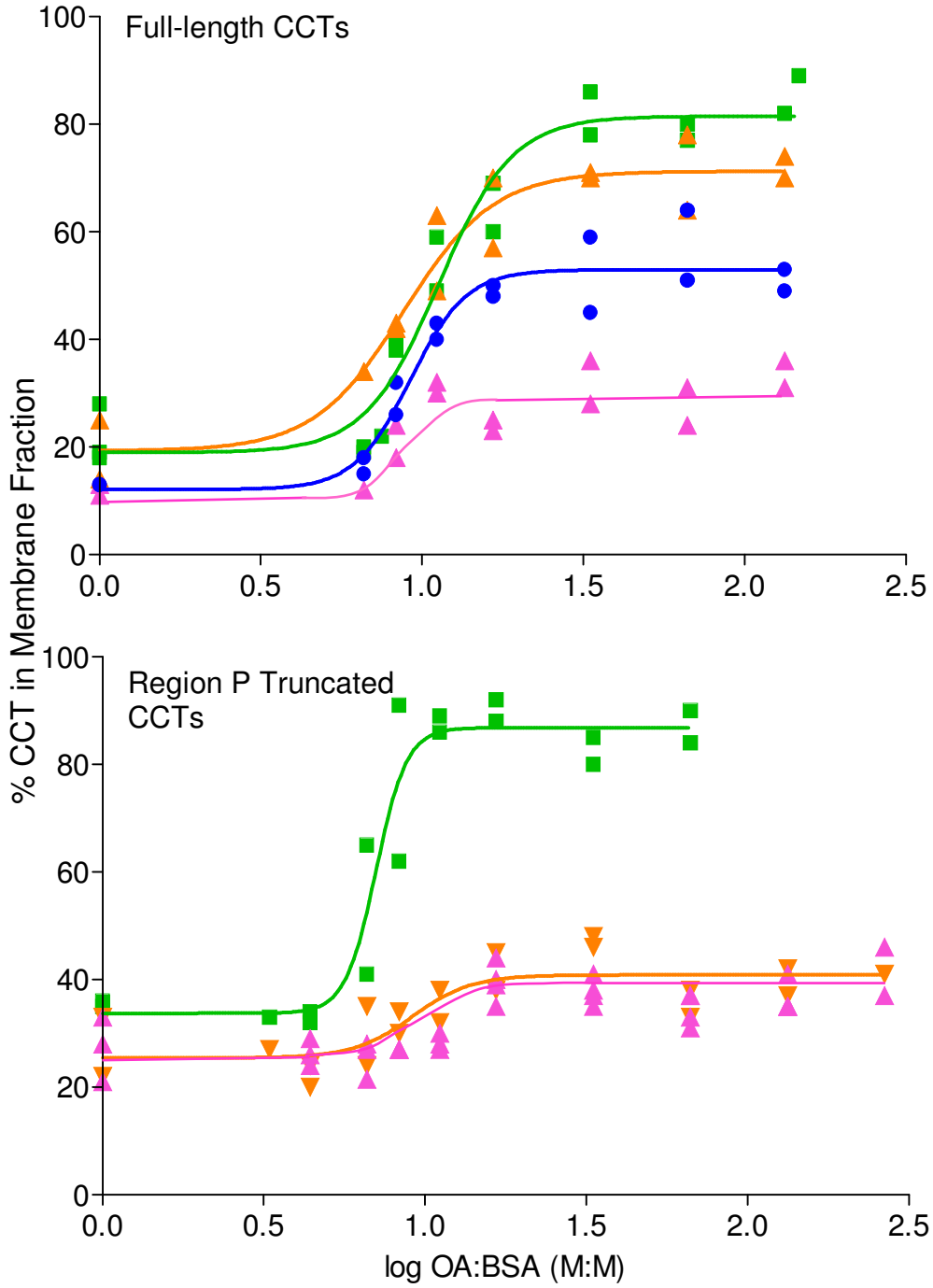

Figure 4.2 Partitioning of CCT Constructs to Oleic Acid-Enriched Cell Membranes

Partitioning curves were aligned to allow for comparison of all constructs. CCTα-derived constructs (green), CCTβ$_2$-derived constructs (pink), CCTαΔNLS-derived constructs (orange), and CCTβ+NLS (blue).

Construct		Basal		Maximum	
		% Partition	Bound/Free	% Partition	Bound/Free
1	CCTα	19 ± 4	0.24	82 ± 3	4.85
	$CCT\beta_2$	12 ± 3	0.14	30 ± 1	0.43
	CCTαΔNLS	19 ± 4	0.24	70 ± 2	2.80
	CCTβ+NLS	12 ± 3	0.14	53 ± 2	1.22
2	$CCT\alpha_{312}$	34 ± 4	0.55	87 ± 3	14.50
	$CCT\beta_{313}$	27 ± 1	0.38	38 ± 1	0.63
	$CCT\alpha\Delta NLS_{312}$	26 ± 3	0.35	41 ± 2	0.72

Table 4.2 Partitioning of CCT Constructs in Cells

Basal and maximum % partitioning was determined as the mean value ± S.E.M of the baseline and plateau of the curves in Figure 4.2, using GraphPad Prism 4. Bound/Free is the ratio of CCT units in the membrane fraction to the CCT units in the soluble fraction.

found that multi-lamellar membrane stacks are formed in cells over-expressing CCTα and CCTα was found in between these stacks. The authors postulated that the two M domains of the CCT dimer engaged separate membranes within the stack and stabilized this architecture. Taneva *et al.* (74), however, found that only one domain M engages the membrane at a time; therefore, the other membrane tethering device must be the NLS (Figure 4.3). The work of Taneva *et al.* (74) in which the NLS was first identified as a membrane binding motif was purely *in vitro* and used mutant CCTs including an NLS deletion mutant which caused a loss of tethering function in CCTα. Here I have shown that the NLS is responsible for the vesicle tethering activity of CCTα using wildtype CCTβ_2, which lacks an NLS. As well, I constructed two gain-of-function mutants (CCTβα-N and CCTβ+NLS) which tethered anionic lipid vesicles. These results further confirm that the NLS is responsible for vesicle tethering and functions as a membrane binding motif.

I have shown that the NLS functions to distinguish the membrane binding affinity of two wildtype, naturally occurring proteins both *in vitro* and in the context of cell membranes. The large difference in binding affinity between CCTα and β_2 persisted when the CCTs were dephosphorylated or when they lacked the phosphorylation region, arguing against differential phosphorylation as the key determinant for binding affinity. However, the consequences of NLS insertion/deletion were moderated by the antagonistic region P. When constructs were dephosphorylated or truncated to remove the entire phosphorylation segment, the effects of NLS insertion/deletion were unequivocal and the magnitudes of effects were very similar whether measured *in vitro* or in cells (compare the analyses of CCTα_{312} and CCTβ_{313} in Table 4.1 and 4.2).

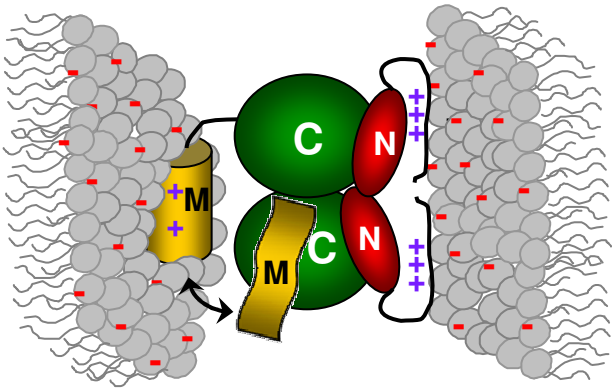

Figure 4.3 The NLS Enables Tethering of Anionic Lipid Vesicles

The CCTα dimer tethers anionic lipid vesicles by a single domain M engaging one vesicle (the two M domains alternate in vesicle binding; see Taneva et al, 2008) and the paired NLS engaging the other vesicle. In this case, domain M and the paired NLS engage different membranes. Vesicle tethering necessitates that M domains and N regions (housing the NLS) are on opposite poles of CCTα. Region P omitted from diagram for clarity.

Previous research has indirectly indicated that NLS sequences may have membrane lipid binding capabilities. In fission yeast the protein mid1p controls the positioning of the cytokinetic ring and localizes to the zone in the middle of the cell where the cleavage ring will develop. This localization (presumably to membrane) depends on a motif that includes a short amphipathic helix and a NLS motif, based on mislocalization of mutants in this motif (117). The results of alternative localizations for mid1p during the cell cycle suggest competition between a nuclear import and membrane binding role for the NLS (117). Studies with four other proteins also highlight a dual function for NLS sequences. The polybasic segment in PLCζ that contains a nuclear-importing NLS sequence can also bind to anionic lipid vesicles *in vitro* (118). A polybasic PM-targeting motif in Rit or Rin GTPases could be converted into a nuclear targeting signal by replacing a single tryptophan with alanine (119). A segment in the Ste5 scaffold protein of mating yeast contains a polybasic motif that mediates its PM targeting (essential for its signaling function in recruiting $G_{\beta\gamma}$ to the PM), and also its nuclear import, which may serve to dampen signaling (120). Lastly, Opi1p, the transcription repressor for phosphatidylinositol metabolism genes in yeast, contains a polybasic sequence identified to alternately function in ER membrane association or nuclear import, depending on the phosphatidic acid concentrations in the ER (121).

This work extends the body of evidence that NLS sequences can act as membrane binding motifs. I have quantified the membrane partitioning effect of an NLS binding motif in concert with an amphipathic helix motif, and have shown that the NLS can enhance membrane partitioning of an amphitropic protein in cells (Figure 4.4 A). I envision that in the case of CCTα, the two functions of the NLS may not necessarily

compete with each other. Rather, once CCTα has been imported into the nucleus and has dissociated from α-importin, its free basic NLS motif can bind electrostatically to sites of high negative charge density on the inner nuclear membrane. Alternatively, in cells where CCTα is found predominantly in the cytoplasm (42-45), membrane binding of the NLS may serve to block binding to α-importin. The mechanism of CCTα retention in the cytoplasm has not been elucidated at this time.

4.3 Role of Region P Phosphorylation on the Membrane Affinity of CCT Isoforms

The binding affinities of all constructs tested *in vitro* were increased by dephosphorylation or by region P truncation. With one exception[1] the effects of region P deletion were equivalent to dephosphorylation, suggesting that region P antagonizes the binding of domain M and that this effect is related to its phosphorylation state. The negative effect of region P was also observed in the context of cell membranes. CCT partitioning into OA-enriched cell membranes was higher when constructs were missing region P, with the exception of CCTαΔNLS$_{312}$ (Table 4.1 and 4.2). The phosphorylation status of the full-length CCTs in these experiments was unknown; thus, I could not extract the quantitative effect of region P phosphorylation from a comparison of the partitioning of full-length versus region P truncated CCTs as was done *in vitro*. Cumulatively, these findings suggest that region P antagonizes the binding of domain M and that this effect is related to its phosphorylation state. The mechanism whereby phosphorylated region P antagonizes membrane binding remains unresolved. Possible

[1] Region P deletion in CCTα to generate CCTα$_{312}$ increased the membrane binding affinity about 3-fold higher than dephosphorylation. This construct as well as CCTβ+NLS$_{313}$ had poor solubility during purification. This finding suggests that region P may also serve to improve CCT solubility in constructs containing NLS motifs.

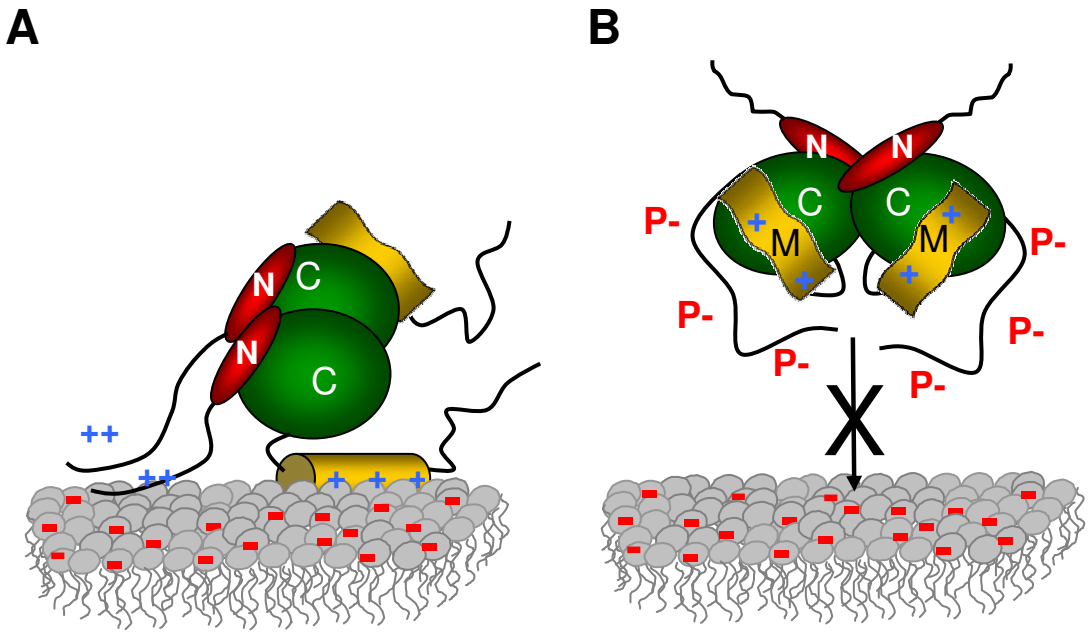

Figure 4.4 Model of Opposing Forces of NLS and Phosphorylation on Domain M Membrane Binding Affinity

A. The NLS, *not* acting in its vesicle tethering capacity, engages the same membrane as domain M. The N region is long and flexible owing to its intrinsic structural disorder and is able to reach the same membrane as domain M. This action does not increase the activity of CCTα directly but may serve to reinforce domain M membrane binding and de-repression by increasing the lifetime of membrane-bound domain M. *B*. Phosphorylation antagonizes membrane binding possibly by electrostatic repulsion from anionic membranes or neutralization of positive charges in domain M responsible for initial electrostatic interactions. In the absence of an NLS to reinforce membrane binding, phosphorylation has a stronger antagonistic effect.

mechanisms include electrostatic repulsion between the phospho-serines proximal to domain M and the negatively charged membrane surface, or neutralization of the positive charges in neighboring domain M (Figure 4.4 B; 90).

Antagonism of membrane binding by phosphorylation of region P is supported by three decades of studies on CCT, starting with the discovery that treatment of cells with conditions inhibitory to kinases resulted in increased CCT activity, membrane binding and PC synthesis, and that phosphatase inhibitors had the opposite effect (100, 122). Many agents which stimulate PC synthesis are associated with CCT dephosphorylation (123, 124) and increased membrane association (76, 77, 79, 94). Similar to work presented here, region P truncation (116) or dephosphorylation (90) has been shown to reduce CCTα affinity for anionic lipid vesicles. Dephosphorylation of CCTα during the cell cycle is associated with increased CCT activity and PC synthesis (125).

On the other hand, reports of the effects of phosphorylation by specific kinases on CCT activity are few. Oxysterol-promoted ERK1/2 phosphorylation of CCTα in MLE cells (predominantly at Ser-315 at the start of region P), was associated with inhibition of activity, but the effect of this phosphorylation on the membrane affinity of the CCT was not explored (86). Other attempts to modulate CCT activity by *in vitro* phosphorylation by various proline-directed kinases or casein kinase II have failed due to poor stoichiometry of phosphorylation (81, 85). Several other investigations into the signaling pathways leading to elevated PC synthesis have suggested links between CCTα or CCTβ_2 to upstream kinases (32, 96, 97), but these studies did not clearly identify the kinase directly modifying CCT, its target site on CCT, or effect on CCT activity/membrane association.

One report suggested that region P can serve as a second activation/lipid binding domain along with domain M (80). This conclusion was based on the finding that while the activity of CCTα truncated at residue 257, mid-way through domain M, was unresponsive to anionic lipid vesicles, the activity of a mutant CCTα with a deletion between residue 257 and the start of region P was lipid responsive. While a straight-forward explanation is that region P provided a second membrane binding motif, it may be that the extension of the truncated amphipathic helix domain with region P peptide helped to stabilize the residual helical conformation of domain M to enhance membrane binding. This idea is supported by helix predictions of these constructs by PROFSec (http://ca.expasy.org). As well, the P segment is equally susceptible to proteolysis in the presence or absence of lipid (39); if it was a binding domain it would be protected like domain M.

The SLV binding measurements suggested that the membrane affinity of CCTβ_2 is more sensitive to phosphorylation than CCTα, such that dephosphorylation or region P truncation produced a greater increase in affinity for PC/PG vesicles. Moreover, deletion of the NLS from CCTα sensitized it to phosphorylation changes. The high phosphorylation state of the CCTβ+NLS (14 phosphorylation sites) may explain this exception to the trend seen with the other constructs, which suggests a mitigating effect of the NLS. The presence of the NLS motif may dampen the effects of phosphorylation on CCT membrane affinity by providing an additional membrane anchor.

4.4 The Different Intrinsic Membrane Affinities of CCT Isoforms May Reflect Their Distinct Cellular Localizations

Why would CCTβ_2 have evolved to bind membranes more weakly than the α-isoform and to rely more on phosphorylation signals to modulate its membrane association and activity? For CCTβ_2, its very low membrane affinity, even for the 40% anionic vesicles or cell membranes highly enriched in OA used in this study, suggest that this isoform would require nearly complete dephosphorylation for membrane translocation. Yet others have shown that cells can function with only CCTβ_2 to provide CDP-choline for PC synthesis, despite its weak membrane binding affinity (26, 30). The different membrane binding affinities of CCT isoforms may have evolved as a consequence of their sub-cellular location. CCTβ_2 is a cytoplasmic enzyme that shuttles on and off the ER membrane, whereas CCTα is often found translocating on and off the inner nuclear membrane. The ER contains approximately 50% of the total membrane area volume within a cell whereas the inner nuclear membrane contains only ~0.2% (126; rat liver hepatocyte). In effect, the local concentration of target membrane for CCTβ_2 is much higher than for CCTα, and therefore CCTβ_2 would not require as high affinity to achieve the same level of membrane binding as CCTα.

4.5 Functional and Evolutionary Significance of Intrinsically Disordered Regulatory domains and Regions in CCT

Membrane binding of domain M alleviates its inhibition of catalysis (67) and is responsible for CCT activation. In addition, the intrinsically disordered regions N and P contribute to the activation by modulating the membrane binding affinity of domain M. Why would such an important function be contained within structural disorder? It has been postulated that disordered regions of proteins allow for flexibility and plasticity in

ligand binding and perform vital functions, contrary to the structure-function paradigm (8-11, 15). According to the "fly-casting model" long disordered regions may increase the capture radius, enabling a weak protein-ligand interaction but at a greater distance (15). When binding and folding are coupled, the binding strength is predicted to increase as the capture radius decreases resulting in faster protein association with its target (10, 15). In the soluble form of CCT, domain M is quasi-unstructured (68); thus it would have a large capture radius for sampling membranes, and its coupling of membrane binding to folding into an α-helix would decrease the entropic penalty associated with folding (10, 11). Contact with a membrane site enriched in anionic lipids or other activating lipids might stabilize foci of helical structure in segments of domain M. Propagation to form a long stable helix with a strong hydrophobic face for membrane insertion may be facilitated by NLS binding, which would increase the time that domain M is resident on the membrane. CCTβ_2 would have an identical search radius to that of CCTα but the interaction between unstructured domain M and membrane would not be reinforced due to the lack of an NLS binding motif, resulting in weaker affinity.

While these data show that the NLS can increase CCT's binding to 40 mol% PG vesicles by an order of magnitude, this translated into only a modest ~2-fold increase in activation efficiency of CCTα compared to CCTβ_2 by the same vesicles. As well, CCT partitioning in cells showed that all constructs, regardless of NLS content, initiated partitioning at approximately the same range of OA enrichment. Thus *in vitro* and in cells, it is the charge-sensing function of domain M that primarily determines the response to anionic lipids and the activation status of CCT. However, the maximal partitioning was influenced by the presence/absence of the NLS motif. Therefore domain

M initiates binding and the NLS serves to reinforce this binding as is reflected in the higher maximal partitioning of constructs possessing NLS motifs. In its cross-bridging mode the NLS might not have this consequence, but there are no data suggesting that the NLS cannot also bind to the same membrane as the M domain (Figure 4.4 B). In terms of activation, it is only when domain M is membrane bound that the active site inhibition is de-repressed. The NLS does not itself assist in the activation of the catalytic domain by lipids, but it can assist the de-repression associated with membrane binding of domain M by increasing the lifetime of the membrane-bound M domain.

The structural disorder of region P may serve a different purpose than that of region N. Phosphorylated regions tend also to be areas of intrinsic disorder (17). The flexibility of region P may allow better access of kinases and phosphatases. If region P adopted a rigid structure the action of such modifying enzymes might be sterically hindered and the fine-tuning of the membrane binding affinity of domain M of CCT would be impossible.

The sequences of the disordered N and P regions of CCTs are the least conserved. Because of their lack of structure, mutations in these regions would not have such deleterious affects on function compared to those within a defined structural fold. For example, mutation of Lys-122 to arginine in CCT deadens the enzyme (64), while mutations in the disordered N region described in this work (CCTβ_2 C34S, region N chimera, NLS mutants) had no effect on the specific activity of CCTs. These disordered regions allow for the evolution of new functions and binding partners because maintaining a specific fold is not necessary. It will therefore not be surprising to find that the poorly conserved disordered amino- and carboxy-terminal segments of CCTs across

phyla have evolved novel regulatory devices to modulate the function of the enzyme that controls PC synthesis.

4.6 Significance of this Work

I had hypothesized that CCTα and CCTβ_2 may have evolved similar but distinct regulatory means and that this differential regulation may reflect their expression and sub-cellular localization. The results of *in vitro* studies as well as those in cells support this hypothesis.

The work presented here represents the first biochemical characterization of CCTβ_2. The regulation of CCTβ_2 is, not surprisingly, similar to that of CCTα but there are distinct differences. The CCTβ_2 isoform has a lower specific activity than CCTα. The specific activities of chimeric CCTs with swapped N segments suggest that this region may contribute to this difference. The crystal structure of CCTα showed that a portion of region N makes intimate contact with the catalytic domain (48). The catalytic domains of CCT isoforms are 90% identical but this portion of region N is only 67% similar (Figure 1.4, Table 1.1). Future structural studies are needed but it appears that region N may also distinguish the specific activities of CCT isoforms.

I found that CCTβ_2 has a weaker membrane binding affinity and is more stringently regulated by phosphorylation owing to the lack of a secondary membrane binding motif. In collaboration with Svetla Taneva, I identified the polybasic NLS as this second binding motif. I have shown that the NLS functions to increase membrane affinity using wildtype CCTs and in the context of cellular membranes suggesting that this phenomenon is not simply an artifact of an *in vitro* analysis. An NLS serving as a

membrane binding motif is completely novel in the realm of CCT research. The NLS at the amino-terminus of the protein can couple with domain M in vesicle cross-bridging, but at the same time can enhance CCT affinity for vesicles, suggests that the NLS can bind both in *cis* and in *trans*, with respect to domain M (see Figure 4.3 and 4.4 B). Its ability to do this highlights an important feature of region N – its intrinsic lack of structure, which makes it long and flexible.

The investigation into the regulatory function of the disordered regions of CCT has broadened our knowledge with respect to the utility of such structural disorder. Research published in this area has focused on scaffold proteins and those involved in protein-protein or protein-DNA interactions. To my knowledge this is the first study to investigate the regulation of a vital metabolic enzyme by protein disorder.

Appendices

Appendix 1: Polymerase Chain Reaction Set-up and Thermocycler Settings

PCR for Subcloning CCTβ$_2$

Reaction components:

100 ng linearized plasmid template DNA
100 ng forward primer
100 ng reverse primer
250 µM dNTPs
2.5 units Pfu Turbo
20 mM Tris-HCl (pH 8.8)
10 mM KCl
10 mM $(NH_4)_2SO_4$
2 mM $MgSO_4$
1 % Triton X-100
1 mg/ml nuclease-free BSA

Thermocycler settings:

cycle 1 - 5
95℃ 2 minutes
94℃ 1 minute
55℃ 1 minute
68℃ 1.5 minutes
} x 4 cycles
cycle 6 - 25
94℃ 1 minute
60℃ 1 minute
68℃ 1.5 minutes
} x 19 cycles
68℃ 5 minutes
4℃ ∞

Site-Directed Mutagenesis

Reaction components:

50 ng plasmid template DNA
125 ng forward primer
125 ng reverse primer
250 µM dNTPs
2.5 units Pfu Turbo
20 mM Tris-HCl (pH 8.8)
10 mM KCl
10 mM $(NH_4)_2SO_4$
2 mM MgSO4
1 % Triton X-100
1 mg/ml nuclease-free BSA

Thermocycler settings:

95℃ 30 seconds
95℃ 30 seconds
55℃ 1 minute
68℃ 2 minutes per kilobase
} x 18 cycles
4℃ ∞

Appendix 2: Oligonucleotide Sequences

Legend: Mutated bases in bold (silent mutations denoted as "s"; mutations causing an amino acid change are labeled "XΔY" where "Y" is the resultant residue)

Inserted bases in lowercase

Deleted bases denoted as "^" (number of bases deleted is above symbol)

$T_M = 81.5 + 0.41$ (% G/C) – (675/N) - % mismatch, where N = length of oligonucleotide

Mutagenesis for Sub-cloning CCTβ$_2$ from pCR2.1TOPO to pBSKS(-)His

Forward:

5' GCC AGT GTG CTG G**A****G** **A**TC **T**CC tCT TGC CAT GCC AGT AGT TAC C 3'
*Bgl*II start

T_M = 79°C length = 43 bases G/C = 56 % mismatch = 9 %

Reverse:

5' GG TGT GCA CTT GT**C** **G**AC CAG GCA CCT TTA CTT CTC ATC C 3'
*Sal*I stop

T_M = 81°C length = 39 bases G/C = 54 % mismatch = 5 %

Mutagenesis to Yield pBSKS(-) His-Xa-CCTβ$_2$ C34S

Forward:

5' G CAC ACA T**C**C CCA CAG CCT **A**G**G** CTG ACC CTG ACT GCA C 3'
CΔS *Avr*II (s)

T_M = 80°C length = 38 bases G/C = 58 % mismatch = 8 %

Reverse:

5' G TGC AGT CAG GGT CAG **C**C**T** AGG CTG TGG G**G**A TGT GTC C 3'
*Avr*II (s) CΔS

T_M = 80°C length = 38 bases G/C = 58 % mismatch = 8 %

Mutagenesis to Yield pBSKS(-) His-Xa-CCTα ΔNLS

Forward:

15
5’ GT TCA GCT AAA GTC AAT TCA ^ GAG GT**G** CCT GGC CCT AAT 3’
abolished
*Kpn*I (s)

T_M = 80°C length = 38 bases G/C = 47 % mismatch = 3 %
(long deletion not included in calculations)

Reverse:

15
5’ ATT AGG GCC AGG **C**AC CTC ^ TGA ATT GAC TTT AGC TGA AC 3’
abolished
*Kpn*I (s)

T_M = 80°C length = 38 bases G/C = 47 % mismatch = 3 %
(long deletion not included in calculations)

Mutagenesis to Yield pBSKS(-) His-TEV-CCTβ$_2$

Forward:

(s) (IΔR)
5’ GCT AGG CAC CAC CAT CAC CAT CA**T** AT**G** GAA aat ctc tat ttt caa GGA AGA
*Nde*I TEV recognition sequence

9
TCT ^ ATG CCA GTA GTT ACC ACT GAT GC 3’
start

T_M = 86°C length = 75 bases G/C = 47 % mismatch = 3 %
(long insertion/deletions not included in calculations)

Reverse:

9
5’ GC ATC AGT GGT AAC TAC TGG CAT ^ AGA TCT TCC ttg aaa ata gag att TTC
start TEV recognition sequence

CAT **A**TG ATG GTG ATG GTG GTG CTT AGC 3’
*Nde*I

T_M = 86°C length = 75 bases G/C = 47 % mismatch = 3 %
(long insertion/deletions not included in calculations)

Mutagenesis to Yield pBSKS(-) His-TEV-CCTβ+NLS

Forward:

polybasic NLS

5' CCA GTA GTT ACC ACT G**C**T **AAA** G**T**G TCA **TC**A A**G**A **AAA** A**GG AG**A AAA TCC
DΔA AΔK EΔV EΔS TΔR GΔK IΔR PΔR

CTT TC**G** AAT GAG CCT CCC 3'
*Bst*BI (s)

T_M = 82°C length = 66 bases G/C = 45 % mismatch = 2 %
(long mutation not included in calculations)

Reverse:

5' GGG AGG CTC ATT **C**GA AAG GGA TTT T**CT CCT TTT** TC**T** T**GA** TGA C**A**C **TTT**
*Bst*BI (s) PΔR IΔR GΔK TΔR EΔS EΔV AΔK

A**G**C AGT GGT AAC TAC TGG 3'
DΔA

T_M = 82°C length = 66 bases G/C = 45 % mismatch = 2 %
(long mutation not included in calculations)

Mutagenesis to Yield pBSKS(-) $CCT\alpha_{312}$ and $CCT\alpha\ \Delta NLS_{312}$

Forward:

5' GGT CGG ATG CTG CAG **TAA G**TC **GAC** CCC AAG CAG AGT CCC AGC AGC
stop *Sal*I

AGC CCT 3'

T_M = 78°C length = 51 bases G/C = 57 % mismatch = 14 %

Reverse:

5' AGG GGT GCT GCT GGG ACT CTG CTT GGG **GTC** GA**C** **TTA** CTG CAG CAT
*Sal*I stop

CCG ACC 3'

T_M = 78°C length = 51 bases G/C = 57 % mismatch = 14 %

Mutagenesis to Yield pBSKS(-) CCTβ$_{313}$ and CCTβ+NLS$_{313}$

Forward:

5' CGG ATG CTA CAG GCC T**A**A T**G**T C**G**A **C**AG CAG AGT CCT GTG AGC AGC 3'
stop *Sal*I

T_M = 79°C length = 45 bases G/C = 51 % mismatch = 9 %

Reverse:

5' GCT GCT CAC AGG ACT CTG CT**G** T**C**G A**C**A T**T**A GGC CTG TAG CAT CCG 3'
*Sal*I stop

T_M = 79°C length = 45 bases G/C = 51 % mismatch = 9 %

Mutagenesis to Yield pBSKS(-) CCTα

Forward:

36 start
5' GG CCG CTC TAG ACG CGT AG**T** AC**T** ^ AGA TCT agg **A**CC ATG GAT GCA CAG
*Sca*I Kozak

AGT TC 3'

T_M = 78°C length = 52 bases G/C = 50 % mismatch = 12 %
(long deleted sequence not included in calculations)

Reverse:

36
5' GA ACT CTG TGC ATC CAT GG**T** cct AGA TCT ^ **A**GT **A**CT ACG CGT CTA GAG
Kozak *Sca*I

CGG CC 3'

T_M = 78°C length = 52 bases G/C = 50 % mismatch = 12 %
(long deleted sequence not included in calculations)

Appendix 3: Protease Inhibitors for Protein Purification

The following protease inhibitors were added to the hypotonic buffer used when homogenizing transfected COS-1. The protease cocktail was adapted from the method of Weinhold *et al.* (127).

Inhibitor (working concentration)	**Inhibitor Stock Concentration**	**Volume for 10 ml Buffer**
Leupeptin (2.5 µg/ml)	5 mg/ml in H_20	5 µl
Chymostatin (2 µg/ml)	2.5 mg/ml in DMSO	8 µl
Antipain (1 µg/ml)	5 mg/ml in H_20	2 µl
Pepstatin (2 µg/ml)	5 mg/ml in DMSO	4 µl
p-amino-benzadine (10 µg/ml)	2 mg/ml in H_2O	50 µl
Benzamidine (10 µg/ml)	2 mg/ml in H_2O	50 µl
PMSF (2 mM)	87 mg/ml in DMSO	40 µl

Appendix 4: Structure of Bis(sulfosuccinimidyl) Suberate and Copper Phenanthrolene

The chemical structures for the lysine-specific chemical crosslinker and the oxidizing agent used in probing the quaternary structure of CCTβ_2 are shown. The length of the cross-linker arm of bis (sulfosuccinimidyl) suberate (boxed) is approximately 12 Å.

Bis (sulfosuccinimidyl) suberate

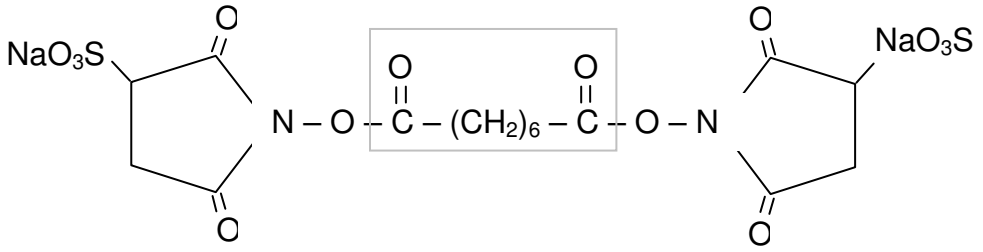

Copper phenanthrolene

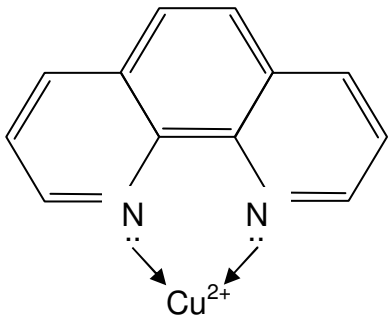

Appendix 5: The Presence of Phosphatase in SLV Binding Assay Does Not Affect CCT Binding

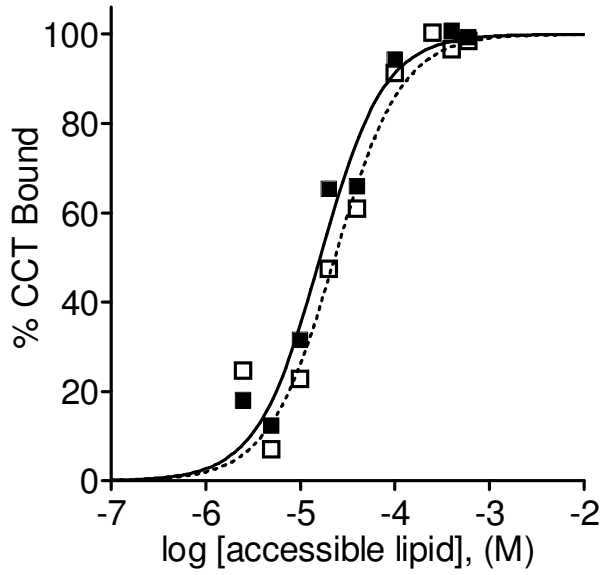

Membrane binding of purified, phosphorylated CCTα was assayed in the presence and absence of pre-quenched PPIα using SLVs composed of PC/PG (3:2) at 20°C. The phosphatase activity of PPIα was quenched by the addition of 20 mM K_2HPO_4 and 2 mM EDTA. CCTα (■) and CCTα + pre-quenched PPIα (□) were assayed in parallel in a single experiment. The individual data points were fit to the equation % Bound = $100K_p$ [L] / (1+K_p [L]), where [L] is the concentration of accessible lipid (½ of total lipid). Partition coefficients (K_p ± 95% confidence interval with respect to the best fit) were calculated from these curves. CCTα = 61.5 ± 21.1 x 10^3 M^{-1}, and CCTα + pre-quenched PPIα = 43.0 ± 16.4 x 10^3 M^{-1}. The curves were fit and analyzed by the f-test using GraphPad Prism 4 (p = 0.1146).

Appendix 6: Expression Level of CCT Constructs Based on Activity

CCT Construct	**Activity (units/mg lysate protein)** ± range or SD
CCTα	93 ± 2
CCTβ$_2$	108 ± 14
CCTαΔNLS	121 ± 16
CCTβ+NLS	106 ± 2
CCTα$_{312}$	102 ± 1
CCTβ$_{313}$	92 ± 0
CCTαΔNLS$_{312}$	106 ± 4

The expression level of each CCT construct was determined based on the activity of cell lysates. COS-1 cells were transiently transfected with untagged CCT constructs for various durations (see "Experimental Procedures" sections 2.2.4 and 3.2.3). Cells were harvested and lysed and the CDP-choline/min/mg of lysates protein was determined by CCT activity assay (see "Experimental Procedures" section 2.2.5). CCTs were activated by 250 μM PG SUVs and saturating substrate conditions were used. The mean activity (units/mg lysates protein) was calculated from a minimum of 2 independent determinations and a range or S.D. was determined.

This method is much more accurate compared to a quantitative Western blot. In a Western blot there is error associated with the sample loading and transfer process. As well, CCT isoforms may have different reactivity to the antibody. Furthermore, the intensity of the signal produced by a Western blot is linear with respect to amount of protein for only a small range. As a result, it is possible to over or under-estimate the amount of protein using a quantitative Western blot. The CCT activity assay follows the conversion of radiolabeled substrate into radiolabeled product. It is therefore sensitive but has less chance for error.

Appendix 7: Determination of CCT Substrate K_m Values

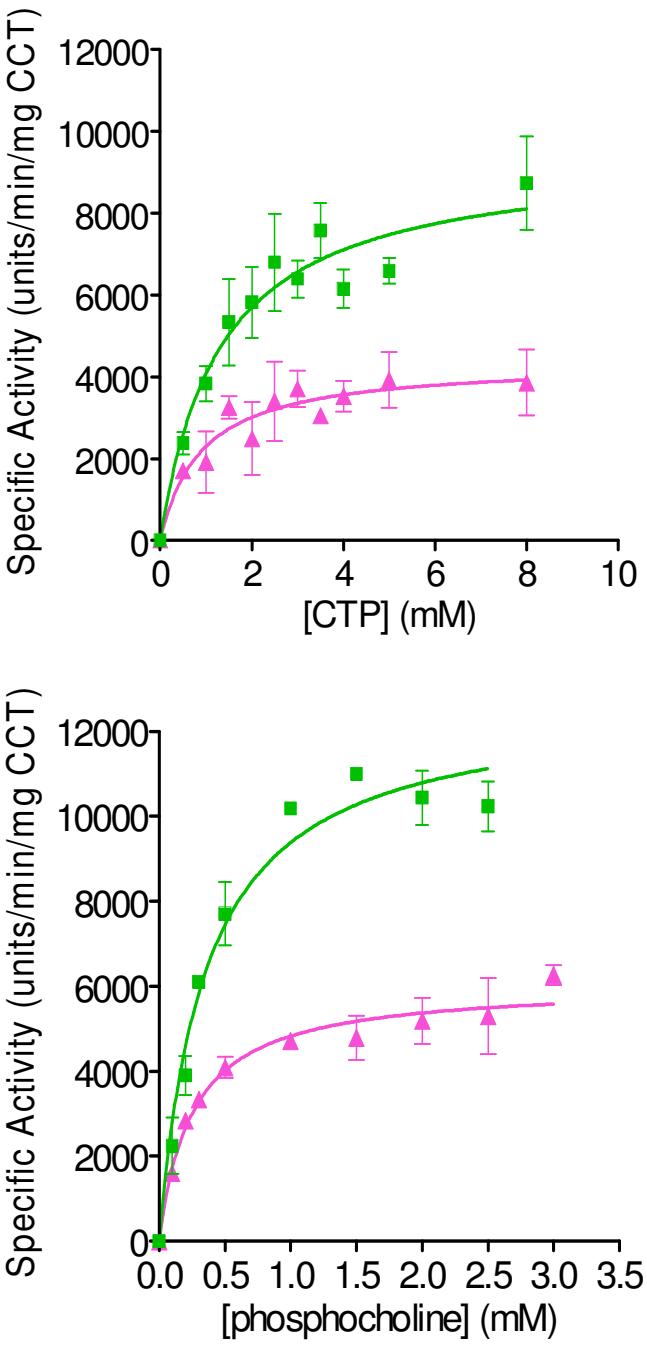

The K_m of CCTα (green) and CCTβ_2 (pink) for CTP (top) and phosphocholine (bottom) were determined from primary plots as described in "Experimental Procedures" section 2.2.5. The K_m values for CTP were approximately the same for the two CCTs (CCTα = 1.3 ± 0.4 mM, CCTβ_2 = 0.9 ± 0.4 mM), and the K_m values for phosphocholine were 0.4 ± 0.06 mM for CCTα and 0.25 ± 0.05 mM for CCTβ_2. Specific activity has units nmol CDP-choline/min/mg CCT.

Reference List

1. Min DS, Park SK, Exton JH (1998) J Biol Chem 273:7044-7051.

2. Manifava M, Sugars J, Ktistakis NT (1999) J Biol Chem 274:1072-1077.

3. Steinberg SF (2008) Physiol Rev 88:1341-1378.

4. Bermudez O, Pages G, Gimond C (2010) Am J Physiol Cell Physiol 299:C189-C202.

5. Colley WC, Sung TC, Roll R, Jenco J, Hammond SM, Altshuller Y, Bar-Sagi D, Morris AJ, Frohman MA (1997) Curr Biol 7:191-201.

6. Chakraborti S (2003) Cell Signal 15:637-665.

7. Dunker AK, Obradovic Z, Romero P, Garner EC, Brown CJ (2000) Genone Inform Ser Workshop Genome Inform 11:161-171.

8. Uversky VN and Dunker AK (2010) Biochim Biophys Acta 1804:1231-1264.

9. Dyson HJ and Wright PE (2005) Nat Rev Mol Cell Biol 6:197-208.

10. Wright PE and Dyson HJ (2009) Curr Opin Struct Biol 19:31-38.

11. Smock RG and Gierasch LM (2009) Science 324:198-203.

12. Johannessen M, Delghandi MP, Moens V (2004) Cell Signal 16:1211-1227.

13. Parker D, Ferreri K, Nakajima T, LaMorte VJ, Evans R, Koerber SC, Hoeger C, Montminy MR (1996) Mol Cell Biol 16:694-703.

14. Radhakrishnan I, Perez-Alvarado GC, Parker D, Dyson HL, Montminy MR, Wright PE (1997) Cell 91:741-752.

15. Shoemaker BA, Portman JJ, Wolynes PG (2000) Proc Natl Acad Sci 97:8868-8873.

16. Sugase K, Dyson HJ, Wright PE (2007) Nature 447:1021-1025.

17. Iakoucheva LM, Radivojac P, Brown CJ, O'Connor TR, Sikes JG, Obradovic Z, Dunker AK (2004) Nucleic Acids Res 32:1037-1049.

18. Pufall MA, Lee GM, Nelson MML, Kang H-S, Velyvis A, Kay LE, McIntosh LP, Graves BJ (2005) Science 309:142-145.

19. Mittag T, Orlicky S, Choy W-Y, Tang X, Lin H, Sicheri F, Kay LE, Tyers M, Forman-Kay JD (2008) Proc Natl Acad Sci 105:17772-17777.

20. Baker JMR, Hudson RP, Kanelis V, Choy W-Y, Thibobeau PH, Thomas PJ, Forman-Kay JD (2007) Nat Struct Mol Biol 14:738-745.

21. Vance JE (1998) Trends Biochem Sci 23:423-428.

22. Cornell RB and Northwood I (2000) Trends Biochem Sci 25:441-447.

23. Lykidis A, Murti G, Jackowski S (1998) J Biol Chem 273:14022-14029.

24. Tang W, Keesler GA, Tabas I (1997) J Biol Chem 272:13146-13151.

25. Karim M, Jacksom P, Jackowski S (2003) Biochim Biophys Acta 1633:1-12.

26. Lykidis A, Baburina I, Jackowski S (1999) J Biol Chem 274:26992-27001.

27. Jackowski S, Rehg JE, Zhang Y-M, Wang J, Miller K, Jackson P, Karim M (2004) Mol Cell Biol 24:4720-4733.

28. Wang L, Magdeleno S, Tabas I, Jackowski S (2005) Mol Cell Biol 25:3357-3363.

29. Cui Z, Houweling M, Chen MH, Record M, Chap H, Vance DE, Terce F (1996) J Biol Chem 271:14668-14671.

30. Zhang D, Tang W, Yao PM, Yang C, Xie B, Jackowski S, Tabas I (2000) J Biol Chem 275:35368-35376.

31. Carter JM, Waite KE, Campenot RB, Vance JE, Vance DE (2003) J Biol Chem 278:44988-44994.

32. Carter JM, Demizieux L, Campenot RB, Vance DE, Vance JE (2008) J Biol Chem 283:202-212.

33. Helmink BA and Friesen JA (2004) Biochim Biophys Acta 1683:78-88.

34. Tilley DM, Evans CR, Larson TM, Edwards KA, Friesen JA (2008) Biochemistry 47:11838-11846.

35. Gupta T and Schupbach T (2003) Development 130:6075-6087.

36. Inatsugi R, Kawai H, Yamaoka Y, Yu Y, Sekiguchi A, Nakamura M, Nishida I (2009) Plant Cell Physiol 50:1727-1735.

37. Cornell RB (1989) J Biol Chem 264:9077-9082.

38. Craig L, Johnson JE, Cornell RB (1994) J Biol Chem 269:3311-3317.

39. Bogan MJ, Agnes GR, Pio F, Cornell RB (2005) J Biol Chem 280:19613-19624.

40. Watkins JD and Kent C (1992) J Biol Chem 267:5686-5692.

41. Wang Y, Sweitzer TD, Weinhold PA, Kent C (1993) J Biol Chem 268:5899-5904.

42. Houweling M, Cui Z, Anfuso CD, Bussiere M, Chen MH, Vance DE (1996) Eur J Cell Biol 69:55-63.

43. Ridsdale R, Tseu I, Wang J, Post M (2001) J Biol Chem 276:49148-49155.

44. Tseu I, Ridsdale R, Lui J, Wang J, Post M (2002) Am J Respir Cell Mol Biol 26:506-512.

45. Fagone P, Sriburi R, Ward-Chapman C, Frank M, Wang J, Gunter C, Brewer JW, Jackowski S (2007) J Biol Chem 282:7591-7605.

46. Wang Y, MacDonald JIS, Kent C (1995) J Biol Chem 270:354-360.

47. Chen BB and Mallampalli RK (2009) Mol Cell Biol 29:3062-3075.

48. Lee J, Johnson J, Ding Z, Paetzel M, Cornell RB (2009) J Biol Chem 284:33535-33548.

49. MacKinnon MA, Curwin AJ, Gaspard ZGJ, Suraci AB, Fernandez-Murray JP, McMaster CR (2009) J Biol Chem 284:7376-7384.

50. Aoyama C, Liao H, Ishidate K (2004) Prog Lipid Res 43:266-281.

51. Henneberry AL, Wright MM, McMaster CR (2002) Mol Cell Biol 13:3148-3161.

52. Lagace TA and Ridgway ND (2005) Mol Cell Biol 16:1120-1130.

53. Gehrig K, Cornell RB, Ridgway ND (2008) Mol Cell Biol 19:237-247.

54. Fricker M, Hollinshead M, White N, Vaux D (1997) J Cell Biol 136:531-544.

55. Echevarria W, Leite MF, Guerra MT, Zipfel WR, Nathanson MH (2003) Nat Cell Biol 5:440-445.

56. Favale NO, Fernandez-Tome MC, Pescio LG, Sterin-Speziale NB (2010) Biochim Biophys Acta 1801:1184-1194.

57. Xie M, Smith JL, Ding Z, Zhang D, Cornell RB (2004) J Biol Chem 279:28817-28825.

58. Kalmar GB, Kay R, Lachance A, Aebersold R, Cornell RB (1990) Proc Natl Acad Sci 87:6029-6033.

59. Park YS, Sweitzer TD, Dixon JE, Kent C (1993) J Biol Chem 268:16648-16654.

60. Park YS, Gee P, Sanker S, Schurter EJ, Zuiderweg ERP, Kent C (1997) J Biol Chem 272:15161-15166.

61. Veitch DP and Cornell RB (1996) Biochemistry 35:10743-10750.

62. Veitch DP, Gilham D, Cornell RB (1998) Eur J Biochem 255:227-234.

63. Dunne SJ, Cornell RB, Johnson JE, Glover NR, Tracey AS (1996) Biochemistry 35:11975-11984.

64. Helmink BA, Braker JD, Kent C, Friesen JA (2003) Biochemistry 42:5043-5051.

65. Weber CH, Park YS, Sanker S, Kent C, Ludwig ML (1999) Structure 7:1113-1124.

66. Wang Y and Kent (1995) J Biol Chem 270:18948-18952.

67. Friesen JA, Campbell HA, Kent C (1999) J Biol Chem 274:13384-13389.

68. Taneva S, Johnson JE, Cornell RB (2003) Biochemistry 42:11768-11776.

69. Johnson JE, Aebersold R, Cornell RB (1997) Biochim Biophys Acta 1324:273-284.

70. Johnson JE and Cornell RB (1994) Biochemistry 33:4327-4335.

71. Johnson JE, Xie M, Sigh LMR, Edge R, Cornell RB (2003) J Biol Chem 278:512-522.

72. Johnson JE, Rao NM, Hui S-W, Cornell RB (1998) Biochemistry 37:9509-9593.

73. Taneva SG, Patty PJ, Frisken BJ, Cornell RB (2005) Biochemistry 44:9382-9393.

74. Taneva S, Dennis MK, Ding Z, Smith JL, Cornell RB (2008) J Biol Chem 283:28137-28148.

75. Watkins JD and Kent C (1990) J Biol Chem 265:2190-2197.

76. Watkins JD and Kent C (1991) J Biol Chem 266:21113-21117.

77. Wang J, MacDonald JIS, Kent C (1993) J Biol Chem 268:5512-5518.

78. Wang Y and Kent C (1995) J Biol Chem 270:18948-18952.

79. Houweling M, Jamil H, Hatch GH, Vance DE (1994) J Biol Chem 269:7544-7551.

80. Lykidis A, Jackson P, Jackowski S (2001) Biochemistry 40:494-503.

81. Cornell RB, Kalmar GB, Kay RJ, Johnson MA, Sanghera JS, Pelech SL (1995) Biochem J 310:699-708.

82. MacDonald JIS and Kent C (1994) J Biol Chem 269:10529-10537.

83. Sanghera JS and Vance DE (1989) J Biol Chem 264:1215-1223.

84. Wieprecht M, Wieder T, Paul C, Geilen CC, Orfanos CE (1996) J Biol Chem 271:9955-9961.

85. Wieprecht M, Wieder T, Geilen CC, Orfanos CE (1994) FEBS Lett 353:221-224.

86. Agassandian M, Zhou J, Tephly LA, Ryan AJ, Carter AB, Mallampalli RK (2005) J Biol Chem 280:21577-21587.

87. Ryan AJ, Andrews M, Zhou J, Mallampalli RK (2006) Arch Biochem Biophys 447:23-33.

88. D'Antuono C, Fernendez-Tome MC, Sterin-Speziale N, Bernik DL (2000) Arch Biochem Biophys 382:39-47.

89. Arnold RS and Cornell RB (1996) Biochemistry 35:9917-9924.

90. Arnold RS, DePaoli-Roach AA, Cornell RB (1997) Biochemistry 36:6149-6156.

91. Jamil H, Hatch GM, Vance DE (1993) Biochem J 291 pt2:419-427.

92. Davies SMA, Epand RM, Hraayenhof R, Cornell RB (2000) Biochemistry 40:10522-10531.

93. Attard, GS, Templer RH, Smith WS, Hunt AN, Jackowski S (2000) Proc Natl Acad Sci 97:9032-9036.

94. Northwood IC, Tang AHY, Crawford B, Drobnies AE, Cornell RB (1999) J Biol Chem 274:26240-26248.

95. Ng MN, Kitos TE, Cornell RB (2004) Biochim Biophys Acta 1686:85-99.

96. Kitos TE, Drobnies A, Ng MN, Wen Y, Cornell RB (2006) Biochim Biophys Acta 1761:261-271.

97. Kitos TE, Choi CM, Cornell RB (2006) Biochim Biophys Acta 1761:272-279.

98. Wimley WC and White SH (1996) Nat Struct Biol 3:842-848.

99. Eisenburg D, Weiss RM, Terwilliger TC (1984) Proc Natl Acad Sci 81:140-144.

100. Hatch GM, Jamil H, Utal AK, Vance DE (1992) J Biol Chem 267:15751-15758.

101. Golfman LS, Bakovic M, Vance DE (2001) J Biol Chem 276:43688-43692.

102. Banchio C, Schang LM, Vance DE (2003) J Biol Chem 278:32457-32464.

103. Banchio C, Schang LM, Vance DE (2004) J Biol Chem 279:40220-40226.

104. Bakovic M, Waite K, Vance DE (2003) J Biol Chem 278:14753-14761.

105. Bakovic M, Waite AK, Vance DE (2000) J Lipid Res 41:583-594.

106. Sugimoto H, Bakovic M, Yamashita S, Vance DE (2001) J Biol Chem 276:12338-12344.

107. Kast HR, Nguyen CM, Anisfeld AM, Ericssoon J, Edwards PA (2001) J Lipid Res 42:1266-1272.

108. Marcucci H, Elena C, Gilardoni P, Banchio C (2008) Biochim Biophys Acta 1781:254-262.

109. Kay R and Humphries RH (1991) Methods Mol Cell Biol 2:254-265.

110. Bradford MM (1976) Anal Biochem 72:248-254.

111. Sohal PS and Cornell RB (1990) J Biol Chem 265:11746-11750.

112. Cornell RB (1991a) Biochemistry 20:5873-5880.

113. Poehling HM and Neuhoff V (1981) Electrophoresis 2:141-147.

114. Buser CA and McLaughlin S (1998) Methods Mol Biol 84:267-281.

115. Murray D, Hermida-Matsumoto L, Buser CA, Tsang J, Sigal CT, Ben-Tal N, Honig B, Resh MD, McLaughlin S (1998) Biochemistry 37:2145-2159.

116. Yang W and Jackowski S (1995) J Biol Chem 270:16503-16506.

117. Celton-Morizur S, Bordes N, Fraisier V, Tran PT, Paoletti A (2004) Mol Cell Biol 24:10621-10631.

118. Nomikos M, Mulgrew-Nesbitt A, Pallavi P, Mihalyne G, Zaitsera I, Swann K, Lai FA, Murray D, McLaughlin S (2007) J Biol Chem 282:16644-16653.

119. Heo WD, Inoue T, Park WS, Kim ML, Park BO, Wandless TJ, Meyer T (2006) Science 314:1458-1461.

120. Winters MJ, Lamson RE, Nakanishi H, Neiman AM, Pryciak PM (2005) Molecular Cell 20:21-32.

121. Loewen CJR, Grasper ML, Jesch SA, Delan C, Ktisrakis NT, Henry SA, Levine TP (2004) Science 304:1644-1647.

122. Pelech SL and Vance DE (1982) J Biol Chem 257:14198-14202.

123. Shiratori Y, Houweling M, Zha X, Tabas I (1995) J Biol Chem 270:29894-29903.

124. Groblewski GE, Wang Y, Ernst SA, Kent C, Williams JA (1995) J Biol Chem 270:1437-1442.

125. Jackowski S (1994) J Biol Chem 269:3858-3867.

126. Weibel ER, Staubli W, Gnagi HR, Hess FA (1969) J Cell Biol 42:68-91.

127. Weinhold PA, Rounsifer ME, Feldman DA (1986) J Biol Chem 261:5104-5110.

128. Bussell RJ and Eliezer D (2003) J Mol Biol 329:763-778.

129. Teruel MN and Meyer T (1998) Cell 103: 181-184.

130. Spector, AA, John K and Fletcher JE (1969) J Lipid Res 10:56-67.